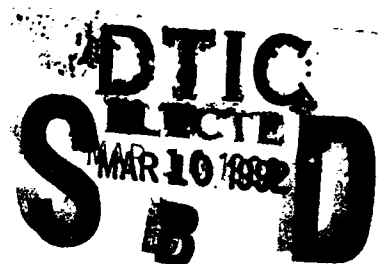


2

NAVAL POSTGRADUATE SCHOOL

Monterey, California

AD-A247 157



THESIS

COMPARISON OF MEASURED AND
TRANSFORMED DIRECTIONAL WAVE SPECTRA
USING A LINEAR REFRACTION MODEL

by

James Cheng Liu

December 1990

Thesis Advisor

Prof. Edward B. Thornton

Approved for public release; distribution is unlimited.

92-06186



92 3 09 134

Unclassified

security classification of this page

REPORT DOCUMENTATION PAGE

1a Report Security Classification Unclassified			1b Restrictive Markings		
2a Security Classification Authority			3 Distribution Availability of Report		
2b Declassification Downgrading Schedule			Approved for public release; distribution is unlimited.		
4 Performing Organization Report Number(s)			5 Monitoring Organization Report Number(s)		
6a Name of Performing Organization Naval Postgraduate School		6b Office Symbol (if applicable) 35	7a Name of Monitoring Organization Naval Postgraduate School		
6c Address (city, state, and ZIP code) Monterey, CA 93943-5000			7b Address (city, state, and ZIP code) Monterey, CA 93943-5000		
8a Name of Funding Sponsoring Organization		8b Office Symbol (if applicable)	9 Procurement Instrument Identification Number		
8c Address (city, state, and ZIP code)			10 Source of Funding Numbers		
			Program Element No	Project No	Task No
			Work Unit Accession No		
11 Title (include security classification) COMPARISON OF MEASURED AND TRANSFORMED DIRECTIONAL WAVE SPECTRA USING A LINEAR REFRACTION MODEL					
12 Personal Author(s) James Cheng Liu					
13a Type of Report Master's Thesis		13b Time Covered From To		14 Date of Report (year, month, day) December 1990	
15 Page Count 96					
16 Supplementary Notation The views expressed in this thesis are those of the author and do not reflect the official policy or position of the Department of Defense or the U.S. Government.					
17 Cosati Codes			18 Subject Terms (continue on reverse if necessary and identify by block number)		
Field	Group	Subgroup	Ocean Waves; Directional Spectra; Wave Refraction		
19 Abstract (continue on reverse if necessary and identify by block number)					
<p>Deep water directional wave spectra, measured by an NDBC 3-meter buoy off Monterey bay, are transformed to shallow water using a linear refraction model. The transformed directional spectra are compared with measured spectra using pressure gauge arrays in shallow waters at Marina and Santa Cruz.</p> <p>The classical Longuet-Higgins et al. (1963) method of computing directional wave spectra and a new exact Fourier coefficients representation method (Grauzinis, 1989) are used to compute directional wave spectra. The new method of computing directional wave spectra, which represents bi-modal distributions of wave energy exactly matching the measured Fourier coefficients to second order, demonstrates improved directional resolution over the classical technique.</p> <p>This work examines the accuracy and limitations of modeling linear refraction by comparing with field observations over complex bathymetry. In general, linear refraction can give reasonable energy and direction estimates starting with deep water spectra, but notable exceptions can occur. The largest prediction error occurred at Marina on 18 January 1988 for the case of a severe storm. This is presumably due to diffractive and non-linear effects of the high waves causing loss of accuracy. The linear refraction model is not suitable for handling such problems.</p>					
20 Distribution Availability of Abstract			21 Abstract Security Classification		
<input checked="" type="checkbox"/> unclassified unlimited <input type="checkbox"/> same as report <input type="checkbox"/> DTIC users			Unclassified		
22a Name of Responsible Individual Prof. Edward B. Thornton			22b Telephone (include Area code) (408) 646-2847		22c Office Symbol 68TM

DD FORM 1473,84 MAR

83 APR edition may be used until exhausted
All other editions are obsolete

security classification of this page

Unclassified

Approved for public release; distribution is unlimited.

Comparison of Measured and
Transformed Directional Wave Spectra
Using A Linear Refraction Model

by

James Cheng Liu
Lieutenant Commander, Navy, Republic of China
B.S., Chung-Cheng Institute of Technology, R.O.C., 1982

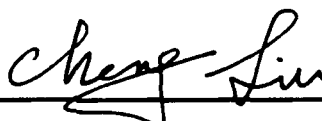
Submitted in partial fulfillment of the
requirements for the degree of

MASTER OF SCIENCE IN METEOROLOGY

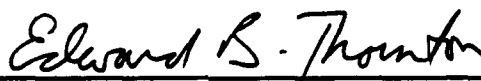
from the

NAVAL POSTGRADUATE SCHOOL
December 1990

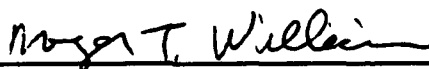
Author:


James Cheng Liu

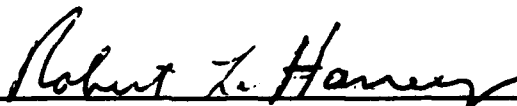
Approved by:



Prof. Edward B. Thornton, Thesis Advisor



Prof. Roger T. Williams, Second Reader



Robert L. Haney, Chairman,
Department of Meteorology

ABSTRACT

Deep water directional wave spectra, measured by an NDBC 3-meter buoy off Monterey bay, are transformed to shallow water using a linear refraction model. The transformed directional spectra are compared with measured spectra using pressure gauge arrays in shallow waters at Marina and Santa Cruz.

The classical Longuet-Higgins et al. (1963) method of computing directional wave spectra and a new exact Fourier coefficients representation method (Grauzinis, 1989) are used to compute directional wave spectra. The new method of computing directional wave spectra, which represents bi-modal distributions of wave energy exactly matching the measured Fourier coefficients to second order, demonstrates improved directional resolution over the classical technique.

This work examines the accuracy and limitations of modeling linear refraction by comparing with field observations over complex bathymetry. In general, linear refraction can give reasonable energy and direction estimates starting with deep water spectra, but notable exceptions can occur. The largest prediction error occurred at Marina on 18 January 1988 for the case of a severe storm. This is presumably due to diffractive and non-linear effects of the high waves causing loss of accuracy. The linear refraction model is not suitable for handling such problems.



Accession For	
NTIS GRA&I	<input checked="checked" type="checkbox"/>
DTIC TAB	<input type="checkbox"/>
Unannounced	<input type="checkbox"/>
Justification	
By	
Distribution/	
Availability Codes	
Dist	Avail and/or Special
A-1	

TABLE OF CONTENTS

I. INTRODUCTION	1
A. MOTIVATION OF STUDY	1
B. HISTORICAL BACKGROUND	1
C. OBJECTIVE	3
II. THEORETICAL BACKGROUND	4
A. THE LINEAR WAVE THEORY	4
1. Formulation	4
B. THE SPECIFICATION OF A WAVE FIELD	7
1. Directional Spectrum	7
2. Classical Approach	8
3. Exact Fourier Coefficient Representation Method	11
C. WAVE SPECTRUM TRANSFORMATION	16
III. DATA ACQUISITION AND SENSORS	21
A. LOCATION	21
B. DEEP WATER WAVE DATA	21
C. SHALLOW WATER WAVE DATA	22
D. WAVE DATA SELECTION	24
E. TRANSFORMATION OF DEEP WAVE SPECTRUM	24
IV. RESULTS AND DISCUSSION	35
A. COMPARISON OF LCS AND EFC MEASURED DIRECTIONAL SPECTRAL DENSITIES	35
B. REFRACTION MODEL PREDICTIONS	36
C. COMPARISON OF DEEP, SHALLOW AND TRANSFORMED DIREC- TIONAL SPECTRAL DENSITIES	56
V. CONCLUSION	66

APPENDIX A. THE SHALLOW WATER ANGLE VERSUS DEEP WATER ANGLE	67
APPENDIX B. THE DEEP, SHALLOW, AND TRANSFORMED DSD	72
RERERENCES	82
INITIAL DISTRIBUTION LIST	84

LIST OF TABLES

Table 1.	LOCATIONS OF SENSORS	21
Table 2.	DEEP WATER WAVE CHARACTERISTICS OF SELECTED CASES	24
Table 3.	SIGNIFICANT WAVE HEIGHT (UNIT: METER)	28
Table 4.	EFFECTS OF LINEAR REFRACTION	34
Table 5.	DEEP WATER BUOY ENERGY (M^2)	35
Table 6.	SHALLOW WATER ARRAY ENERGY (M^2)	36
Table 7.	COMPARISON OF TRANSFORMED AND MEASURED DATA DIFFERENCE IN DEGREE	55
Table 8.	MEASURED AND TRANSFORMED ENERGY SPECTRUM DATA AT MARINA (M^2/HZ)	55
Table 9.	MEASURED AND TRANSFORMED ENERGY SPECTRUM DATA AT SANTA CRUZ (M^2/HZ)	55

LIST OF FIGURES

Figure 1.	Location of sensors and bathymetry in Monterey Bay	2
Figure 2.	Typical spreading function of the LCS method	12
Figure 3.	Distribution of energy	14
Figure 4.	Three model distribution	16
Figure 5.	Transformation constant along a ray path	20
Figure 6.	Floating Buoy	22
Figure 7.	Slope Pressure Array	23
Figure 8.	Measured spectral densities on 3 January 1988, 0800 PST	25
Figure 9.	Measured spectral density on 18 January 1988, 0200 PST	26
Figure 10.	Measured spectral density on 29 January 1988, 2100 PST	27
Figure 11.	Ray traces from Marina to deep water	29
Figure 12.	Ray traces from Marina to deep water	30
Figure 13.	Ray traces from Santa Cruz to deep water	31
Figure 14.	Ray traces from Santa Cruz deep water	32
Figure 15.	Example of the shallow water angle versus deep water angle	33
Figure 16.	The flow chart of measurement calculation	36
Figure 17.	The energy direction of deep water on 3 Jan 1988.	37
Figure 18.	The energy direction of shallow water at Marina on 3 Jan 1988.	38
Figure 19.	The energy direction of shallow water at Santa Cruz on 3 Jan 1988.	39
Figure 20.	The LCS directional spectral density in 3-D plot	40
Figure 21.	The EFC directional spectral density in 3-D plot	41
Figure 22.	The LCS directional spectral density in contour plot	42
Figure 23.	The EFC directional spectral density in contour plot	43
Figure 24.	The LCS directional spectral density in 3-D plot	44
Figure 25.	The EFC directional spectral density in 3-D plot	45
Figure 26.	The LCS directional spectral density in contour plot	46
Figure 27.	The EFC directional spectral density in contour plot	47
Figure 28.	The LCS directional spectral density in 3-D plot	48
Figure 29.	The EFC directional spectral density in 3-D plot	49
Figure 30.	The LCS directional spectral density in contour plot	50
Figure 31.	The EFC directional spectral density in contour plot	51

Figure 32. The LCS & EFC directional spectral densities in 2-D plot	52
Figure 33. The LCS & EFC directional spectral densities in 2-D plot	53
Figure 34. The LCS & EFC directional spectral densities in 2-D plot	54
Figure 35. The deep, shallow, and transformed DSD	57
Figure 36. The deep, shallow, and transformed DSD	58
Figure 37. The deep, shallow, and transformed DSD	59
Figure 38. The deep, shallow, and transformed DSD	60
Figure 39. The deep, shallow, and transformed DSD	61
Figure 40. The deep, shallow, and transformed DSD	63
Figure 41. The deep, shallow, and transformed DSD	64
Figure 42. The deep, shallow, and transformed DSD	65
Figure 43. The shallow water angle versus deep water angle	67
Figure 44. The shallow water angle versus deep water angle	68
Figure 45. The shallow water angle versus deep water angle	69
Figure 46. The shallow water angle versus deep water angle	70
Figure 47. The shallow water angle versus deep water angle	71
Figure 48. The deep, shallow, and transformed DSD	72
Figure 49. The deep, shallow, and transformed DSD	73
Figure 50. The deep, shallow, and transformed DSD	74
Figure 51. The deep, shallow, and transformed DSD	75
Figure 52. The deep, shallow, and transformed DSD	76
Figure 53. The deep, shallow, and transformed DSD	77
Figure 54. The deep, shallow, and transformed DSD	78
Figure 55. The deep, shallow, and transformed DSD	79
Figure 56. The deep, shallow, and transformed DSD	80
Figure 57. The deep, shallow, and transformed DSD	81

ACKNOWLEDGMENTS

I wish to thank Professor Edward B. Thornton for his guidance and advice during this research. His encouragement and patience made this study a joyful learning experience. I would also like to thank Professor Roger T. Williams for his careful review and nice suggestions. Thanks are due for the assistance from Mr. Robert Wyland and Mrs. Mary Bristow to use linear refraction model program. I am very thankful to my old brother Dr. Kevin Liu, for his continual pushing and reminding. My deepest gratitude should go to my mom, whose enduring confidence and support for these years made this possible. I am grateful to my country, Republic of China, for providing me this opportunity to explore my new horizon.

I dedicate this thesis to my dear wife, Mei-lan, for her inexhaustible supply of love, encouragement and understanding.

I. INTRODUCTION

A. MOTIVATION OF STUDY

Wave climatology plays an important role in coastal dynamics. A basic problem is how to use deep water wave data to predict shallow water wave characteristics, which would allow predictions of waves at any nearshore location using only the measurement at one deep ocean location. But there are two associated questions. First, how to characterize ocean wave behavior? Second, how to transform waves from deep water to shallow water? Since directional characteristics of ocean waves are important to understand for wave generation and wave refraction behavior, we choose to use the directional wave spectral density (DSD) for characterizing the ocean wave behavior and we will use a linear refraction model to transform the deep water DSD to shallow water.

The area of Monterey Bay has been selected for this comparative study of ocean waves. This area presents an interesting problem for predicting directional wave spectra because of its variable shoreline orientation relative to prevalent eastward waves and the presence of the Monterey submarine canyon which is the largest in the western hemisphere and causes substantial perturbations on the nearshore wave field. Figure 1 shows the irregular bathymetry of the Monterey submarine canyon and three sensors locations used in the comparison study.

A NOAA, 3m buoy is used in deep water to measure the three orthogonal components of the wave field heave, pitch, and roll directly. In shallow water, square slope arrays, 6m on a side composed of 4 pressure sensors each are used to measure and compute the equivalent three orthogonal wave components at Marina and Santa Cruz.

B. HISTORICAL BACKGROUND

Historically, Monterey Bay was the first, and presumably one of the most intensively studied, locations for wave refraction. Wave refraction diagrams of Monterey Bay were first constructed in 1948 by Johnson, O'Brien and Isaac (Wiegel, 1964). The first intensive refraction studies were performed for amphibious landing exercises at Fort Ord (1954) followed by studies by the Corps of Engineers (1958) for the small craft harbor at Santa Cruz. Wave refraction and littoral drift calculations have been performed by Dorman (1969) and Arnal et al. (1973). All these studies were performed using hand-drawn refraction diagrams. More recently, numerical refraction calculations have been made for a number of specific marine construction sites (e.g., Thornton (1978, 1980))

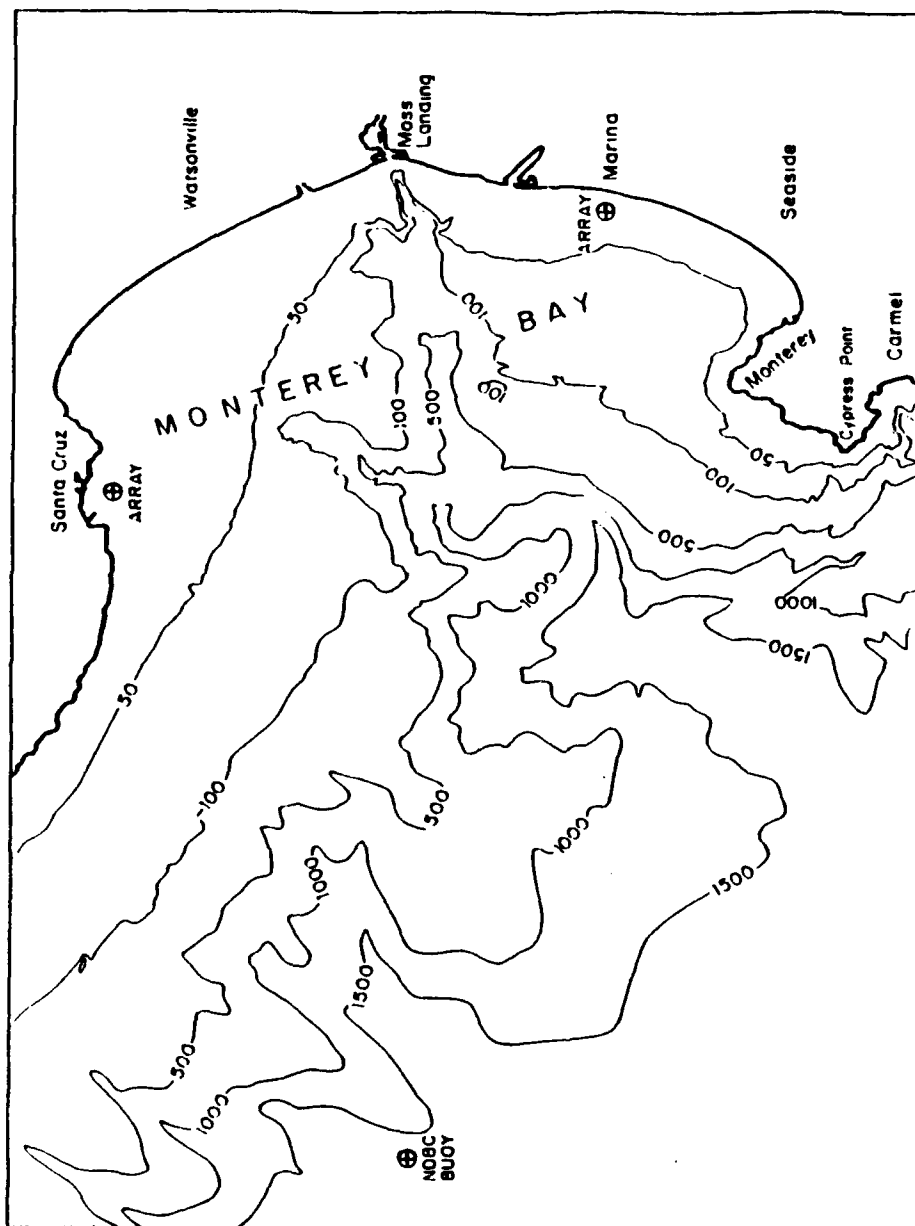


Figure 1. Location of sensors and bathymetry in Monterey Bay

and erosion studies (Oradiwe, 1986; McGee, 1986). The present work is an extension of the work by Khalid (1989) who used the low resolution spectral estimator method of Longuet-Higgins, Cartwright and Smith (1963).

C. OBJECTIVE

The objective of this study is to investigate whether linear refraction can be used to transform directional wave spectra from deep to shallow water over complex bathymetry. Several different ways of computing directional spectral density (DSD) are presented. The deep water DSD are transformed to shallow water using the refraction approach originally proposed by Longuet-Higgins (1957). These transformed spectra are compared with DSD measured directly in shallow water for which the data had been acquired from pressure gauge arrays located at Marina and Santa Cruz. In Chapter II. of this thesis, linear wave theory, two methods of computing directional wave spectrum, and wave spectrum transformation using the theoretical approach will be addressed. Chapter III. describes the data acquisition and sensors. Chapter IV. contains the results and discussion. Conclusions are presented in Chapter V.

II. THEORETICAL BACKGROUND

A. THE LINEAR WAVE THEORY

1. Formulation

Linear surface gravity wave theory has been successful in describing many observed wave phenomena. In the formulation of this theory, see for instance Kinsman (1965), the basic assumptions can be summarized as

- wave frequencies, ω , are much greater than the earth's rotation frequency, Ω
- the fluid is homogeneous, or $\omega \gg N$, the Brunt- Väisälä frequency
- surface tension effects are negligible, or $\omega_{cp} \gg \omega$, where ω_{cp} is the frequency of the capillary waves
- the fluid motion is irrotational, or $\nabla \times \vec{V} = 0$, which allows the velocity potential, ϕ , to be defined in terms of the water particle velocity vector as $\vec{V} = -\nabla\phi$
- the fluid is incompressible, or $\nabla \cdot \vec{V} = 0$

The combination of the assumptions of irrotationality and incompressibility leads to the basic equation of linear wave theory, Laplace's equation

$$\nabla^2 \phi = 0 \quad (1)$$

Analytical solutions to this equation are obtained by applying the following boundary conditions:

- waves are periodic in space and time
- the bottom boundary is horizontal and impermeable, which is prescribed by

$$w|_{-h} = -\frac{\partial \phi}{\partial z}|_{-h} = 0 \quad (2)$$

- the linearized kinematic free surface boundary condition is expressed as

$$\frac{\partial \eta}{\partial t} - w|_{\eta} = 0 \quad (3)$$

and the linearized dynamic boundary condition as

$$g\eta - \frac{\partial \phi}{\partial t}|_{\eta} = 0 \quad (4)$$

where w is the scalar vertical velocity, h is the local water depth, η is the instantaneous free surface elevation, g is the acceleration of gravity, and t is time.

In the linearization process, it is assumed that the wave amplitude a is small when compared to the wavelength L and depth, or that $\frac{a}{L} \ll 1$ and $\frac{a}{h} \ll 1$. These restrictions make the linear wave theory strictly applicable to small amplitude waves of infinitesimal steepness. The resulting solution to the wave equation is a single harmonic function. Invoking the superposition principle, the instantaneous sea surface elevation can be represented as an infinite sum of sinusoids as expressed by

$$\eta(t) = \sum_{n=1}^{\infty} \eta_n = \sum_{n=1}^{\infty} a_n \cos(\vec{K}_n \cdot \vec{x} - \omega_n t + \epsilon_n) \quad (5)$$

where \vec{K}_n is the horizontal vector wavenumber, $\vec{x} = (x, y)$ is the position vector, ω_n is the circular frequency and ϵ_n is the initial phase angle. The dispersion relationship is obtained from the solution of the wave equation in applying the surface boundary conditions

$$\omega^2 = gk \tanh(kh) \quad (6)$$

The spectral component index n is now dropped for convenience.

Two limiting regions can be considered, deep and shallow water wave approximations. These simplified solutions correspond to the consideration of asymptotic forms for the hyperbolic functions entering the basic solution definitions. These extreme cases are generally identified by the ratio $\frac{h}{L}$, where h is the local water depth and L is the wavelength as computed by the expressions corresponding to each one of the cases. For $h/L > 1/2$ the solution is considered as belonging to the deep water limit and for $h/L < 1/20$ the solution corresponds to the shallow water case. In between the full solution must be considered and the solution is known as the intermediate water wave solution.

The solution of the linear wave equation can be used to describe the wave induced motions. In particular, the relation between wave elevation η and subsurface pressure head p is described by

$$\eta(t) = \left[\frac{\cosh kh}{\cosh k(h+z)} \right] [p(t) + z] \quad (7)$$

Open ocean data are invariably collected in the form of time series of processes that are inherently random. Spectral analysis techniques are a natural first choice to study these data. The previously presented solution to the Laplace's equation gives rise to simple spectral relationships between the sea surface elevation spectrum and pressure spectra when considering the water column as a constant parameter linear system. Un-

der such a system, any two quantities are connected in the spectral space via a transfer function as

$$S_y(\omega) = |H(\omega)|^2 S_x(\omega) \quad (8)$$

where $S_y(\omega)$ and $S_x(\omega)$ are respectively the output and input energy-density spectra and $H(\omega)$ is the transfer function. The constant parameter linear system preserves the input frequency at the output and modifies the amplitude and phase of each component of the input independently. Similar types of relations can be deduced for the cross-spectral quantities. For the case of the open ocean wave field and considering the pressure head as input and sea surface elevation spectra as output, the applicable transfer function for the pressure is

$$H_p(\omega) = \frac{\cosh kz}{\cosh k(h+z)} \quad (9)$$

which is the same term as in the brackets of Eq.(7).

It was noted in the formulation of the linear wave theory that specific phase relations exist between the sea surface elevation and pressure. The relative phase between two quantities in spectral terms is defined as

$$\Phi_{xy}(\omega) = \arctan \frac{Q_{xy}(\omega)}{C_{xy}(\omega)} \quad (10)$$

where $Q_{xy}(\omega)$ is the quadrature spectrum and $C_{xy}(\omega)$ is the co-spectrum of the two quantities.

The spectral transfer function relating pressure head to surface elevation as a function of frequency and depth, Eq.(9), can be modified to include differential distance and elevation between two sensors of an array to compute energy and cross - spectra of surface slope in the x - direction as

$$S_{\frac{d\eta}{dx}}(f) = \frac{1}{\Delta x^2} \left[\frac{\cosh kh}{\cosh k(h+z)} \right]^2 S_{\Delta p_x}(f) \quad (11)$$

$$S_{\eta, \frac{d\eta}{dx}}(f) = \frac{1}{\Delta x} \left[\frac{\cosh kh}{\cosh k(h+z)} \right]^2 S_{p, \Delta p_x}(f) \quad (12)$$

where ΔP_x is subsurface pressure difference between two sensors on the x-axis and Δx is differential distance along the same axis. Similarly, pressure power spectra and cross - spectra can be computed along y-axis.

B. THE SPECIFICATION OF A WAVE FIELD

The complete description of the wave field requires knowledge of frequency and directional wave spectra. Directional spectra are commonly measured by pitch and roll buoy and multi-element arrays, which represent spectra measured at a point. The methods for computation of the directional wave spectrum are generally classified as

- Model fitting methods - based on the parametric representation of the spectrum as the classical Longuet-Higgins et al (1963) method.
- Model independent methods (Davis and Regier, 1977), that can be divided into a priori and data adaptative methods.

A priori methods require in advance a definition of criteria to be verified without reference to the data in use. The data adaptative methods are based in a posteriori assumptions about the spectrum, which depart from characteristics of the input data. Any of these processes of estimation are conditioned by the traditional constraints inherent in time series analysis of statistical reliability and resolution.

1. Directional Spectrum

The wavenumber-frequency characteristic of sea waves is contained in the wave spectrum as given by the Fourier transform of the correlation function $R(\vec{r}, \tau)$

$$S(\vec{K}, \omega) = \frac{1}{(2\pi)^3} \iint R(\vec{r}, \tau) e^{-i(\vec{K} \cdot \vec{r} - \omega\tau)} d\vec{r} d\tau \quad (13)$$

This quantity is simply the three dimensional distribution of variance generally known as the power spectrum. The knowledge of the wave field at fixed positions (Munk et al., 1963), permits the computation of the correlation function. The definition of the power spectrum as given by Eq.(13) leads by inverse transforming to the correlation function, that is

$$R(\vec{r}, \tau) = \iint S(\vec{K}, \omega) e^{i(\vec{K} \cdot \vec{r} - \omega\tau)} d\vec{K} d\omega \quad (14)$$

which for the assumed stationary wave field is an even function. Consequently, the power spectrum is real and symmetric about zero frequency. The correlation function can then be rewritten as a cosine transform of the power spectrum

$$R(\vec{r}, \tau) = \int \int S(\vec{K}, \omega) \cos(\vec{K} \cdot \vec{r}) \cos(\omega \tau) d\vec{K} d\omega \quad (15)$$

The correlation function can now be redefined as

$$R(\vec{r}, \tau) = \int \int S(\vec{K}, \omega) (\cos(\omega \tau) \cos(\vec{K} \cdot \vec{r}) + \sin(\omega \tau) \sin(\vec{K} \cdot \vec{r})) d\vec{K} d\omega \quad (16)$$

The power spectrum can then be calculated in terms of cosine and sine transforms of the correlation

$$S(\vec{K}, \omega) = \int [C(\vec{r}, \omega) + iQ(\vec{r}, \omega)] e^{-i\vec{K} \cdot \vec{r}} d\vec{r} \quad (17)$$

where $C(\vec{r}, \omega)$ and $Q(\vec{r}, \omega)$ are respectively the co- and quadrature spectra of the correlation. Such functions could be calculated if the correlation is known as continuous function of the spatial coordinate, although real world observations lead to the collection of data in a small number of positions. Approximate methods of computing directional spectrum from observations of the wave field at discrete positions must then be considered.

2. Classical Approach

Lonquet-Higgins, Cartwright and Smith (1963) following the suggestions of Barber (1946), developed a method of computing the directional spectrum from the motions of a floating buoy. The method is based on relationships between the cross spectral quantities of the heave, pitch, and roll of the buoy and the Fourier coefficients of the directional spectrum. The directional spectrum can be represented as a Fourier series

$$S(f, \theta) = \frac{a_0}{2} + \sum_{n=1}^{\infty} a_n \cos n\theta + b_n \sin n\theta \quad (18)$$

where θ is the wave direction and the coefficients a_n and b_n are only frequency dependent and represent the frequency distribution of energy. Separating the frequency and directional contributions, as it is usually done, the directional spectrum can be rewritten as

$$S(f, \theta) = S(f)D(f, \theta) \quad (19)$$

where $D(f, \theta)$ is the spreading function. $D(f, \theta)$ corresponds to a unity area weighting function that redistributes the energy contained in the power spectrum over direction, ideally reproducing real world conditions. The three measured quantities obtained with a buoy can be directly related with the harmonic representation of the sea surface. The heave corresponds to the instantaneous sea surface elevation and the pitch and roll are associated with the spatial partial derivatives of the surface elevation. Considering a single harmonic of the sea surface representation

$$\eta(t) = a \cos(\vec{K} \cdot \vec{x} - \omega t) \quad (20)$$

the two horizontal cartesian components of the sea slope can be written as

$$\eta_x(t) = \frac{\partial \eta(t)}{\partial x} = \{-iK \cos \theta\} \eta(t) \quad (21)$$

$$\eta_y(t) = \frac{\partial \eta(t)}{\partial y} = \{-iK \sin \theta\} \eta(t) \quad (23)$$

Cross spectral quantities can be computed for the instantaneous surface elevation and surface slope, and related with the Fourier coefficients of the directional spectrum. These cross spectral quantities can be represented as

$$C_{\eta\eta}(f) = S(f) \int_0^{2\pi} D(f, \theta) d\theta \quad (23)$$

$$Q_{\eta\eta_x}(f) = KS(f) \int_0^{2\pi} D(f, \theta) \cos \theta d\theta \quad (24)$$

$$Q_{\eta\eta_y}(f) = KS(f) \int_0^{2\pi} D(f, \theta) \sin \theta d\theta \quad (25)$$

$$C_{\eta_x \eta_x}(f) = K^2 S(f) \int_0^{2\pi} D(f, \theta) \cos^2 \theta d\theta \quad (26)$$

$$C_{\eta_y \eta_y}(f) = K^2 S(f) \int_0^{2\pi} D(f, \theta) \sin^2 \theta d\theta \quad (27)$$

$$C_{\eta_x \eta_y}(f) = K^2 S(f) \int_0^{2\pi} D(f, \theta) \cos \theta \sin \theta d\theta \quad (28)$$

Considering the directional spectrum in terms of its first five Fourier coefficients, that is

$$S(f, \theta) = \frac{a_0}{2} + a_1 \cos \theta - b_1 \sin \theta + a_2 \cos 2\theta + b_2 \sin 2\theta \quad (29)$$

, it can be shown that these coefficients are given in terms of the cross spectral quantities, Eqs.(23-28), by

$$a_0 = \frac{1}{\pi} C_{\eta\eta} \quad (30)$$

$$a_1 = \frac{1}{\pi K} Q_{\eta\eta_x} \quad (31)$$

$$b_1 = \frac{1}{\pi K} Q_{\eta\eta_y} \quad (32)$$

$$a_2 = \frac{1}{\pi K^2} (C_{\eta_x \eta_x} - C_{\eta_y \eta_y}) \quad (33)$$

$$b_2 = \frac{2}{\pi K^2} C_{\eta_x \eta_y} \quad (34)$$

and equivalently, if a normalization by auto-spectrum is done, the Fourier coefficients of the unit area spreading function are determined. This approach constitutes the classical LCS method. The approximate representation of the directional spectrum in terms of its Fourier series truncated to its first five coefficients leads to a directional distribution of energy as given by a cosine-bell function. Such a representation is of limited resolution, and typically has large negative side lobes (Figure 2).

To solve the problem of the unrealistic negative side lobes, LCS imposed a constraint of positivity on the directional spreading function which resulted in a smoothing effect. However this approach has the consequence that the resolution of a distribution narrower than $\cos^4(\frac{\theta}{2})$ is not possible. It must be noted that this artifice does not solve the real problem that is related to unresolved harmonics of the severely truncated Fourier series representation. Also, the LCS approach is not capable of representing multi-modal distributions of energy that are frequently observed in the real ocean, as can be concluded from the truncated Fourier series given by Eq.(29) and shown in (Figure 2).

The method just described can also be applied to measurements using slope arrays, which consist of multi-point arrangements of pressure transducers. Typically the sensors in the slope arrays are arranged in a square. The real slope is approximated by dividing the differential pressure of a pair of sensors by their separation while assuming the sea surface slope as constant between each pair of sensors. The method of computing the directional distribution of energy then proceeds as before for the case of measurements with a floating buoy. The sea surface elevation is obtained from the time series of pressure by applying the appropriate transfer function. The approximation of the surface slope introduces errors in the computation given by (Seymour and Higgins, 1977)

$$\delta_i = \frac{\partial \eta}{\partial x_i} - \frac{\sin(\vec{K}b\alpha_i)}{\frac{\vec{K}b\alpha_i}{2}} \frac{\partial \eta}{\partial x_i} \quad (35)$$

where $\alpha_i = (\cos \theta, \sin \theta)$ for $i=1,2$ and b is the horizontal sensor separation. It can be seen that the error of such an approximation is a function of the wavenumber vector and the size of the array, decreasing in magnitude as these quantities are reduced. It is then natural to employ arrays as small as possible, limited by the resolution and accuracy of the pressure sensors.

3. Exact Fourier Coefficient Representation Method

The LCS approach provides a way of computing the first five Fourier coefficients of the series expansion of the directional spreading function. These coefficients are obtained via cross-spectral analysis of triorthogonal components of the wave field measurements. The number of Fourier coefficients are limited because of the measurement technique normally used, floating buoy or slope array of four sensors in a square.

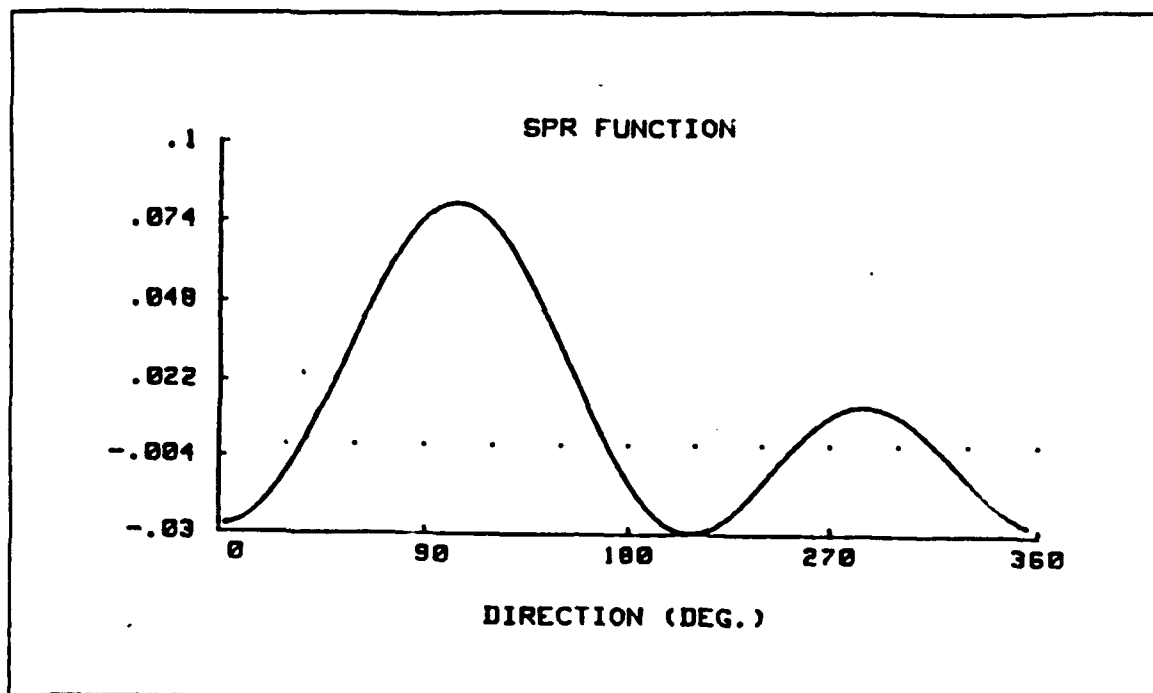


Figure 2. Typical spreading function of the LCS method: Small directional resolution and unrealistic negative side lobes.

Such a system can only give information of the wave field through second order terms. The coefficients determined can be represented by an infinite number of different distributions whose Fourier expansion is common. Examples of distributions having the same Fourier coefficients can be seen in Figure 3. It is then natural to choose a physically realisable distribution, which matches the coefficients determined by observation and more exactly simulates the true directional distribution.

Grauzinis(1989) exploits the matching of a set of Fourier coefficients by different distributions to develop a new method of computing directional spectra. The previously defined directional spreading function $D(\theta)$ can be represented as

$$D(\theta) = \{1 + 2 \sum_k [a_k \cos(k\theta_k) + b_k \sin(k\theta_k)]\} \frac{1}{2\pi} \quad (37)$$

where a_k and b_k are the unitary Fourier coefficients. Such coefficients enter the definition of the polar coefficients c_k and θ_k as given by

$$C_k = a_k + ib_k = c_k e^{ik\theta_k} \quad (37)$$

Any symmetric unity area function can be determined solely by its canonical coefficients defined as

$$m_k = \int_{-\pi}^{\pi} X(\theta) \cos k\theta d\theta \quad (38)$$

where $X(\theta)$ is any arbitray unit area function symmetric around $\theta = 0$. This representation is simply the cosine transform of an even function. It is seen that a relation can be established between the canonical coefficients and the Fourier coefficients.

$$a_k + ib_k = c_k e^{ik\theta_k} = m_k e^{ik\beta_k} \quad (39)$$

where the polar form is now used for the Fourier coefficients of the spreading function. Using linear superposition, any unit area function can be reproduced by a weighted sum of symmetric unit area density functions oriented at different directions as given by

$$c_k e^{ik\theta_k} = \sum_j w_j m_k(j) e^{ik\beta_j} \quad (40)$$

where w_j is the weighting factor and β_j is the orientation of each of the components considered in the series. Eq.(40) constitutes the generating equation for the polar coefficients where on the right hand side w_j , $m_k(j)$ and β_j are unknowns. The left hand side of Eq.(40) is determined from the cross spectral quantities of the wave field typically known through second order. A system of equations can be established as

$$m_1 [w_1 e^{i\beta_1} + w_2 e^{i\beta_2}] = c_1 e^{i\theta_1} \quad (41)$$

$$m_2 [w_1 e^{i2\beta_1} + w_2 e^{i2\beta_2}] = c_2 e^{i2\theta_2} \quad (42)$$

which can be seen to be underdetermined. It must be noted that in the system Eq.(41-42) it is assumed that the canonical coefficients are common to both of the distributions of energy considered. This was the approach followed by Grauzinis (1989) to obtain analytic solutions for the system of generation equations. By the condition of orthogonality of the exponentials of different order and the side condition that the sum of the weights must be equal to unity, analytic solutions are formed. The analytic

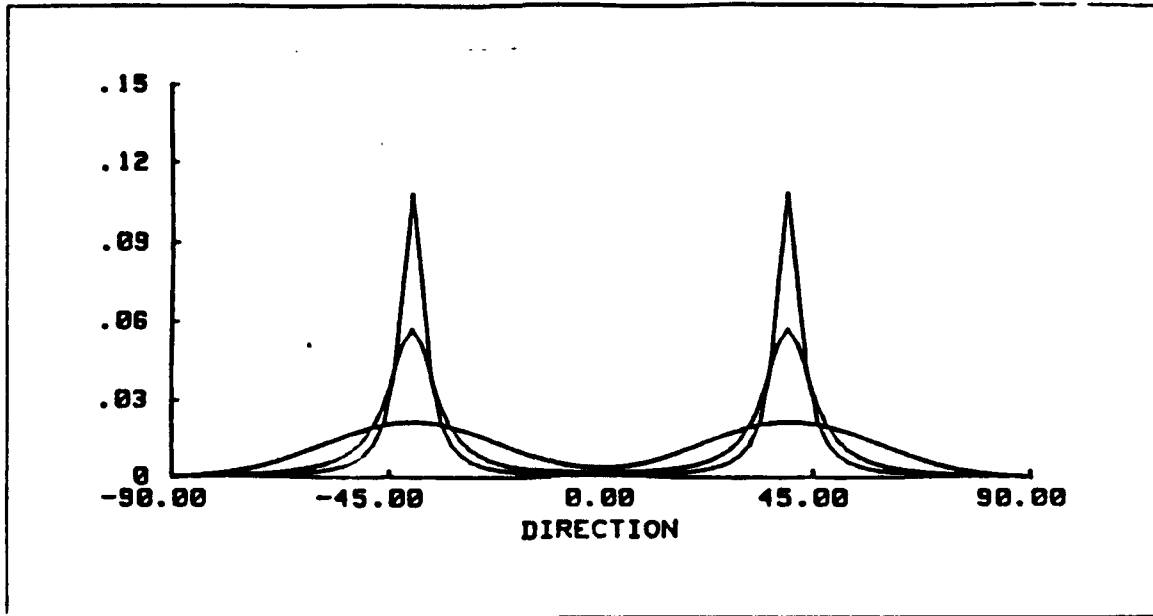


Figure 3. Distribution of energy: The three distribution have a common Fourier expansion.

solutions constitute an implicit underdetermined system of four equations. The unknowns of this system are the two canonical coefficients, the orientation of the two unit area density functions and one of the weighting functions. To solve this system, further constraints are needed. Assuming a functional relationship between the canonical coefficients m_1 and m_2 particular solutions are obtained. The original relationship adopted was a power law between the two canonical coefficients

$$m_2 = m_1^r \quad (43)$$

that for different values of r originated different distributions of energy as analytic solutions. Such distributions are of decreasing sharpness as the magnitude of the exponent increases. For the values of the exponent 2, 3 and 4, the resulting distributions in its unimodal form are represented in Figure 4 using two different orientations and weights also allows this method to represent bimodal distributions of energy. The variable sharpness of the model distributions considered will permit the matching of observed distributions of considerably more peakedness than the classical LCS method. For a canonical coefficient of .9, the half-power width of the distribution D4 is 12 degrees, that is about one-third of the typical resolution of the cosine-bell distribution.

Knowledge of Fourier coefficients of order higher than the second introduces considerable advantage to this method. Some of the constraints can be dropped, such as the functional relationship of the canonical coefficients. Moreover, the matching of coefficients of higher order increases the resolution of the method.

The exact matching of the Fourier coefficients through second order of any spreading function can be obtained by the method just described. The problem of what criteria to use for the selection of the distribution that best matches the real data must also be considered. It should be emphasized that there exist an infinity of distributions that can be considered to match the same set of Fourier coefficients. The problem of selecting the best fitting distribution partly amounts to the matching of the ocean peakedness. Cartwright (1963) considered this problem when computing directional wave spectra by the LCS method. He concluded that information could be obtained from the ratio of the magnitude of the coefficients C_k , Eq.(37). The magnitude of such coefficient is given by

$$|C_k| = \sqrt{a_k^2 + b_k^2} \quad (44)$$

Recalling the functional relationship of the canonical coefficients introduced to allow for the solution of the generating system, Eq.(43), it is concluded that in the Grauzinis method it is more natural to consider the ratio of the natural logarithms of the C_k coefficients, that is

$$LogRatio = \frac{\ln(C_2)}{\ln(C_1)} \quad (45)$$

which represents the greatest power-law of the canonical coefficients that can match the input Fourier coefficients. Cartwright (1963) verified that the ratios obtained from the observed data were consistently greater than the values corresponding to the cosine-bell function of the LCS method. It was hypothesized that such difference could be due to the multimodality of the wind-wave spectrum. Recalling that the ratio of the coefficients C_k as an indicator was deduced from uni-modal considerations; it does not seem correct to make use of it to infer of the adequacy of multi-modal distributions. Grauzinis (1989) points out that the natural logarithmic ratio will exceed the power law of canonical coefficients increasingly as the beam separation gets larger. Moreover, noise affects the coefficients C_2 and C_1 differently. Eqs.(23-28) show that the effects of noise are cancelled for the coefficient a_2 , and consequently the LogRatio will be decreased.

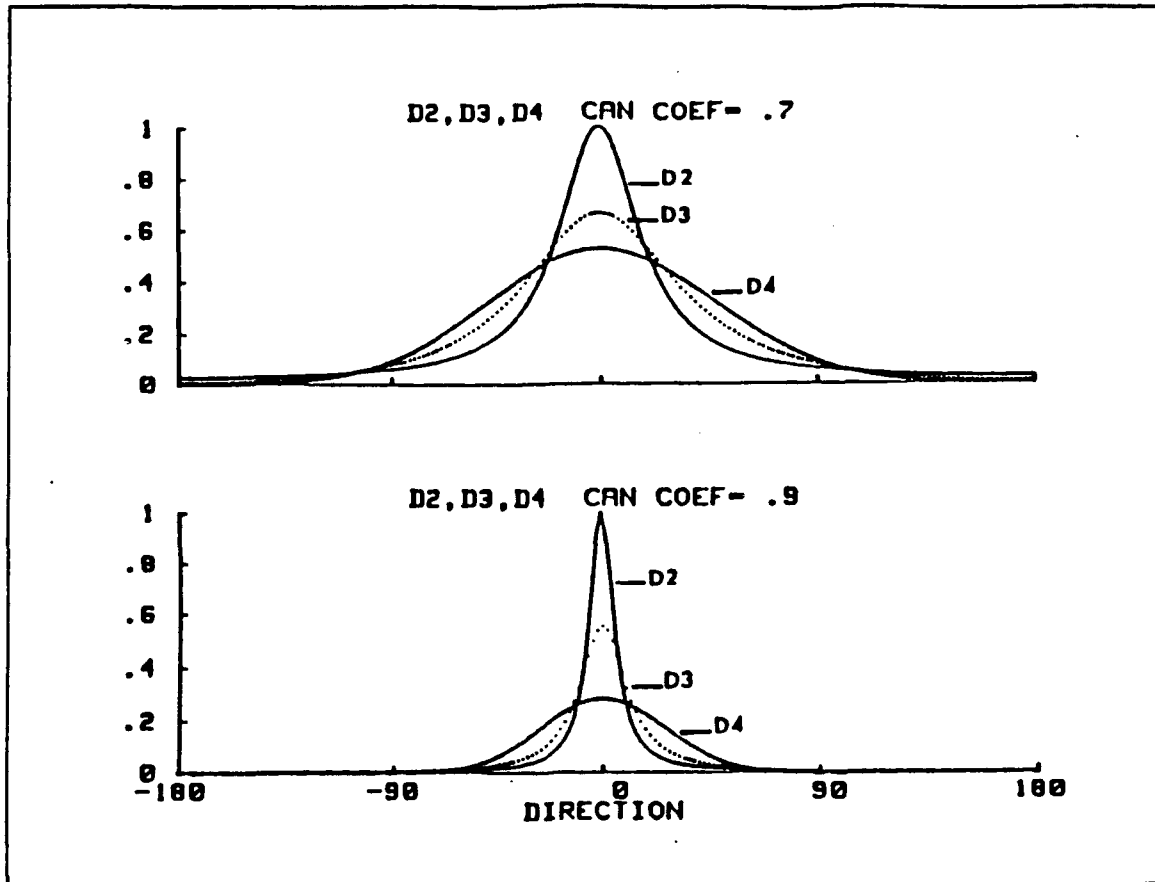


Figure 4. Three model distribution: Uni-modal representation of three different model distributions for two values of the canonical coefficient. D2, D3 and D4 correspond respectively to the exponent 2, 3 and 4 for the functional relationship of the canonical coefficients Eq.(43). The sharpness of the distribution decreases with the magnitude of exponent. For a value of the canonical coefficient equal to .9 the half power width of D4 is 12 degrees.

C. WAVE SPECTRUM TRANSFORMATION

According to M  haut   and Wang (1982), all the formulations of wave spectrum transformation over a shoaling bottom are based on the premise that the wave energy associated with a narrow frequency band stays within that band during the transformation and that it obeys linear superposition. (The shift of energy from frequency to frequency is considered to be the results of nonlinearity.) For each frequency, the energy level, which is characterized by the square of a free surface elevation, $\eta^2(f)$, is treated as

an invariant during the transformation. Therefore, the law of transformation which has been established for monochromatic waves is applied as if each value, $\eta(f)$, were identical to a periodic wave of the same amplitude and frequency, and that the energy contained in each band and direction travels along its corresponding wave ray at group velocity.

The first rigorous theoretical approach to the evolution of the wave spectrum is due to Longuet-Higgins (1957), who demonstrated that the energy spectral density in the wave number space remains constant as one follows any wave group along a wave ray (Phillips 1966). The demonstration is based on the conservation of energy and the law of wave refraction. It is shown that $S(k_1, k_2) = \text{constant}$ along a wave orthogonal, or $\frac{d}{dt} S(k_1, k_2) = 0$. Other demonstrations have also been presented by Karlsson (1969), Collins (1972), and Krasitskiy (1974) in analogy with geometrical optics and the ray particle analogy.

Following their approach, let us consider a wave spectrum defined in terms of space (x, y) , time (t) , and wave number (k_1, k_2) as $S(k_1, k_2, x, y, t)$. By virtue of the aforementioned principle ($\frac{dS}{dt} = 0$), then

$$\frac{\partial S}{\partial t} + \frac{\partial S}{\partial x} \frac{dx}{dt} + \frac{\partial S}{\partial y} \frac{dy}{dt} + \frac{\partial S}{\partial k_1} \frac{dk_1}{dt} + \frac{\partial S}{\partial k_2} \frac{dk_2}{dt} = 0 \quad (46)$$

The first term is generally taken equal to zero under steady-state condition. The second and third terms are the convective terms and are due to the variation of energy level as a result of the spatial variation. The two last terms are due to shoaling and refraction. $\frac{dx}{dt}$ is the velocity of energy propagation in the x direction and

$$\frac{dx}{dt} = \frac{\partial \omega}{\partial k_1} = V \cos \theta = V_x \quad (47)$$

Similarly:

$$\frac{dy}{dt} = \frac{\partial \omega}{\partial k_2} = V \sin \theta = V_y \quad (48)$$

where V : group velocity, k : wave number. Since $\omega^2 = gk \tanh kh$, ω is a function of k and h . The depth, h , depends exclusively on (x, y) , thus we can write $\omega = \omega[k, h(x, y)] = \omega(k, x, y)$. Then

$$\frac{d\omega}{dt} = \frac{\partial \omega}{\partial k_1} \frac{dk_1}{dt} + \frac{\partial \omega}{\partial x} \frac{dx}{dt} + \frac{\partial \omega}{\partial k_2} \frac{dk_2}{dt} + \frac{\partial \omega}{\partial y} \frac{dy}{dt} \quad (49)$$

For periodic waves, a phase function, α , can be defined such that $\frac{\partial \alpha}{\partial x_i} = -k_i$ and $\frac{\partial \alpha}{\partial t} = \omega$. Then differentiability of α requires:

$$-\frac{\partial k_i}{\partial t} = \frac{\partial \omega}{\partial k_j} \frac{\partial k_i}{\partial x_j} + \frac{\partial \omega}{\partial x_i} = V_j \frac{\partial k_i}{\partial x_j} + \frac{\partial \omega}{\partial x_i} \quad (50)$$

At a position moving with group velocity, i.e., along a wave ray given by

$$\frac{dx_i}{dt} = V_i = \frac{\partial \omega}{\partial k_i} \quad (51)$$

we obtain from Eq.(50):

$$\frac{dk_i}{dt} = -\frac{\partial \omega}{\partial x_i} \quad (52)$$

It is easily verified by inserting Eqs.(51-52) into Eq.(49) that ω , in fact, remains constant along a wave ray. Inserting these relationships into Eq.(46) and introducing the spectrum in terms of frequency and direction

$$S(k_1, k_2) = \frac{1}{k} S(k, \theta) = \frac{V}{k} S(\omega, \theta) = \frac{V}{2\pi k} S(f, \theta) \quad (53)$$

or

$$S(f, \theta, x, y) = \frac{2\pi k}{V} S(k_1, k_2, x, y) \quad (54)$$

finally yields, after some algebraic operation:

$$dt = \frac{V}{2\pi\omega} \left\{ \cos \theta \frac{\partial [CVS(f, \theta)]}{\partial x} + \sin \theta \frac{\partial [CVS(f, \theta)]}{\partial y} + \frac{1}{C} \left(\sin \theta \frac{\partial C}{\partial x} - \cos \theta \frac{\partial C}{\partial y} \right) \frac{\partial [CVS(f, \theta)]}{\partial \theta} \right\} \quad (55)$$

in which $C =$ the phase velocity, $C = \frac{\omega}{k}$. It is recalled that the ray equations are (Munk and Arthur 1951)

$$\begin{aligned} \frac{dx}{ds} &= \cos \theta; \frac{dy}{ds} = \sin \theta \\ \frac{d\theta}{ds} &= \frac{1}{C} \left(\sin \theta \frac{\partial C}{\partial x} - \cos \theta \frac{\partial C}{\partial y} \right) \end{aligned} \quad (56)$$

in which s = the distance along a ray. Inserting these into Eq.(55) yields simply:

$$\frac{V}{2\pi\omega} \frac{d}{ds} [CVS(f, \theta)] = 0 \quad (57)$$

i.e.:

$$CVS(f, \theta) = \text{constant} \quad (58)$$

along a wave ray. Note:

$$\frac{dS(k_1, k_2)}{dt} = \frac{V}{2\pi\omega} \frac{d}{ds} [CVS(f, \theta)] = 0 \quad (59)$$

The result obtained in Eq.(59) is the same as Longuet-Higgins. Eq.(58) can be written further as

$$\frac{V}{k} S(f, \theta, x, y) = \text{constant}$$

or

$$S(\omega, \theta) = \frac{k}{k_0} \frac{V_0}{V} S_0(\omega, \theta_0) \quad (61)$$

where the subscript refers to deep water quantities. In other words, the ratio between shallow water DSD and deep water DSD is a universal function of depth and wavenumber where

$$\frac{k}{k_0} \frac{V_0}{V} = \left[\tanh kh \left(1 + \frac{2kh}{\sinh 2kh} \right)^{\frac{1}{2}} \right]^{-2} \quad (62)$$

Figure 5 shows the plots and numerical values of the ratio between deep and shallow DSD Eq.(62) at Marina and Santa Cruz versus different frequencies.

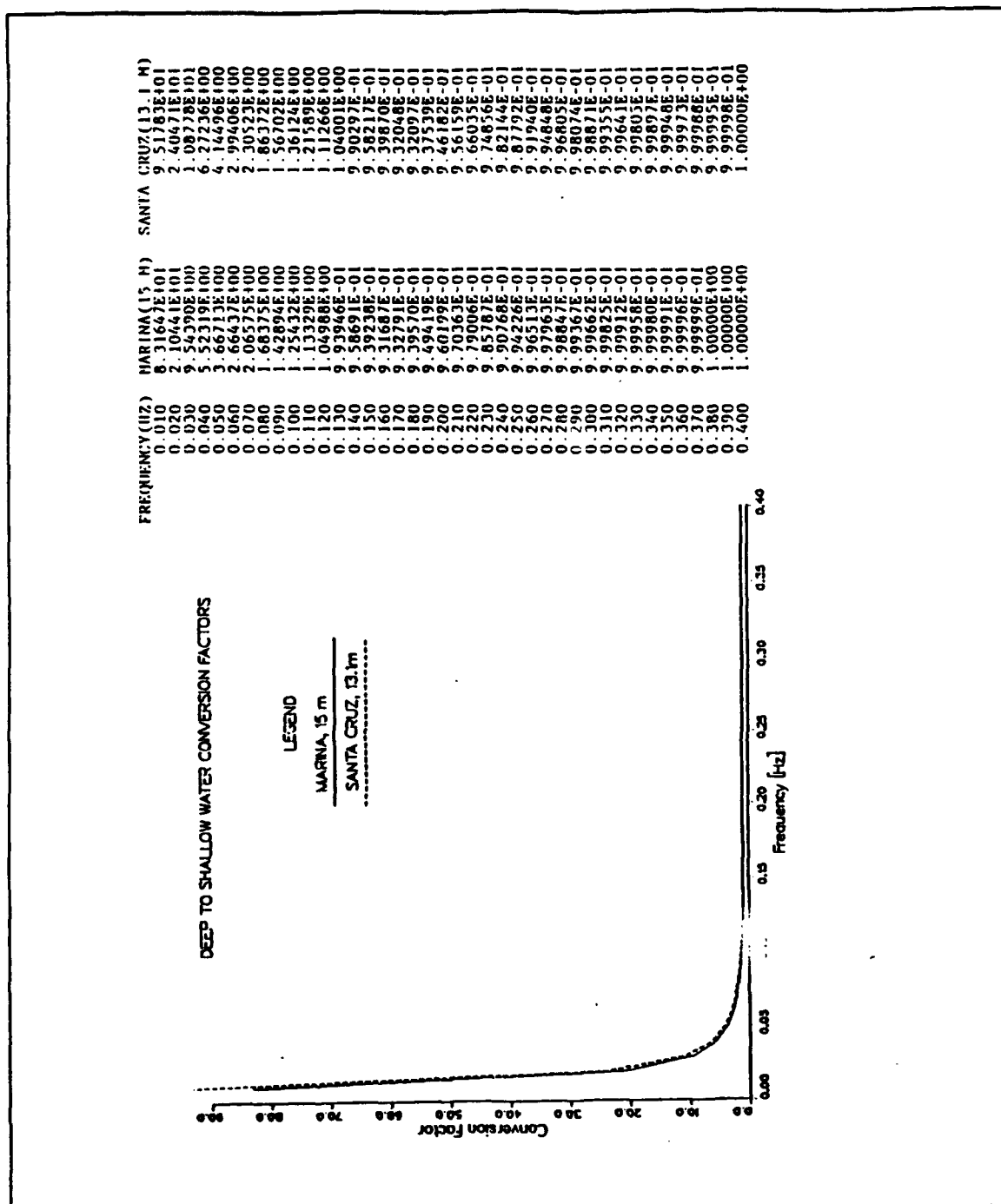


Figure 5. Transformation constant along a ray path

III. DATA ACQUISITION AND SENSORS

A. LOCATION

Monterey Bay was selected as the study area, which poses complex problems due to the highly irregular bathymetry of the Monterey submarine canyon. A deepwater wave buoy and two shallow water slope arrays were utilized for wave data acquisition. The locations of sensors are listed in Table 1, see Figure 1 for bathymetry and location.

Table 1. LOCATIONS OF SENSORS

No.	Type of Sensor	Location	Depth (M)
1.	NDBC roll/pitch wave buoy	36°48.0'N, 122°23.0'59.0"W	2003
2.	Array of pressure gauges (4) Marina	36°42.0'N, 121°48.9'W	15.0
3.	Array of pressure gauges (4) Santa Cruz	36°57.0'N, 122°0.2'W	13.1

In comparing coincident data sets, on the average, a time lag of one hour was assumed for the waves to travel from the deep water buoy to the shallow water array sites.

B. DEEP WATER WAVE DATA

Deep water wave data of the pitch/roll buoy were obtained from the NDBC (National Data Buoy Center). The NDBC 3-meter buoy measures heave, pitch, and roll movements with respect to a 3-axes magnetometer. The magnetometer axes are aligned with fore and after (bow positive), athwartship (starboard positive) and vertical (positive upward) axes of a buoy, see Figure 6.

The analog sensor measures vertical acceleration and displacement, hull pitch and roll. The magnetometer bow and starboard output, together with vertical displacement, pitch and roll output from analog sensors are sent to the Directional Wave Data Analyzer (DWDA) after voltage amplification and filtering.

The hull azimuth angle is calculated from bow and starboard magnetic components with necessary corrections made for pitch, roll, and hull magnetic fields. The magnetic azimuth is converted into true azimuth using the magnetic variation for the site. The true azimuth is then used to calculate East-West and North-South components of hull

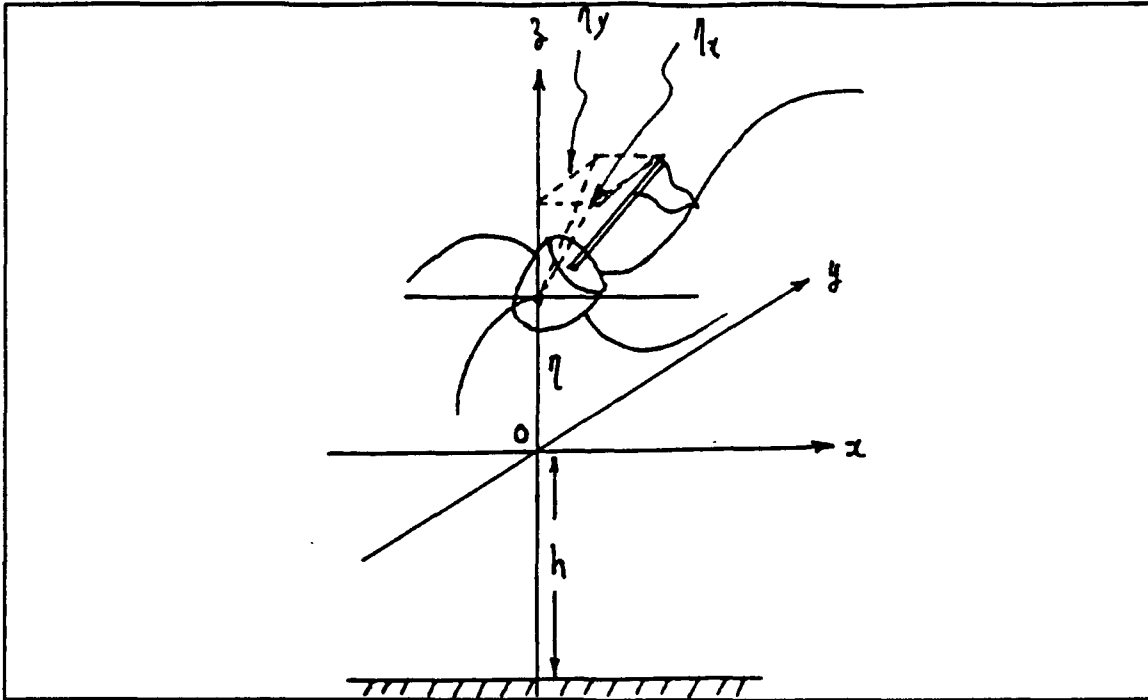


Figure 6. Floating Buoy

slope. One hertz time record of hull displacement and slope are stored in DWDA for spectral analysis and transmission to shore station through GOES (Steele et al., 1985).

Data provided on magnetic tape included environmental parameters, wave spectra, directional wave parameters, and co and quad-spectra. Directional wave parameter data were utilized to determine directional wave spectrum.

C. SHALLOW WATER WAVE DATA

The calibrated data for the pressure gauge arrays were obtained from the Scripps Institute of Oceanography. Array consists of four pressure gauges located in a six-meter square area which measures pressure head in centimeters of water, See Figure 7. Each sensor is located about 50 to 100 cm above the bottom. Pressure power spectrum is calculated which in turn is transformed into surface elevation η and surface slopes η_x and η_y spectra by applying linear wave theory transfer function as described in Chapter II.

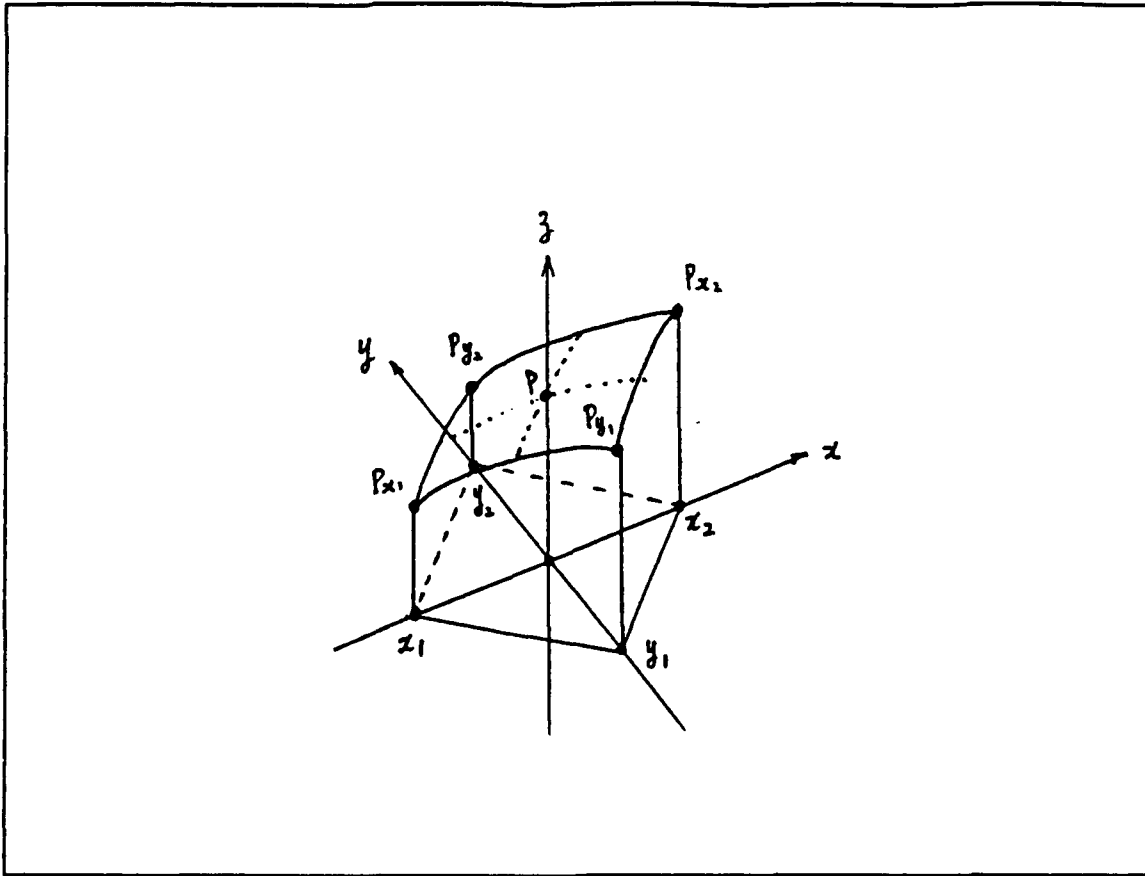


Figure 7. Slope Pressure Array

For the computation of the cross-spectra, the following values were utilized:

- sampling interval = $\Delta t = 2$ sec
- total data points = 2048
- data points for one sample = 64
- nyquist frequency = 0.25 Hz
- frequency bandwidth = $\Delta f = 0.0078125$ Hz

The spectra were cut at a frequency of 0.2 Hz in the higher frequency range due to overestimation by the transfer function. The wave-period for high quality estimate is approximately 5-20 seconds.

D WAVE DATA SELECTION

Selected wave cases from January 1988 were used in the analysis. During the winter season, weather conditions were generally favorable for creating higher energy waves. The selected days are 3 January 0800 PST, 18 January at 0200 PST and 29 January at 2100 PST. These periods provide two cases of narrow band energy spectra at different frequencies and directions and a third case of a major storm event. The California coast was hit by an unusually severe storm during 16-18 January 1988 which resulted in high waves, strong winds, and sea level well in excess of predicted values (Cayan, et al., 1988). Widespread damage occurred along the southern California coast. This storm developed about 300 NM west of San Francisco on 16 January 1988 traveled south-east at about 33 knots. The storm center passed off Monterey Bay on the morning of 17 January 1988 continuing on its SE track and making landfall at Avila Beach in Central California. The energy spectra for these cases are depicted in Figure 8, 9, and 10 comparing the deep water buoy and shallow water pressure gauge measurements at Marina and Santa Cruz. Deep water wave characteristics of selected cases are given in Table 2.

Table 2. DEEP WATER WAVE CHARACTERISTICS OF SELECTED CASES

Characteristics	3 Jan 88	18 Jan 88	29 Jan 88
$H_{sig.}$	1.87 m	5.12 m	2.65 m
$Freq_{peak}$	0.13 Hz	0.07 Hz	0.09 Hz
$Freq_{mean}$	0.18 Hz	0.10 Hz	0.12 Hz
$Direction_{mean}$	280°	300°	275°

Reviewing Table 2 and other published data, deep water waves generally travel eastward during the month of January with slight variability of about 20° on either side of true East. This direction is dominant in the energetic middle frequency range of 0.08 to 0.13 Hz. At other frequencies, the direction tends to be variable.

The significant wave heights, calculated as $H_s = 4\sqrt{\sigma^2}$, where σ^2 is variance calculated as the area under the energy density spectra, are given in Table 3.

E. TRANSFORMATION OF DEEP WAVE SPECTRUM

The directional spectrum density at wavenumber space is constant along ray path. Transforming from wavenumber space to frequency and direction space, the shallow water DSD is related to the deep water DSD by a universal function of depth, h , and wavenumber, k , or frequency, f , Eq.(62), however, the relationships between the shallow

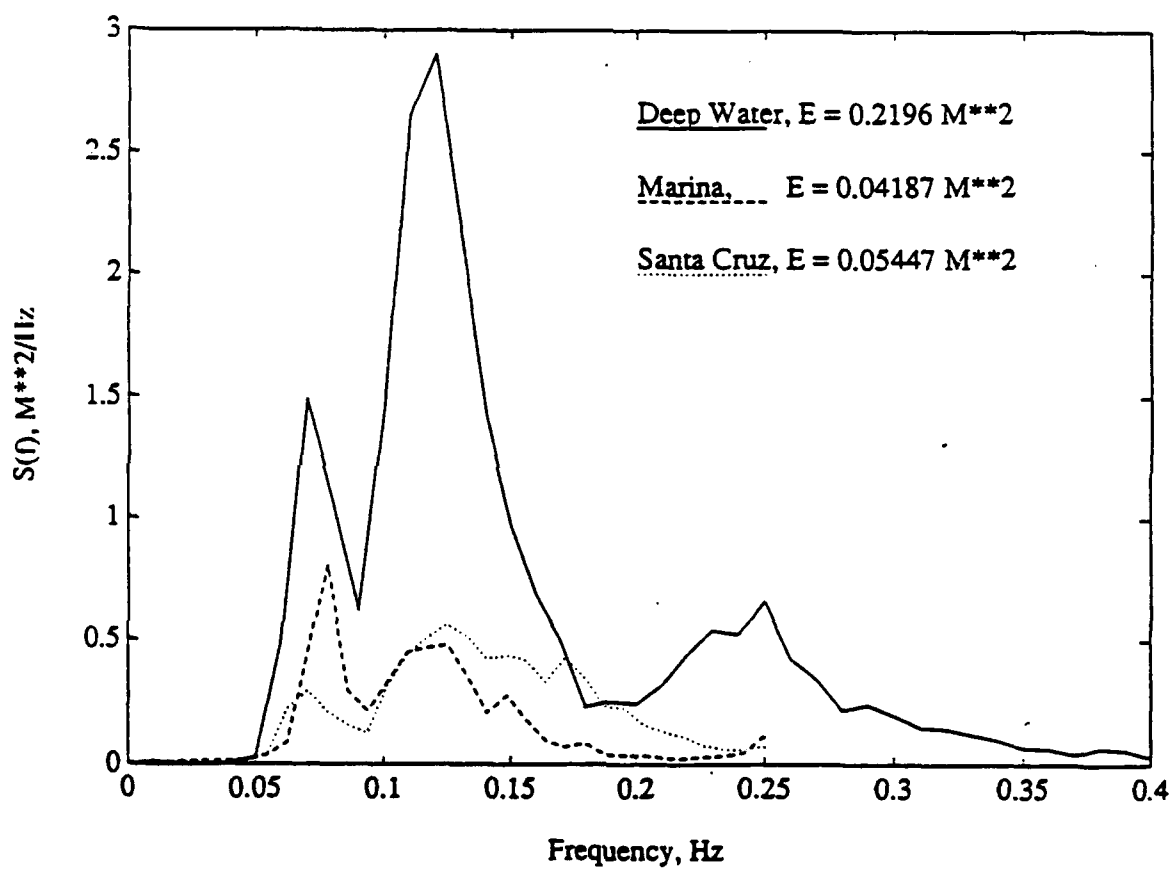


Figure 8. Measured spectral densities on 3 January 1988, 0800 PST

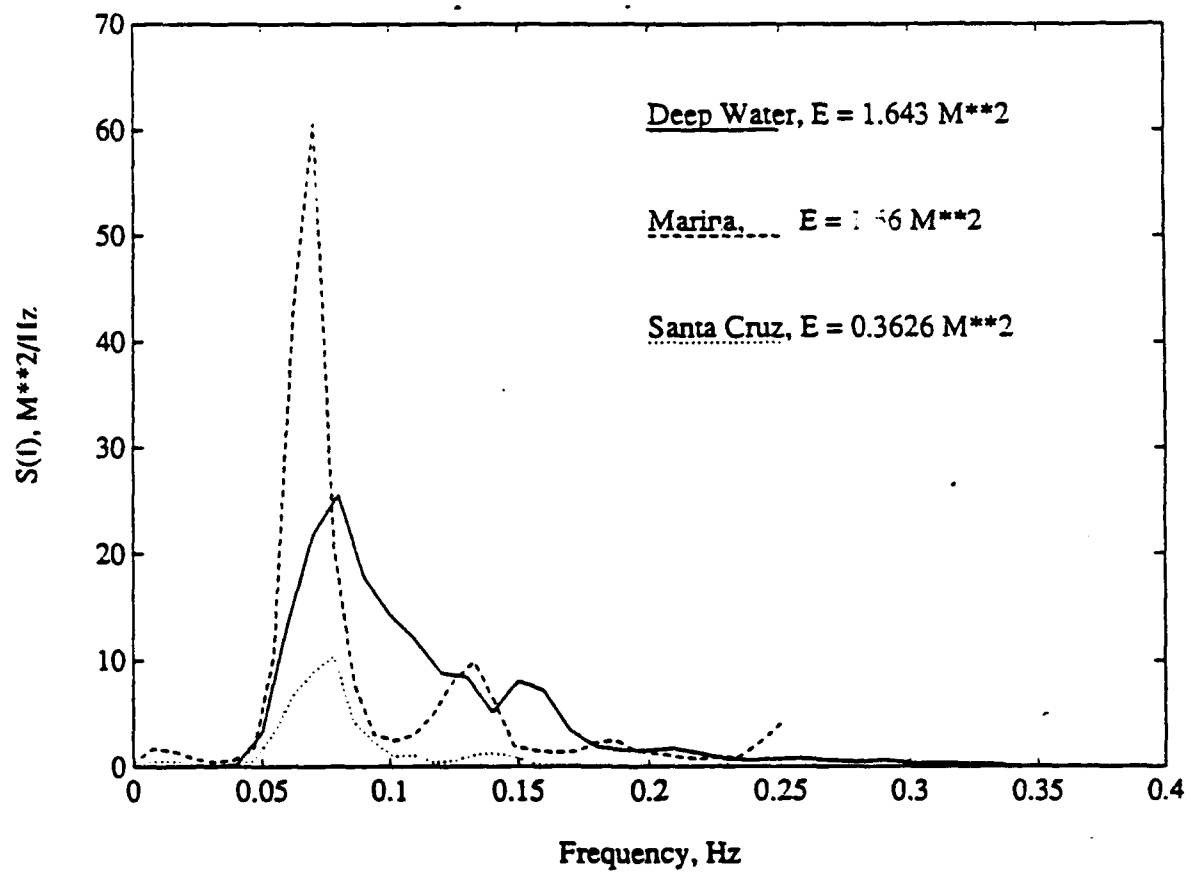


Figure 9. Measured spectral density on 18 January 1988, 0200 PST

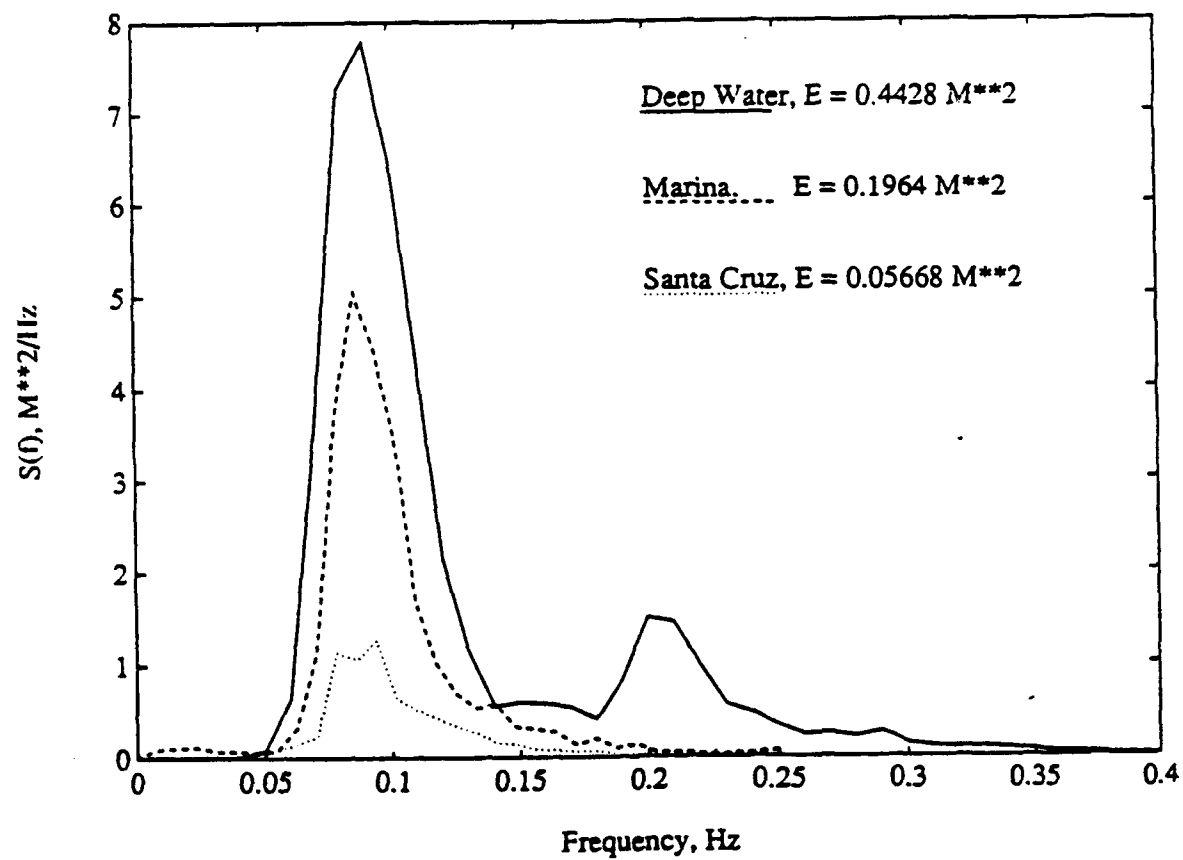


Figure 10. Measured spectral density on 29 January 1988, 2100 PST

Table 3. SIGNIFICANT WAVE HEIGHT (UNIT: METER)

	Buoy	Marina	Santa Cruz
3 Jan 1988	1.87 M	0.8 M	0.9 M
18 Jan 1988	5.12 M	5.15 M	2.4 M
29 Jan 1988	2.65 M	1.77 M	0.94 M

water angle and deep water angle are still to be found. The Dobson linear refractive model was used for this purpose. The reverse projection method was employed. That is, the linear refraction model program was run backward from shallow water location to deep water, beginning at the shallow water locations at Marina and Santa Cruz. Figure 12 - 15. show rays at the particular frequencies of 0.03, 0.06, 0.09, 0.13 Hz from Marina and Santa Cruz propagated offshore in increments of 0.5 degrees over the range of all possible incoming wave angles. Once the deep water is reached, the rays are stopped and deep water wave directions are recorded. As can be seen the low frequency waves are more refracted by the bathymetry than high frequency waves.

An example of the shallow water angle versus deep water angle at Marina for 0.06 Hz is shown in Figure 15. The dotted line is the least square first order fit, where a is the slope and b is the intersection at shallow water angle axis when deep water angle becomes zero.

The slope and intercept of least square linear fits at various frequencies and locations are given in Table 4 and plots given in Appendix A. As frequency increases, the slope increases to one and the offset decreases toward zero. Since slope less than one amounts to shrinking the deep water angular range, it indicates that smaller slope will concentrate wave energy into a smaller direction range and decrease the spectral density. The offset is equivalent to rotating the deep water DSD to a different direction.

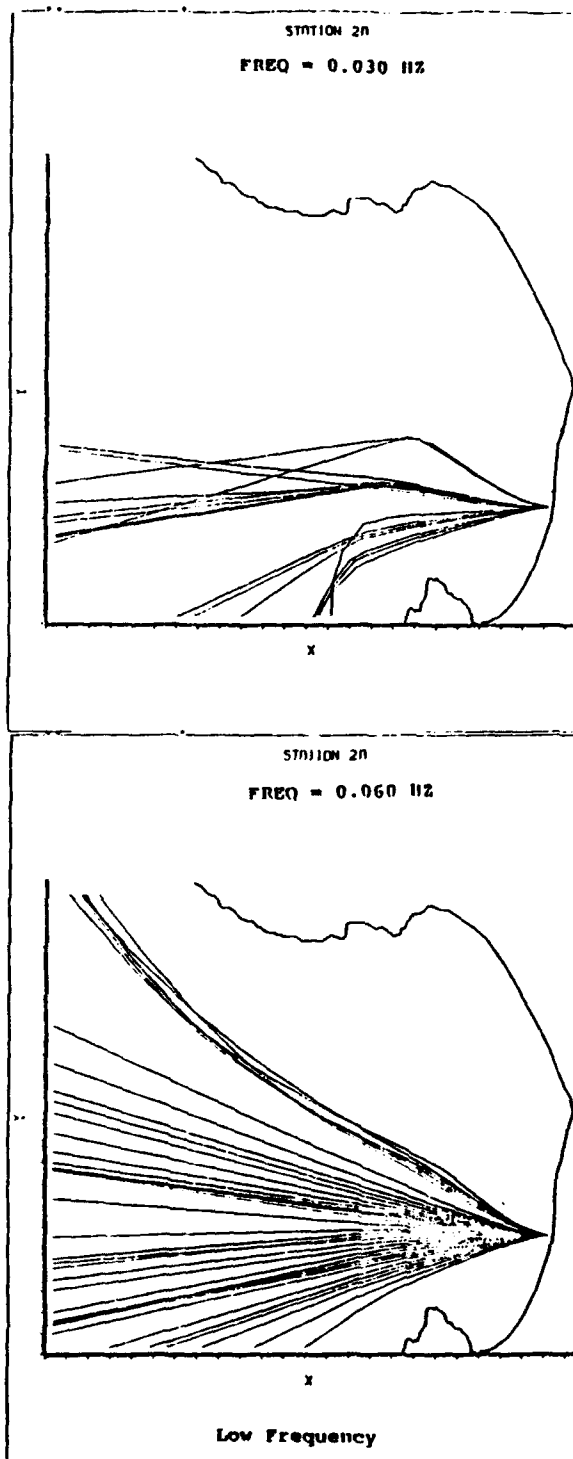


Figure 11. Ray traces from Marina to deep water

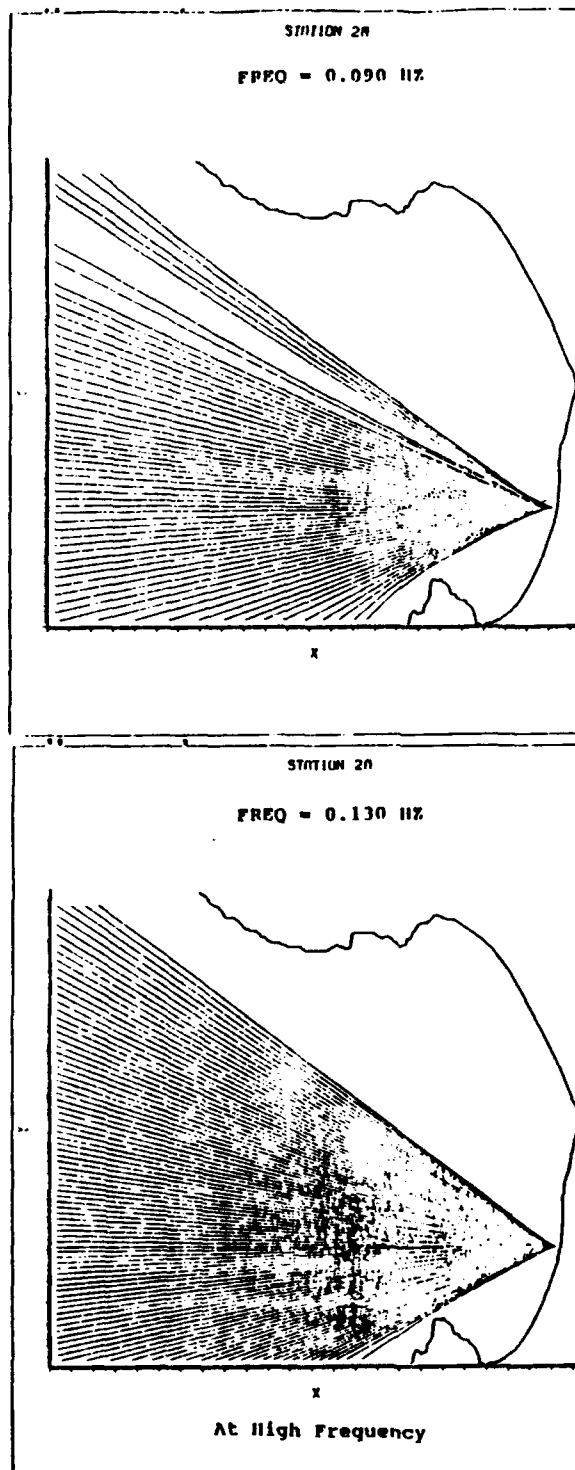


Figure 12. Ray traces from Marina to deep water

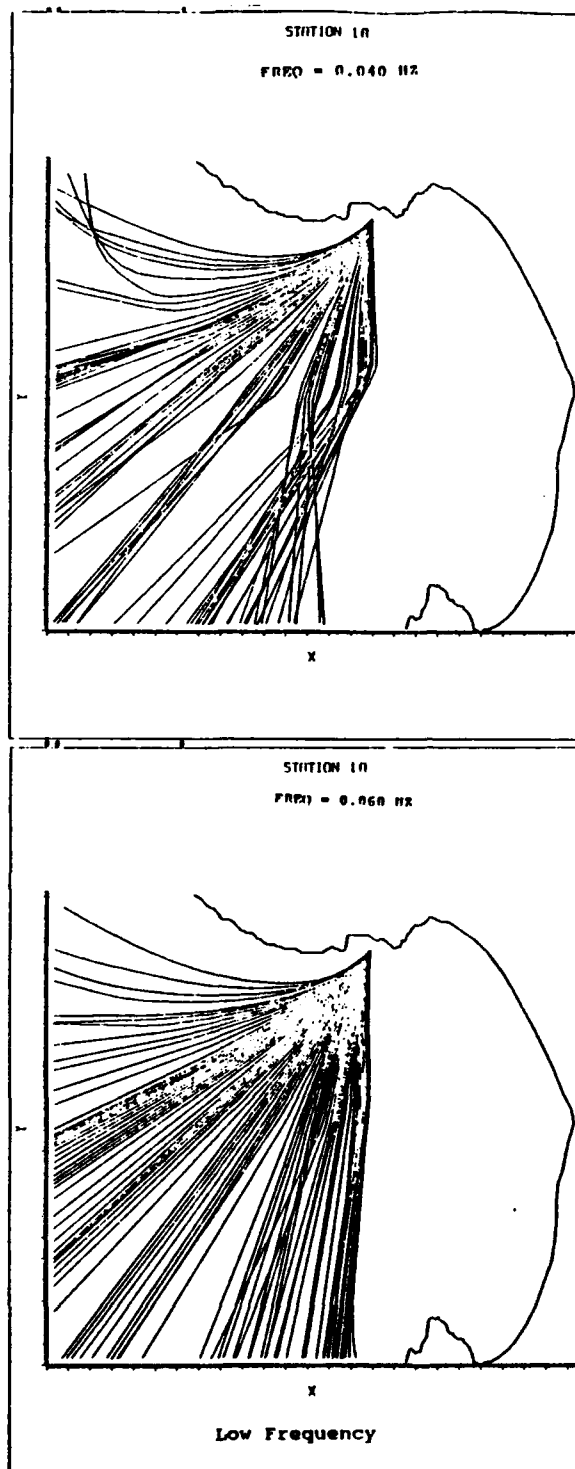


Figure 13. Ray traces from Santa Cruz to deep water

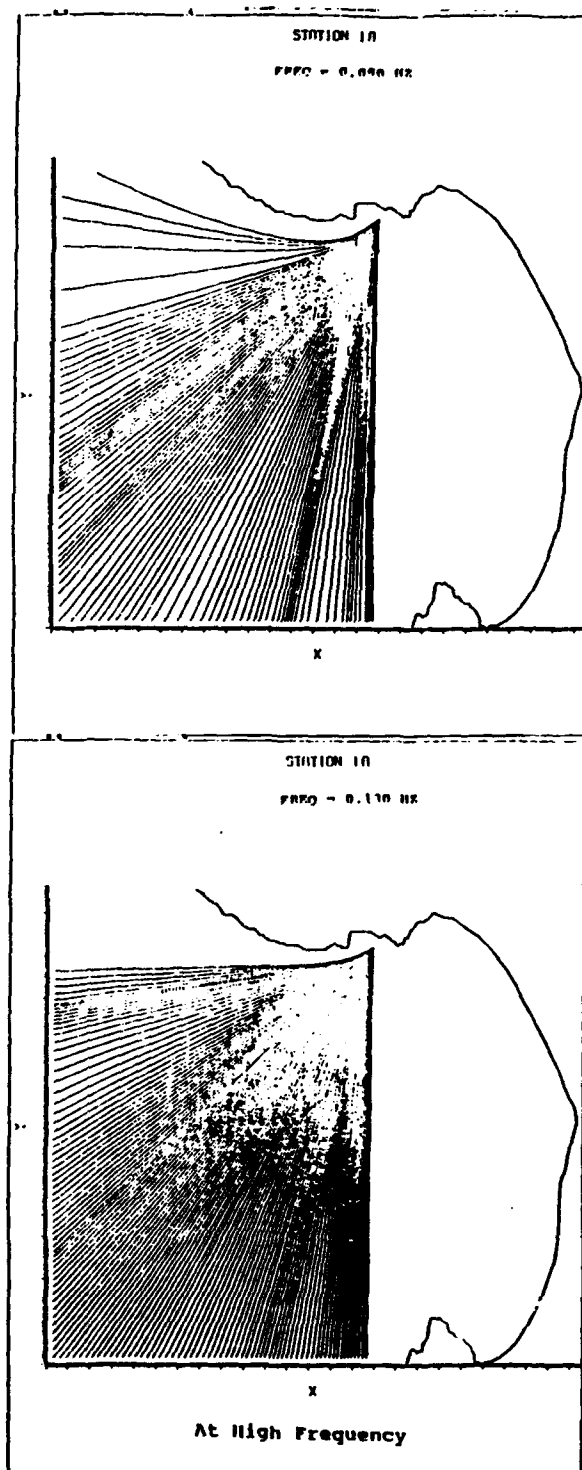


Figure 14. Ray traces from Santa Cruz deep water

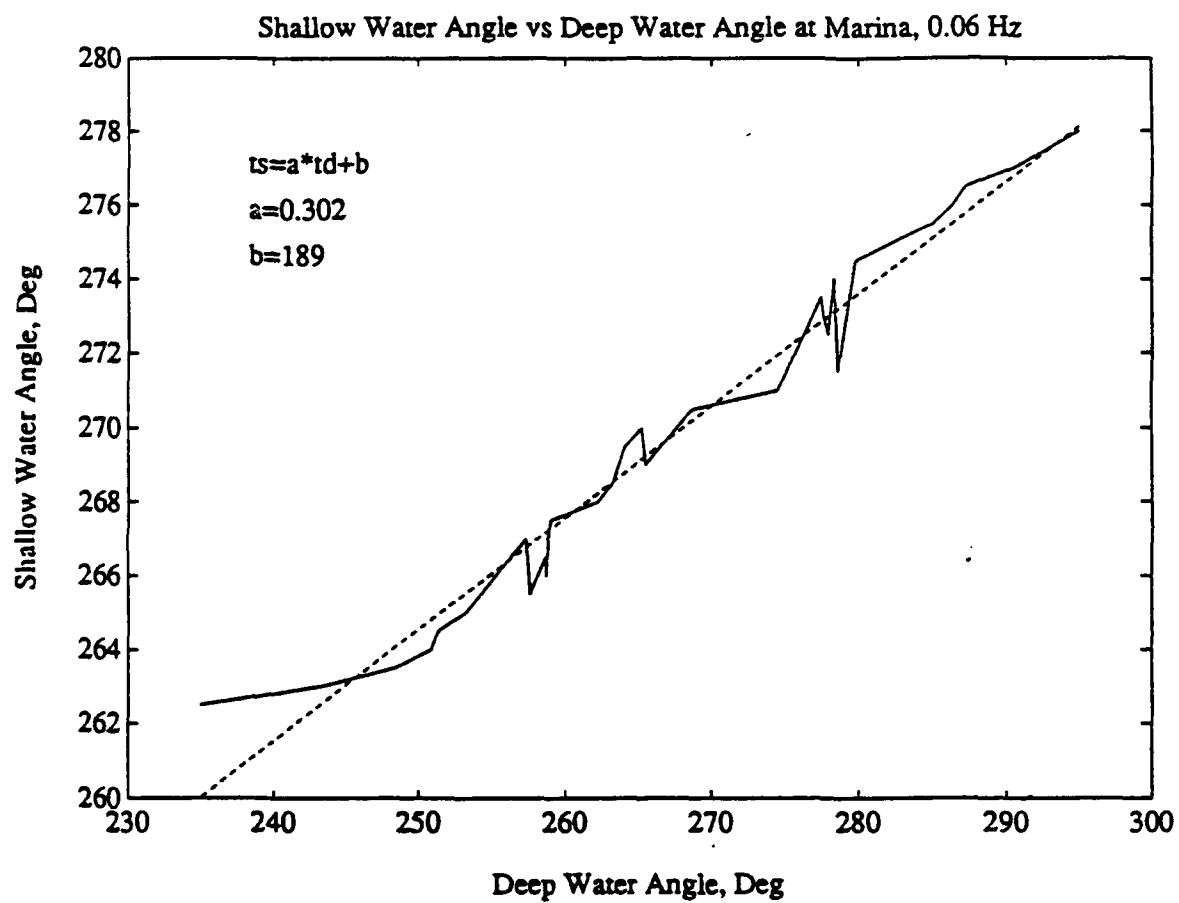


Figure 15. Example of the shallow water angle versus deep water angle

Table 4. EFFECTS OF LINEAR REFRACTION

Frequency	Marina		Santa Cruz	
	slope	offset	slope	offset
0.03 Hz	0.1164	242.0	0.3290	126.9
0.06 Hz	0.3020	189.0	0.3974	116.6
0.09 Hz	0.4165	157.9	0.4998	98.0
0.13 Hz	0.6938	82.8	0.6824	62.1

IV. RESULTS AND DISCUSSION

A. COMPARISON OF LCS AND EFC MEASURED DIRECTIONAL SPECTRAL DENSITIES

A flow chart of the calculation of measurements is shown in Figure 16. The TRIDEN program calculates the EFC spectrum and compares it with the spectrum measured in shallow water. The directional distribution of measured waves in polar plot form are shown in Figures 17, 18, and 19 at the three locations, Buoy, Marina, and Santa Cruz on 3 January 1988. These axis are aligned with the earth directions. The deep water wave approach from northwest or west. Four frequencies, 0.03, 0.06, 0.09 and 0.13 Hz are examined. At Marina, waves come mostly from west, and at Santa Cruz, from southwest. The plots show the energy is more widely distributed in deep water and that the spectrum narrows in shallow water, except in the lowest frequency.

The energy density distribution as a function of frequency and direction are shown in Figures 20 - 31, for 3 January 1988 at deep water Buoy, Marina, and Santa Cruz. Both of the LCS method and EFC method indicate the same directionality of measured data, but EFC method shows a much sharper peak than LCS method. Also LCS results sometimes show negative side lobes, which do not exist in the EFC results.

The wave energy spectra at frequency 0.13 Hz, are shown in Figures 32, 33, and 34. Again, the EFC method results in much higher resolution. For this reason, only the EFC are discussed for other results. The other two days, 18 and 29 January 1988, 3-D and 2-D also show similar results. All graphs are given in Appendix B. The deep water buoy and shallow water array (Marina and Santa Cruz) energies are compared in Table 5, 6 for the different methods. As can be seen the LCS and EFC methods give the same total energies under the spectra.

Table 5. DEEP WATER BUOY ENERGY (M^2)

DATE	EFC		LCS
	D2	COMPOSITE	
3 Jan 88, 0800	0.22	0.22	0.22
18 Jan 88, 0200	1.642	1.641	1.642
21 Jan 88, 2100	0.443	0.442	0.443

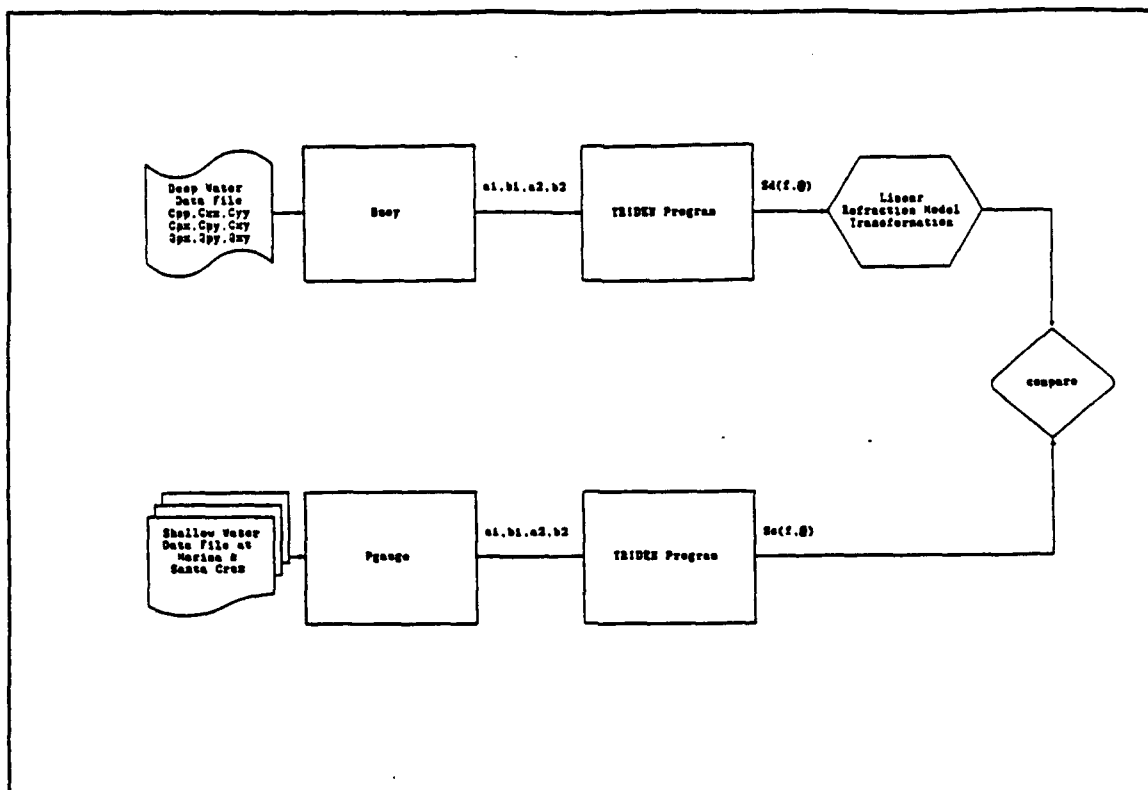


Figure 16. The flow chart of measurement calculation

Table 6. SHALLOW WATER ARRAY ENERGY (M^2)

DATA	EFC				LCS	
	D2		COMPOSITE			
	Marina	Santa Cruz	Marina	Santa Cruz	Marina	Santa Cruz
3 Jan 88, 0800	0.042	0.054	0.042	0.054	0.042	0.054
18 Jan 88, 0200	1.659	0.363	1.656	0.362	1.656	0.362
21 Jan 88, 2100	0.196	0.057	0.196	0.057	0.196	0.057

B. REFRACTION MODEL PREDICTIONS

The deep water spectrum is transformed to shallow water using Eq.(62). The shallow water spectrum is simply equal to deep water spectrum multiplied by shoaling.

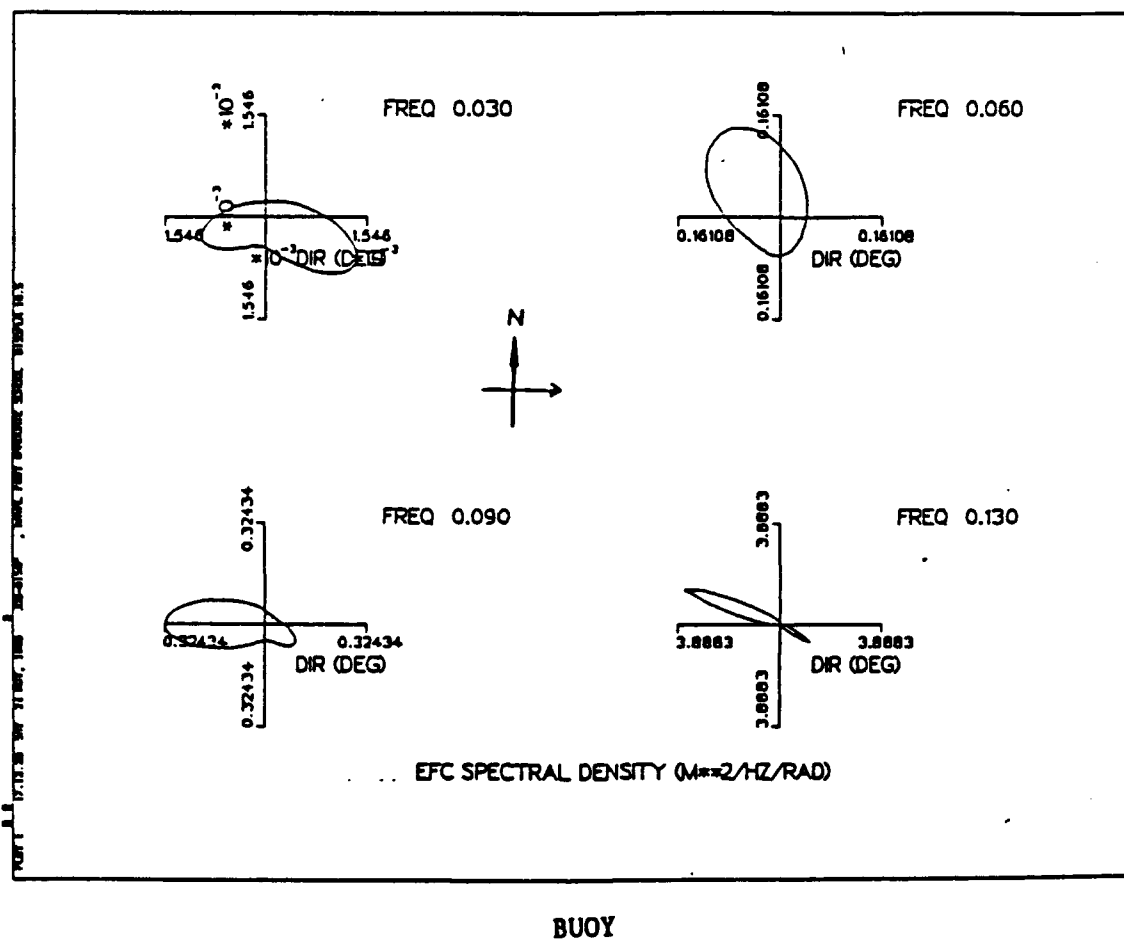


Figure 17. The energy direction of deep water on 3 Jan 1988.

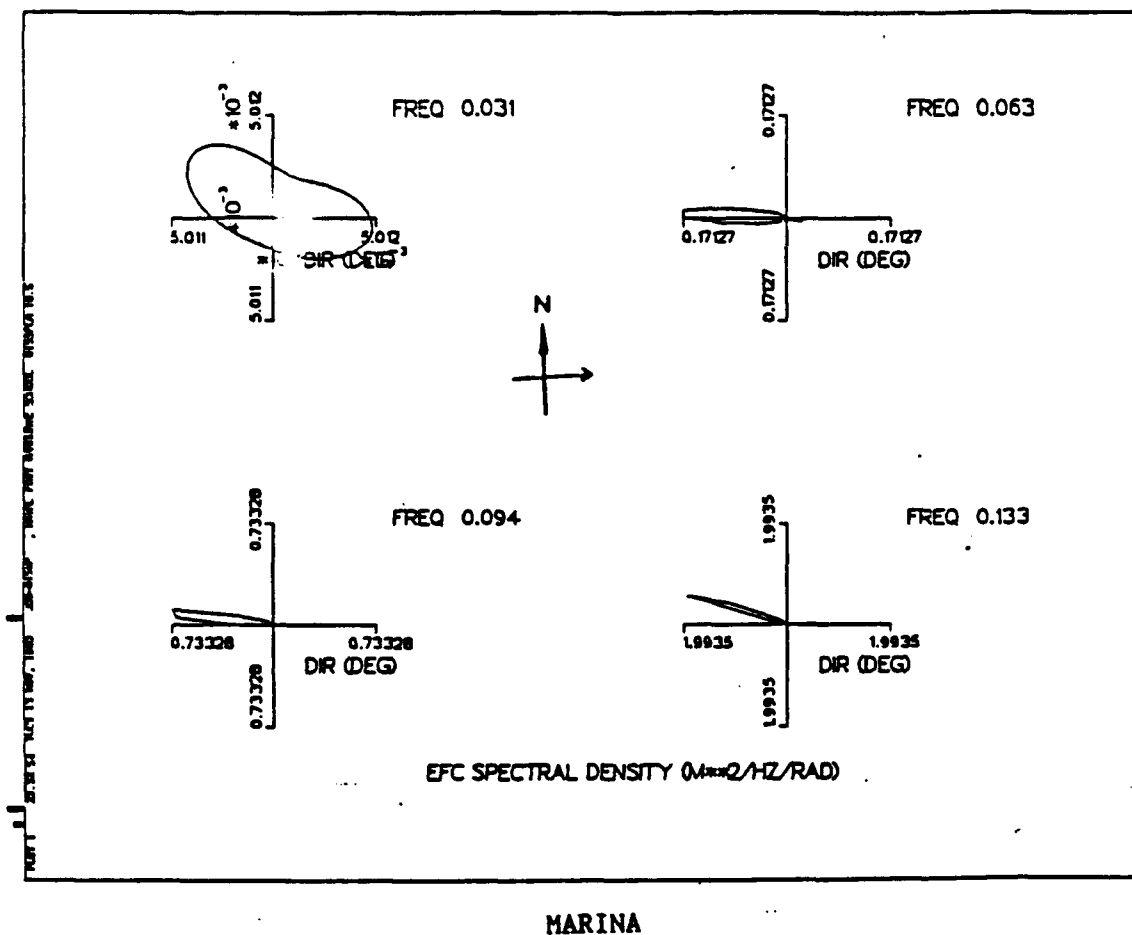


Figure 18. The energy direction of shallow water at Marina on 3 Jan 1988.

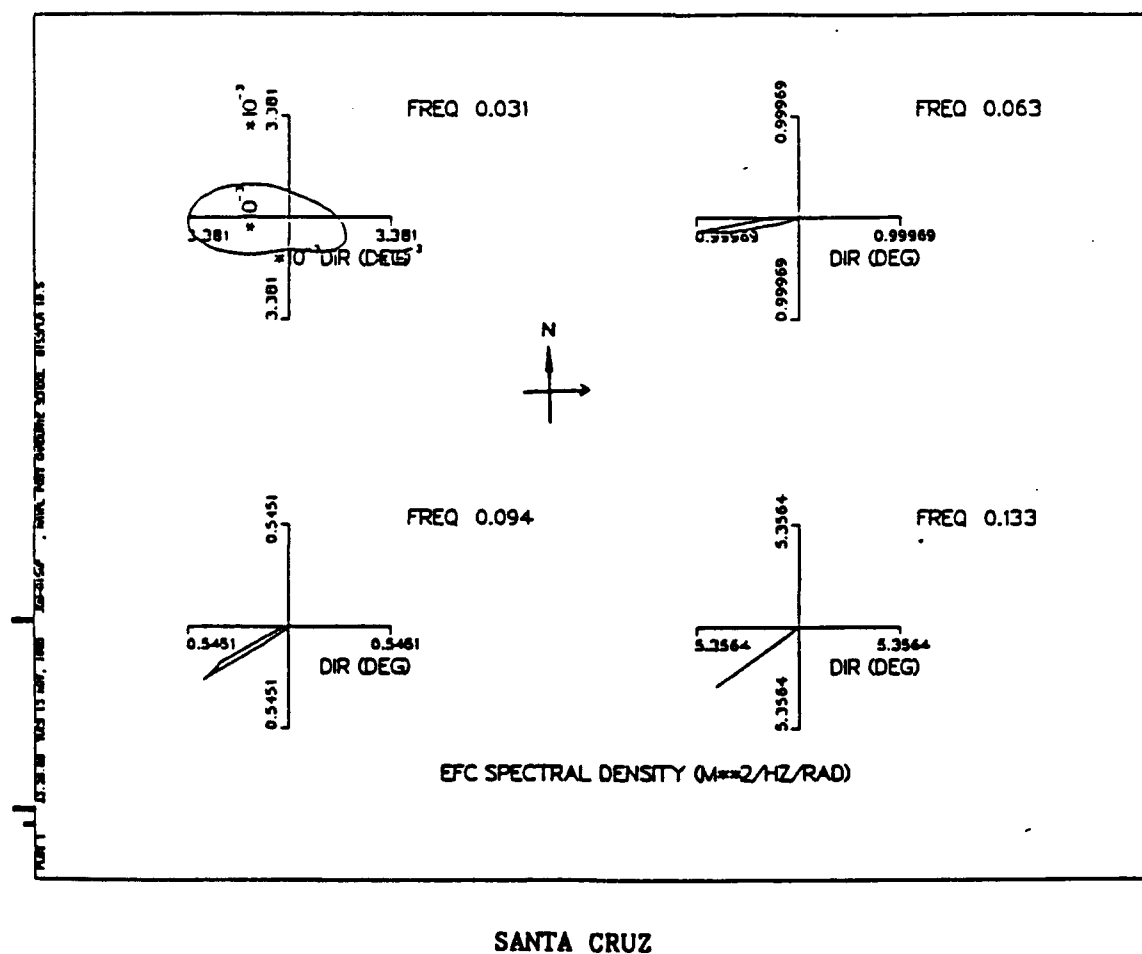


Figure 19. The energy direction of shallow water at Santa Cruz on 3 Jan 1988.

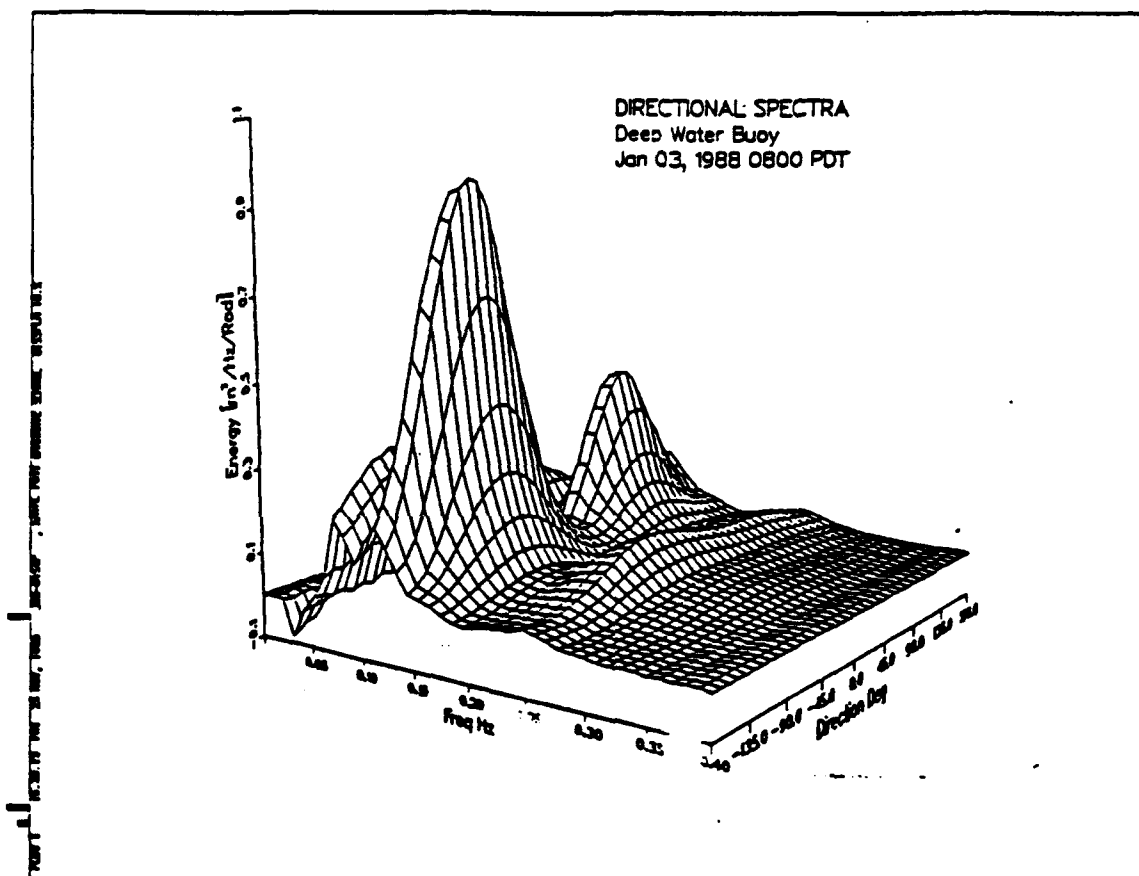


Figure 20. The LCS directional spectral density in 3-D plot: On 3 Jan 1988 at deep water Buoy.

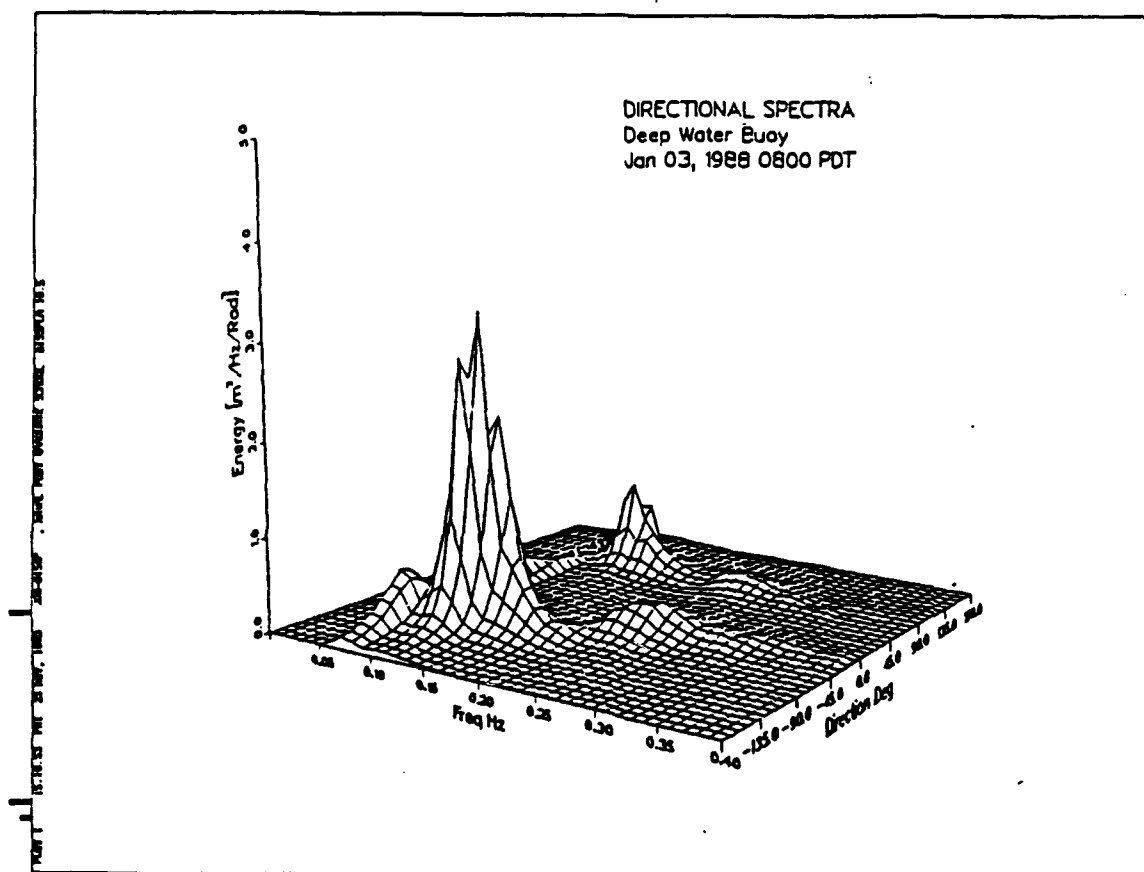


Figure 21. The EFC directional spectral density in 3-D plot: On 3 Jan 1988 at deep water Buoy.

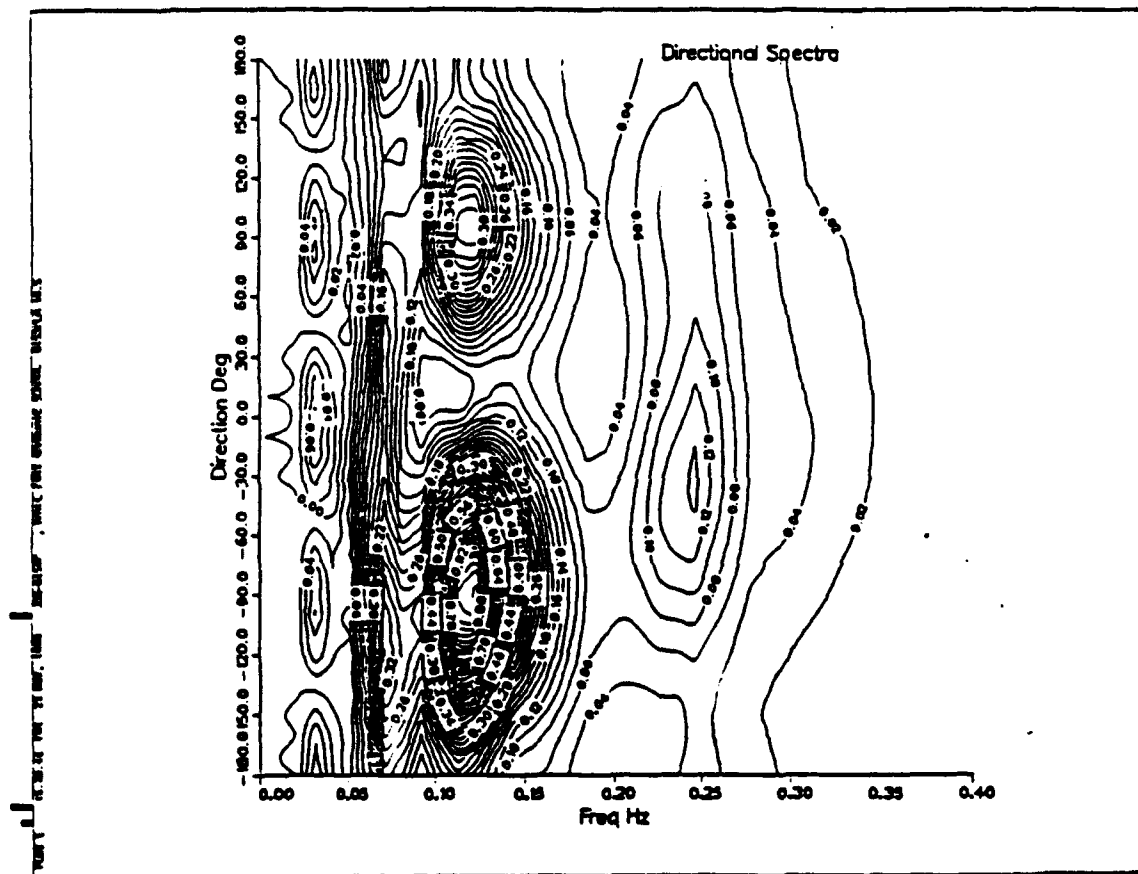


Figure 22. The LCS directional spectral density in contour plot: On 3 Jan 1988 at deep water Buoy.

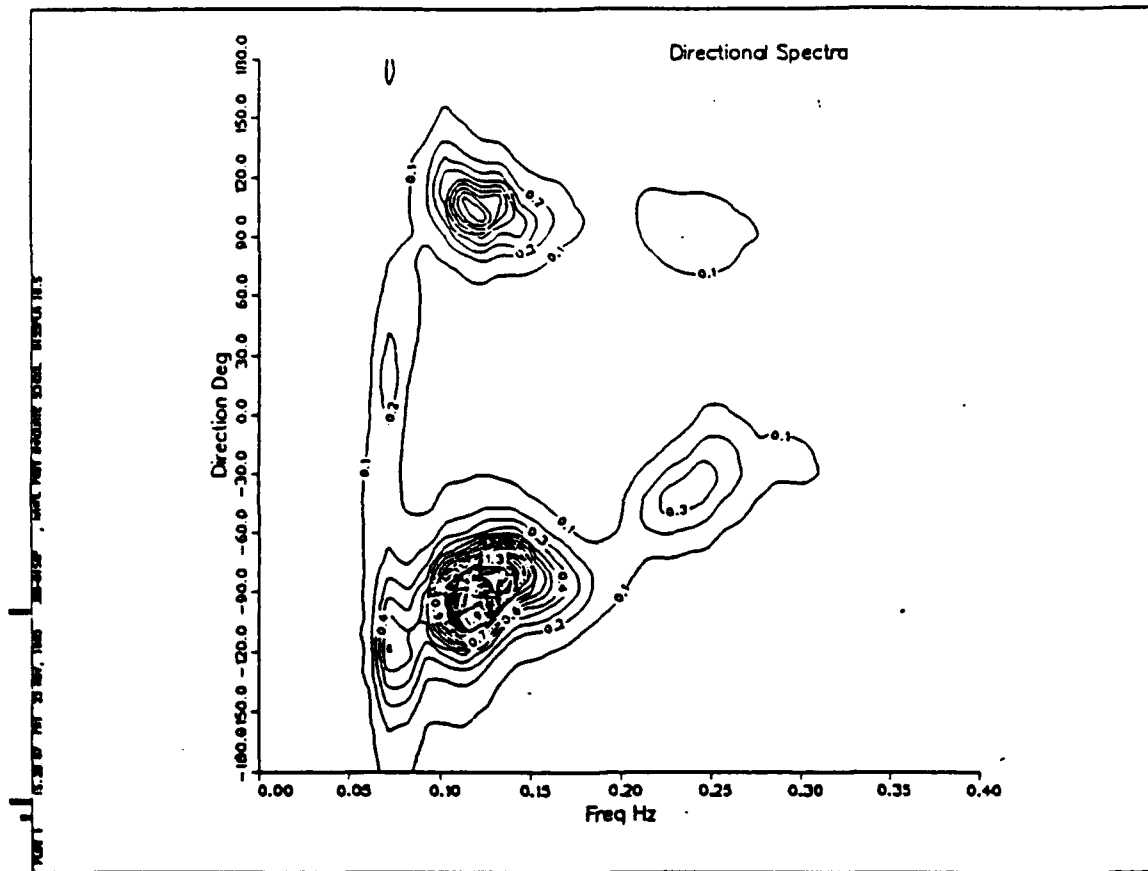


Figure 23. The EFC directional spectral density in contour plot: On 3 Jan 1988 at deep water Buoy.

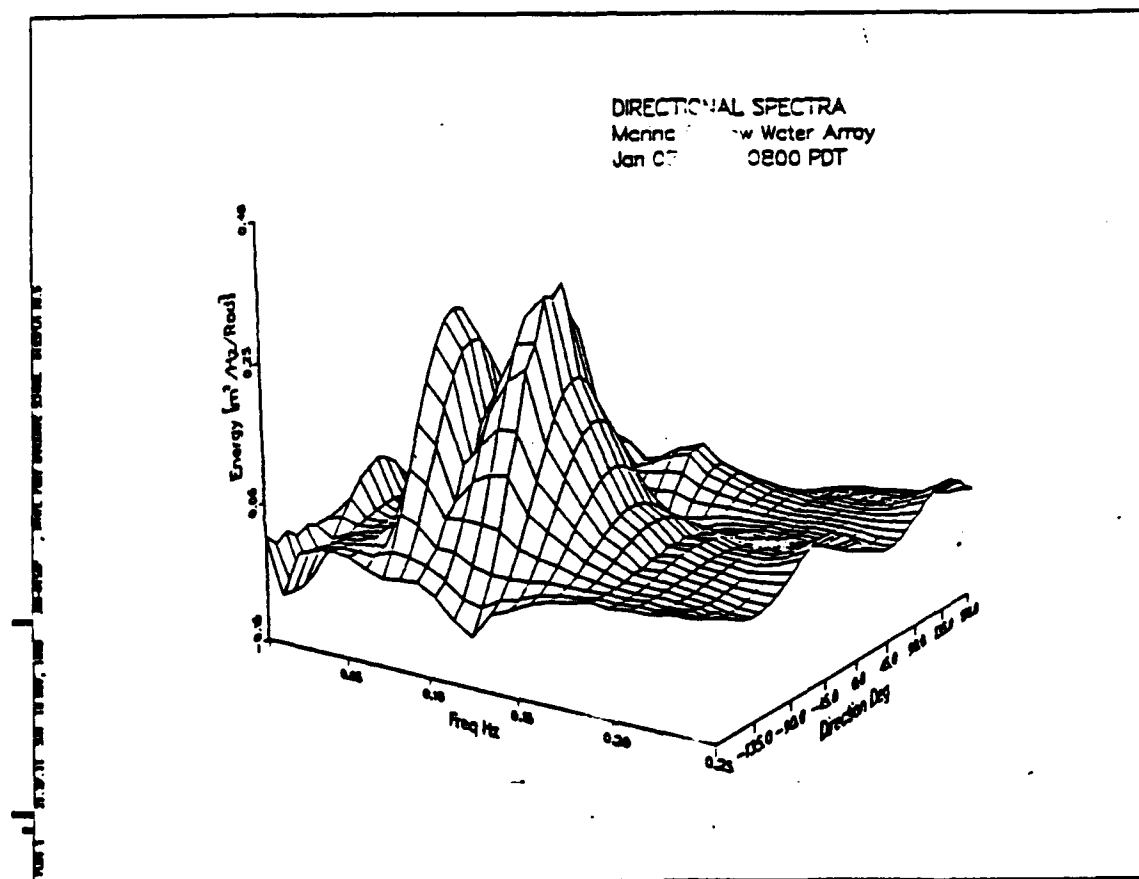


Figure 24. The LCS directional spectral density in 3-D plot: On 3 Jan 1988 at Marina.

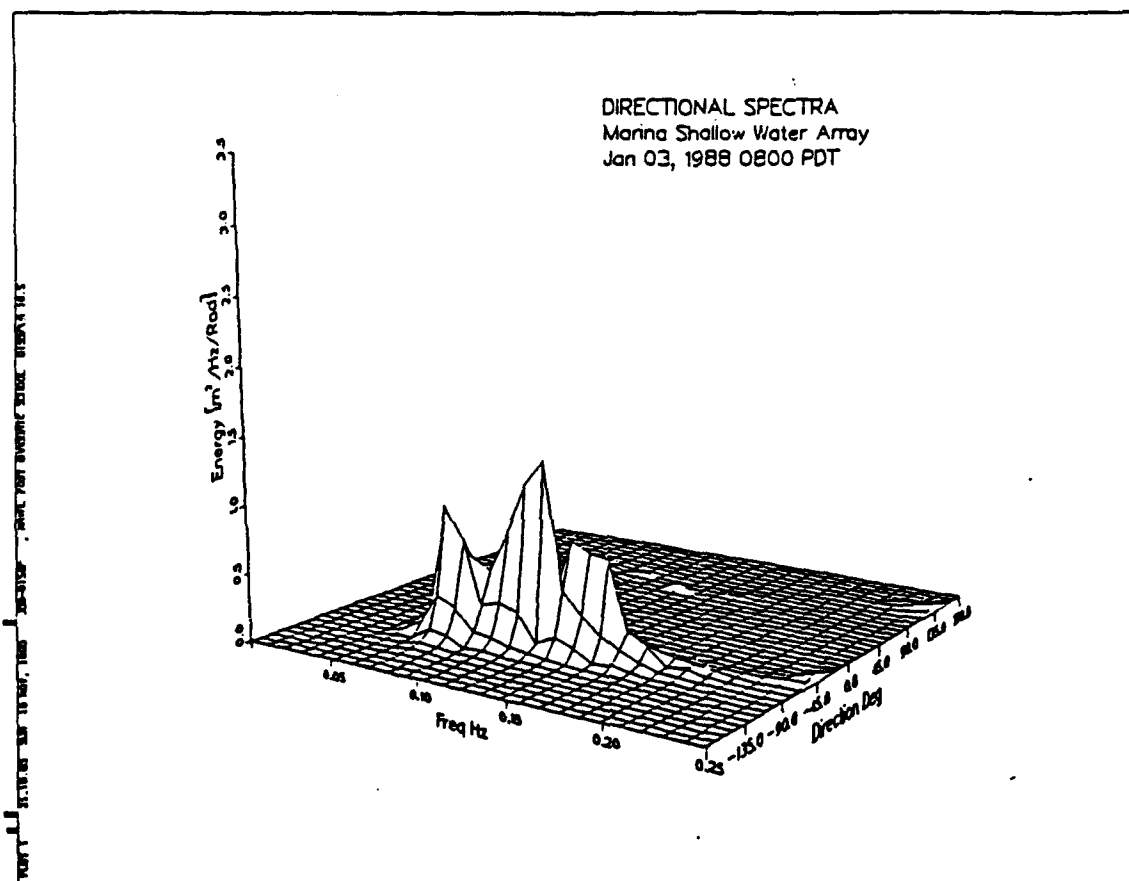


Figure 25. The EFC directional spectral density in 3-D plot: On 3 Jan 1988 at Marina.

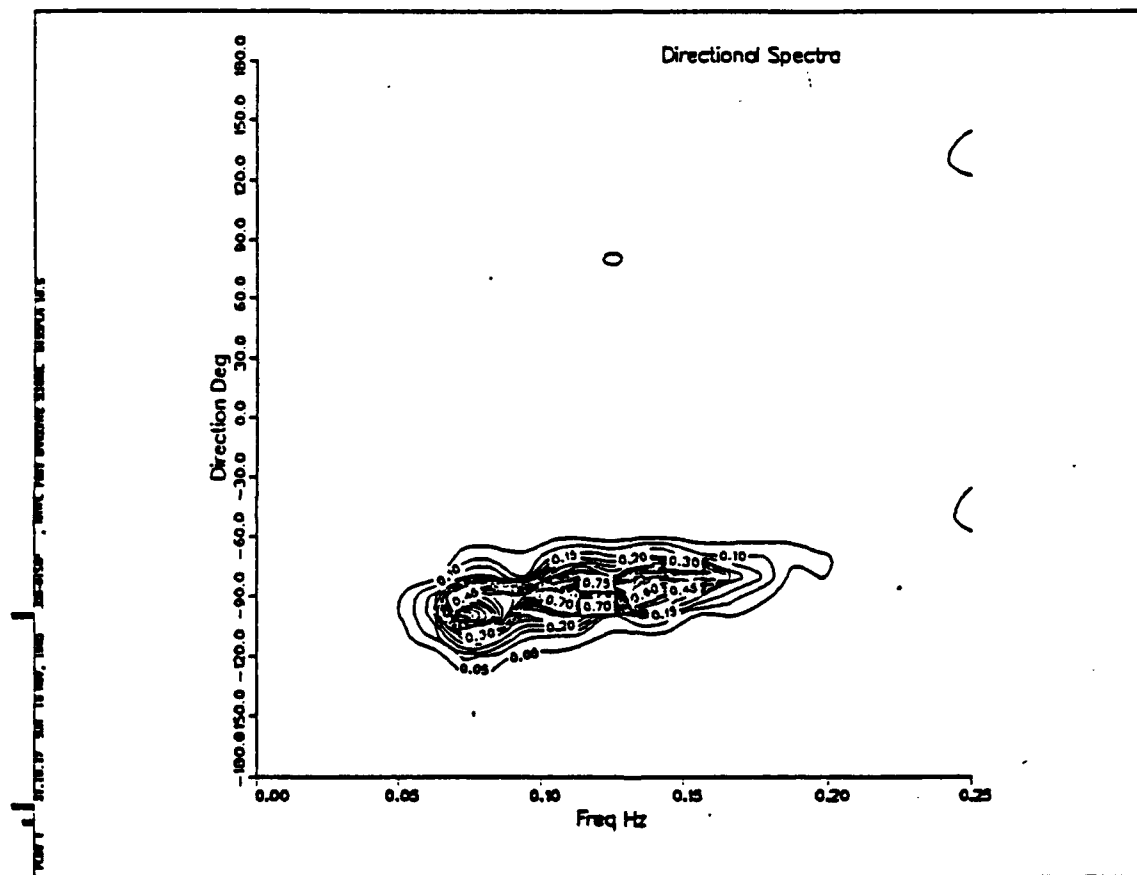


Figure 27. The EFC directional spectral density in contour plot: On 3 Jan 1988 at Marina.

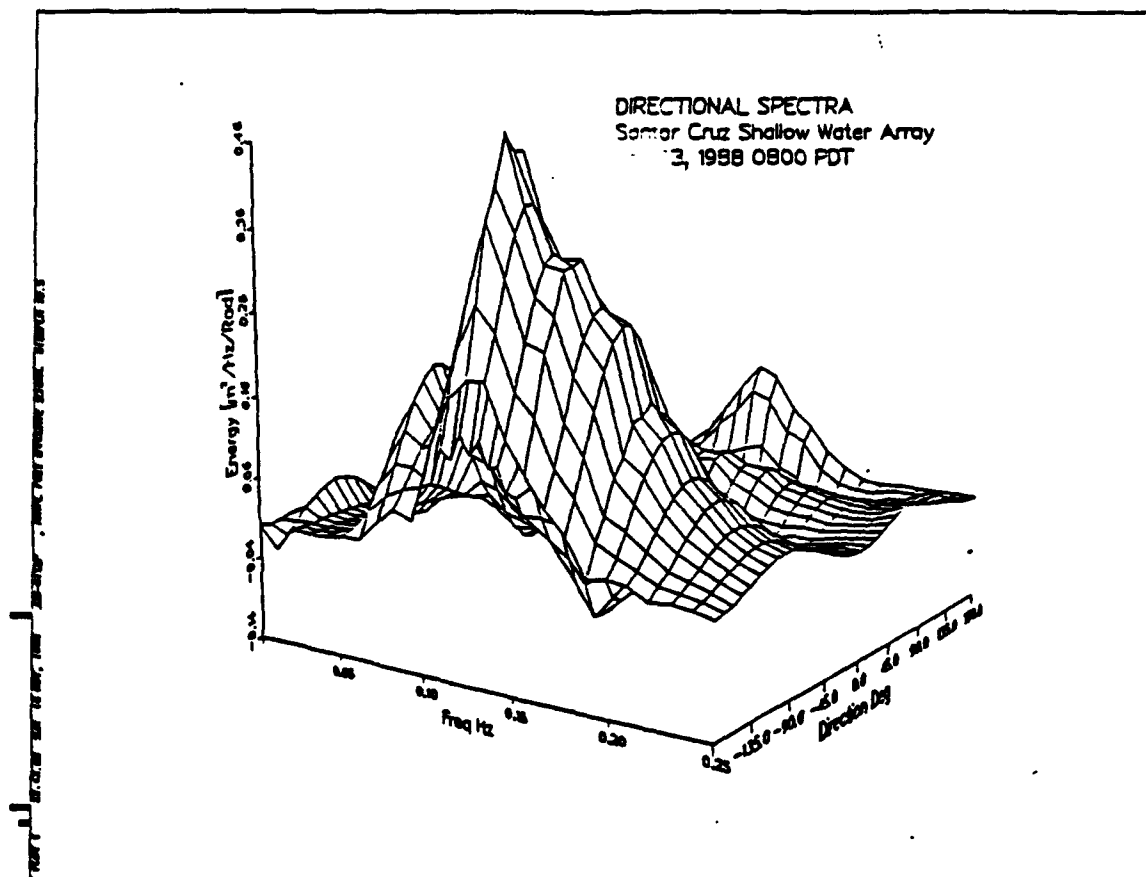


Figure 28. The LCS directional spectral density in 3-D plot: On 3 Jan 1988 at Santa Cruz.

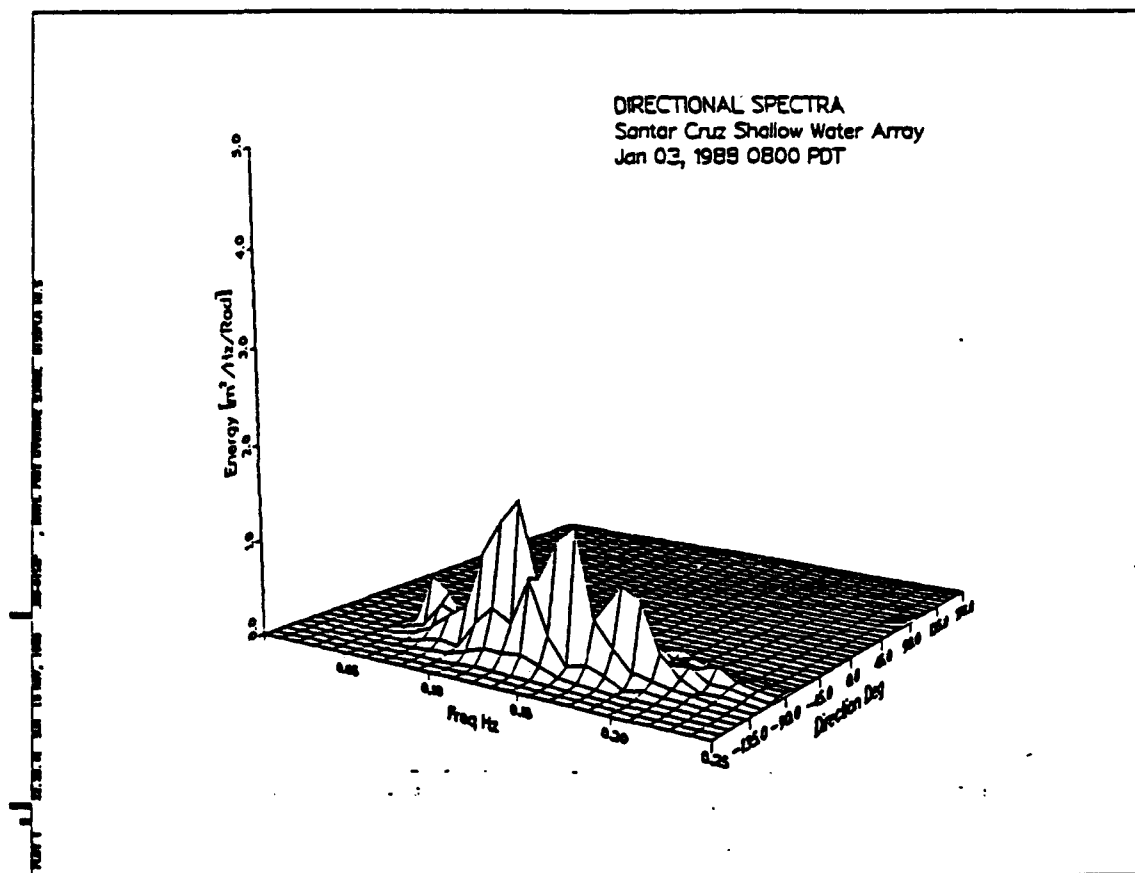


Figure 29. The EFC directional spectral density in 3-D plot: On 3 Jan 1988 at Santa Cruz.

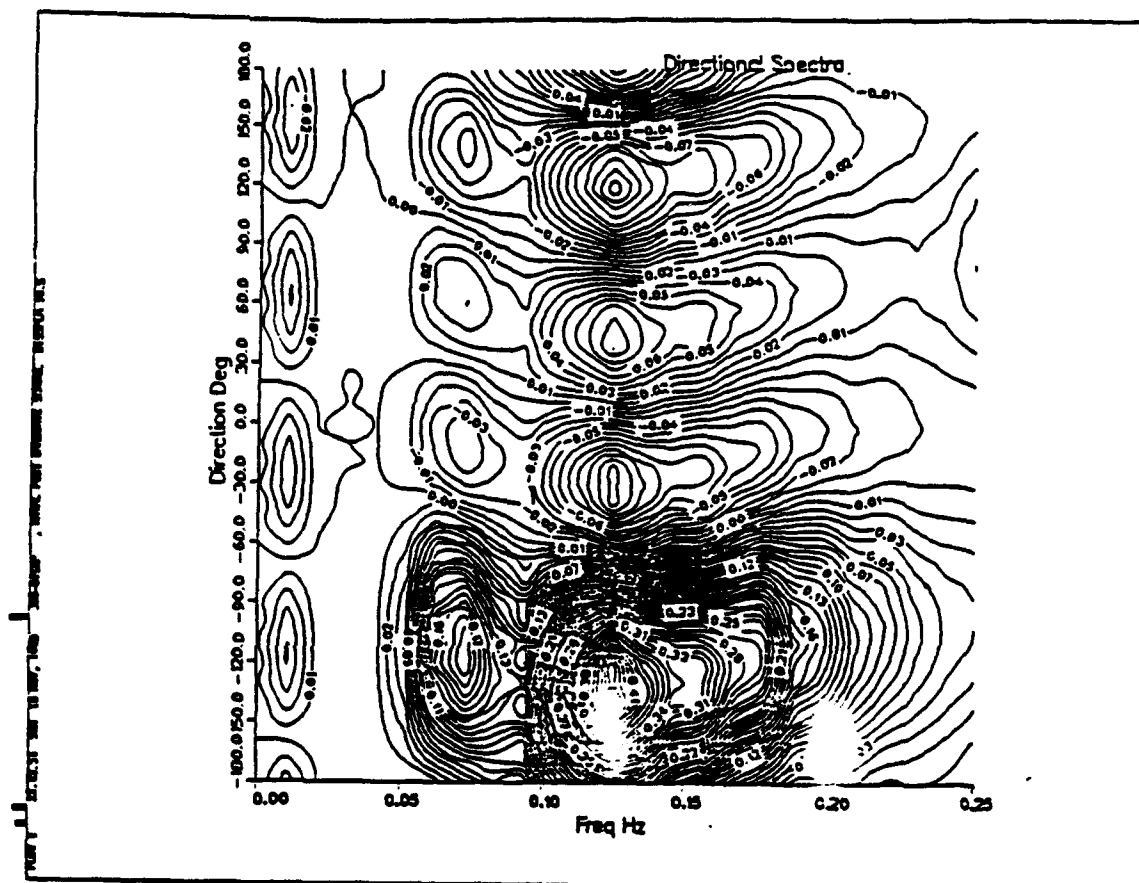


Figure 30. The LCS directional spectral density in contour plot: On 3 Jan 1988 at Santa Cruz.

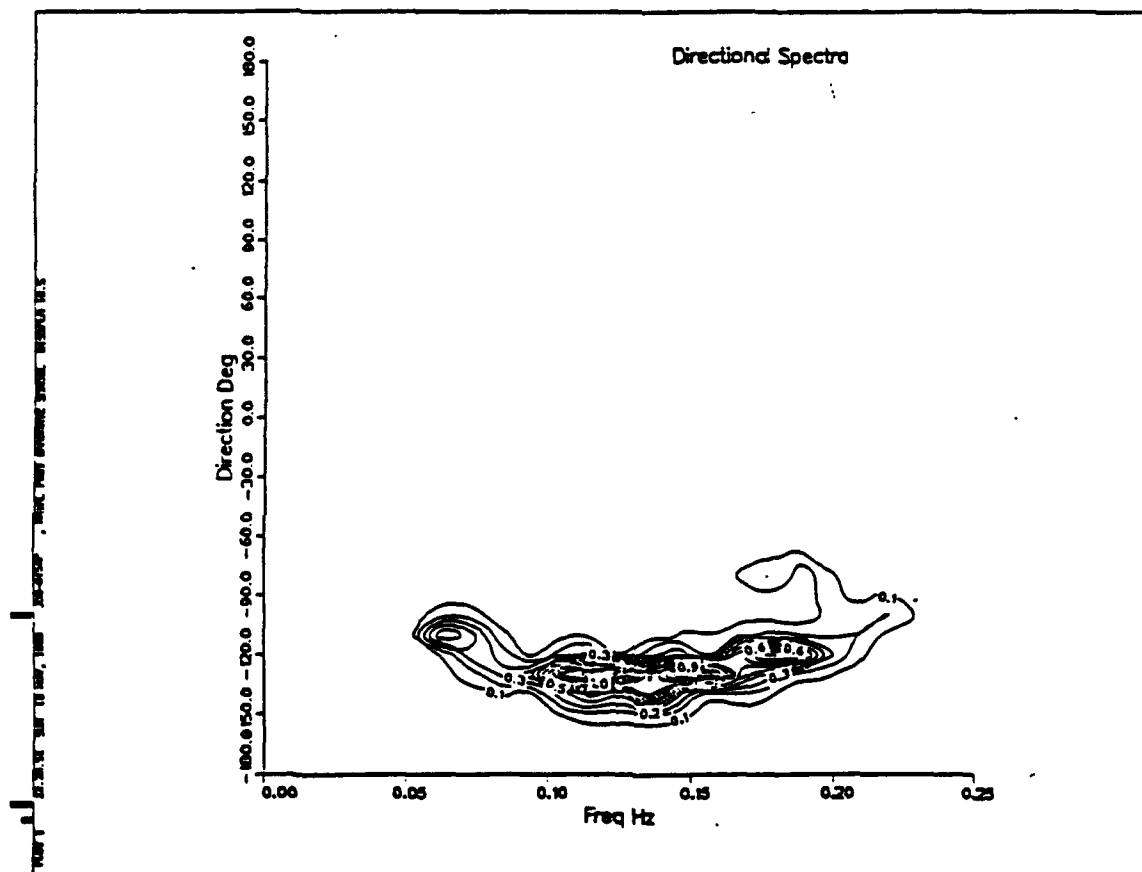


Figure 31. The EFC directional spectral density in contour plot: On 3 Jan 1988 at Santa Cruz.

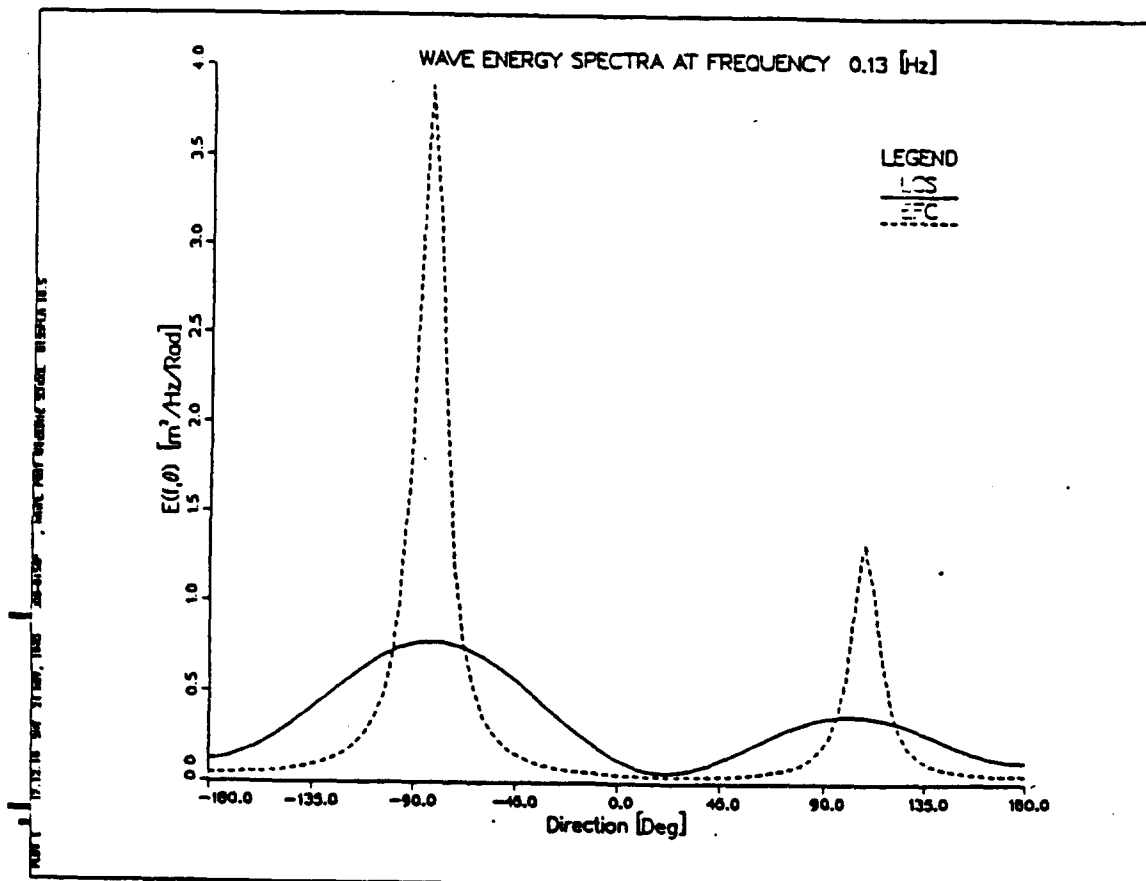


Figure 32. The LCS & EFC directional spectral densities in 2-D plot: On 3 Jan 1988 at deep water Buoy.

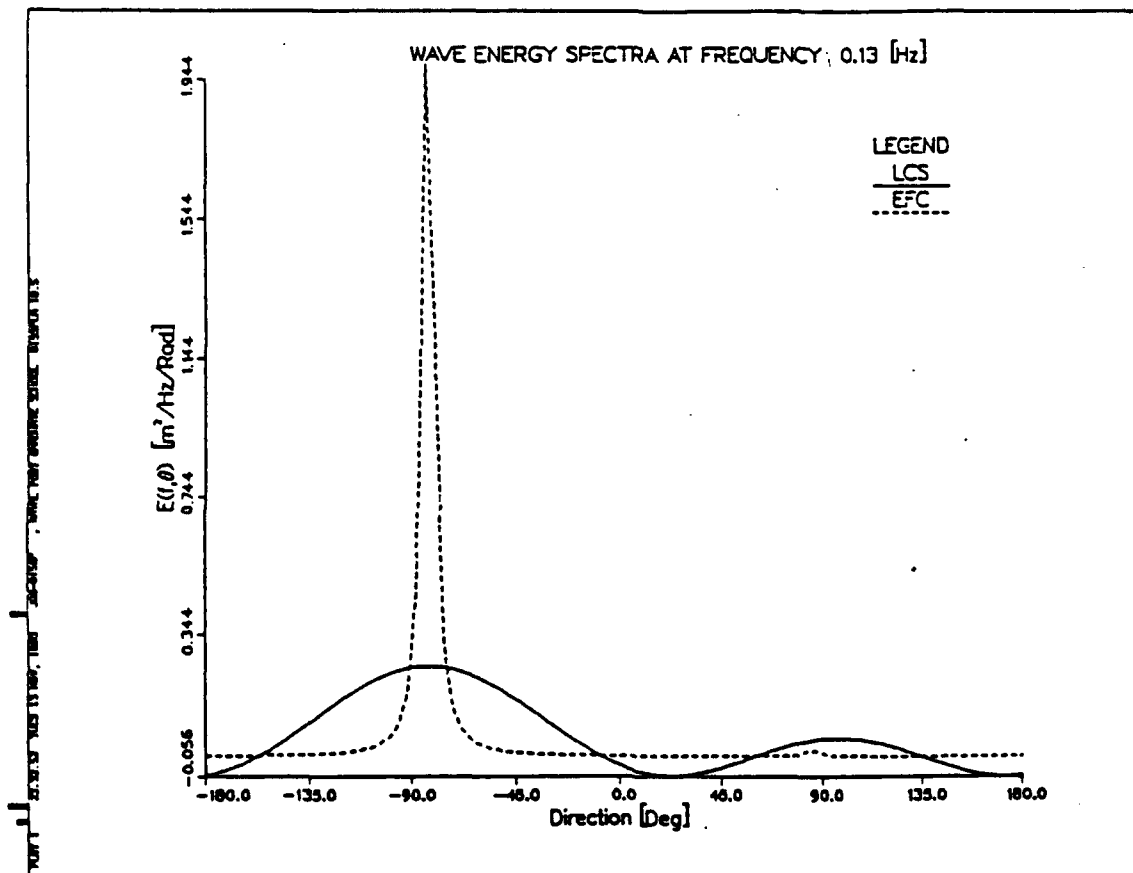


Figure 33. The LCS & EFC directional spectral densities in 2-D plot: On 3 Jan 1988 at Marina.

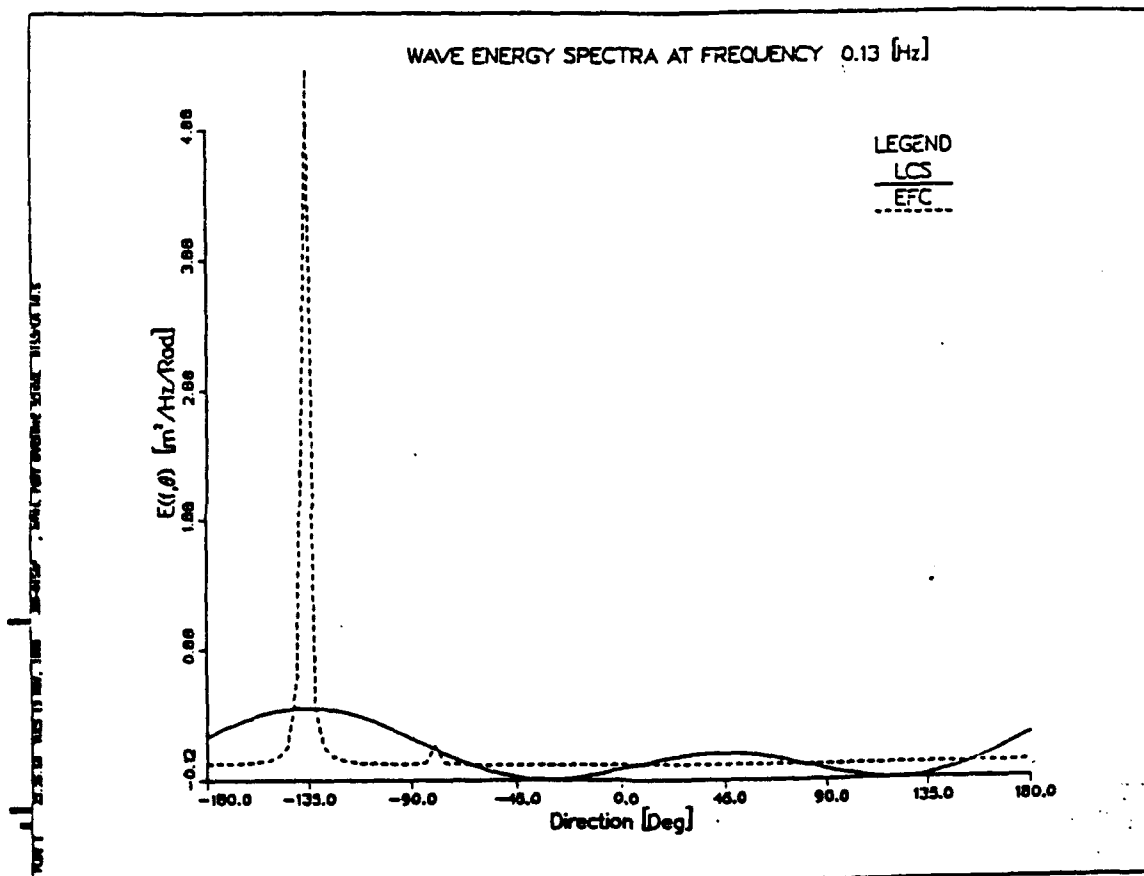


Figure 34. The LCS & EFC directional spectral densities in 2-D plot: On 3 Jan 1988 at Santa Cruz.

Table 7. COMPARISON OF TRANSFORMED AND MEASURED DATA DIFFERENCE IN DEGREE

Location	Marina			Santa Cruz		
Frequency	0.06 Hz	0.09 Hz	0.13 Hz	0.06 Hz	0.09 Hz	0.13 Hz
03 Jan 1988	25°	0°	0°	15°	0°	30°
18 Jan 1988	30°	95°	50°	5°	15°	25°
29 Jan 1988	5°	0°	5°	40°	5°	5°

Table 8. MEASURED AND TRANSFORMED ENERGY SPECTRUM DATA AT MARINA (M^2/HZ)

FREQ.	0.06 Hz		0.09 Hz		0.13 Hz	
	MEAS-URED	TRANS-FORMED	MEAS-URED	TRANS-FORMED	MEAS-URED	TRANS-FORMED
3 Jan 88, 0800	0.026	0.123	0.062	0.078	0.401	0.449
18 Jan 88, 0200	12.8	3.85	1.54	2.46	4.11	2.90
29 Jan 88, 2100	0.103	0.103	1.28	1.28	0.180	0.205

Table 9. MEASURED AND TRANSFORMED ENERGY SPECTRUM DATA AT SANTA CRUZ (M^2/HZ)

FREQ.	0.06 Hz		0.09 Hz		0.13 Hz	
	MEAS-URED	TRANS-FORMED	MEAS-URED	TRANS-FORMED	MEAS-URED	TRANS-FORMED
3 Jan 88, 0800	0.072	0.187	0.045	0.118	0.205	0.277
18 Jan 88, 0200	2.87	3.25	1.03	2.00	0.411	1.54
29 Jan 88, 2100	0.062	0.16	0.616	1.03	0.168	0.205

$(\frac{V_o}{V})$, and dispersion, $(\frac{K}{K_o})$ and the energy density is replotted based on the angle conversion between deep and shallow water, determined by the linear wave refraction model.

The Marina location is shadowed by Point Pinós in the southwest and Point Santa Cruz in the northwest. High frequency waves, 0.11 Hz and above, are limited to directions from 235°-310° at the array site, whereas low frequency waves may arrive from even southerly directions after considerable refraction (refer to Figures 11, 12).

The Santa Cruz site poses more complex problems than Marina because of its location. The waves approaching from the westerly direction make almost a 90° turn to arrive at the shoreline. The low frequency waves travelling north and north-eastward may arrive at this location. The ray patterns show (Figures 13, 14) scattered and crossing rays (caustics) from the west or higher approach angle at low frequency. The ray patterns become more regular with increasing frequency.

C. COMPARISON OF DEEP, SHALLOW AND TRANSFORMED DIRECTIONAL SPECTRAL DENSITIES

Transformed and measured shallow wave directional spectra for Marina are compared in Figure 35 - 37. On 3 January 1988 for 0.06 Hz, the result shows about a 25 degree angle difference between transformed and measured DSD, and the transformed spectral energy is overestimated. For 0.09 Hz, the transformed and measured shallow waves have the same directional spectral distribution, but the measured data has greater energy density than the transformed. On the same day at 0.13 Hz, the result shows good prediction in directionality. Both frequencies indicate the transformed DSD have narrower distributions compared with deep water DSD, because the shrinking of the angle distribution concentrates the energy in shallow water during transformation. The refraction effects are greatest at lower frequency. On 18 January 1988 for 0.09 Hz at Marina, the results (Figure 38) show a poor prediction, the directionality having a 95 degree difference, which is at low relative energy within the spectrum and appears to be a spurious result. On 29 January 1988, the results show a 5 degree difference or less at all frequencies.

Results of the Santa Cruz location are depicted in Figure 40 - 42. The results are different from Marina. On 18 January 1988 at 0.09 Hz, the prediction has a 15 degree difference, which is better than that at Marina. On 3 January at 0.09 Hz and 29 January at 0.13 Hz both provide satisfactory results. Table 7 summarize the three days 3, 18, and 29 January 1988 at different frequencies and locations comparing transformed and measured directionality angle differences.

The variance within half power band width of the directional spectra at Marina and Santa Cruz on all these days are given in Tables 8 and 9. By examining Tables 7 - 9 and focusing on the energy peak frequencies for the three days, 0.13 Hz on 3 January 1988, 0.06 Hz on 18 January 1988 and 0.09 Hz on 29 January 1988, we can compare the energy and directional difference between measured and transformed data at Marina and Santa Cruz. At Marina, the directions are the same on 3 and 29 January 1988, but has

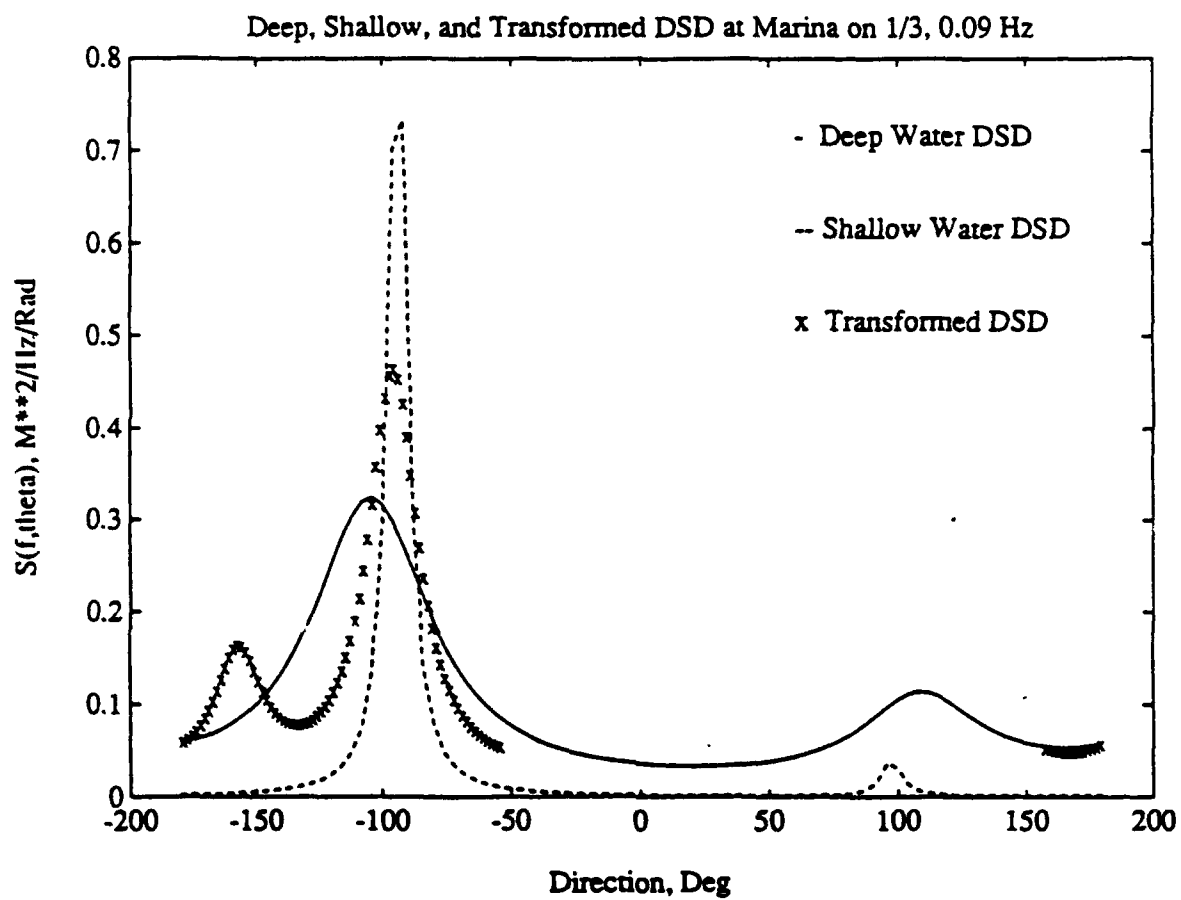


Figure 35. The deep, shallow, and transformed DSD: On 3 Jan 1988 at Marina, 0.09 Hz.

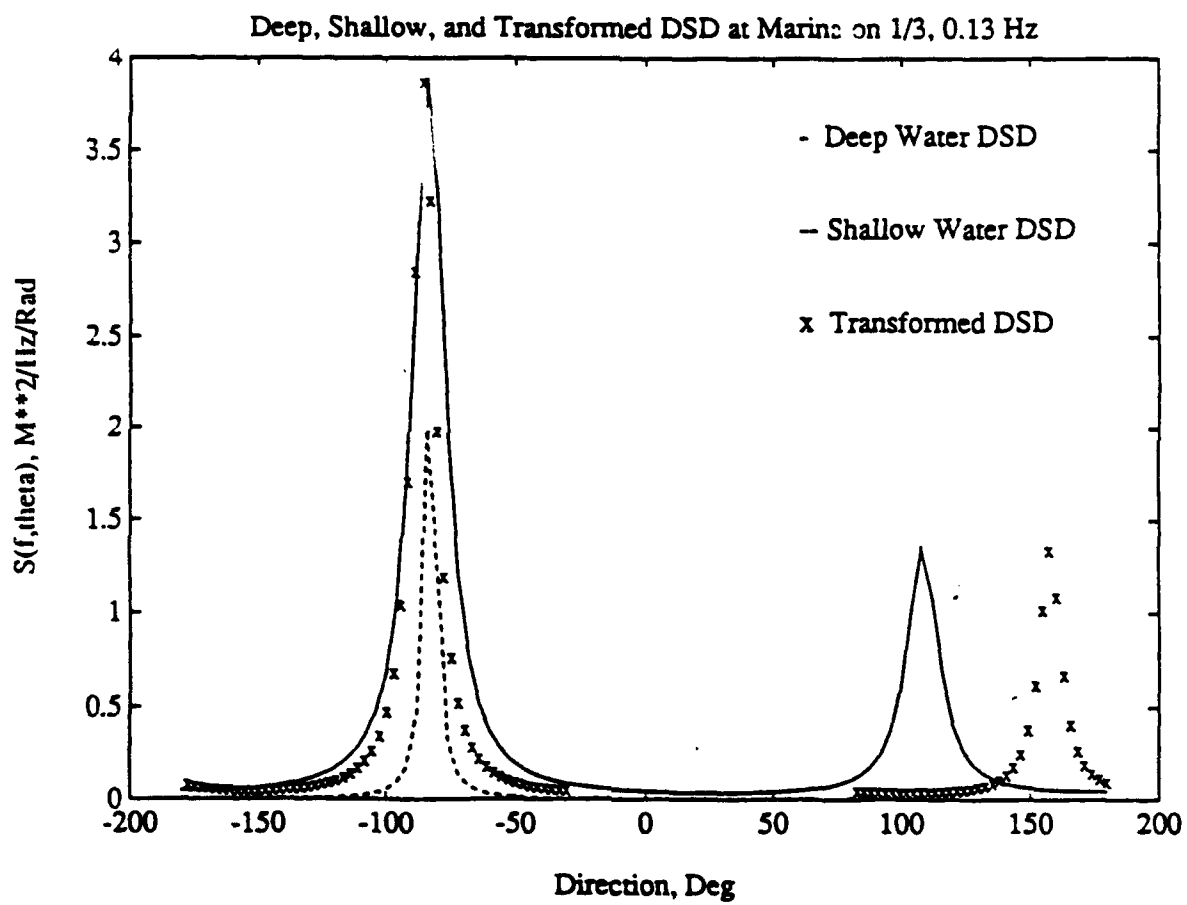


Figure 36. The deep, shallow, and transformed DSD: On 3 Jan 1988 at Marina, 0.13 Hz.

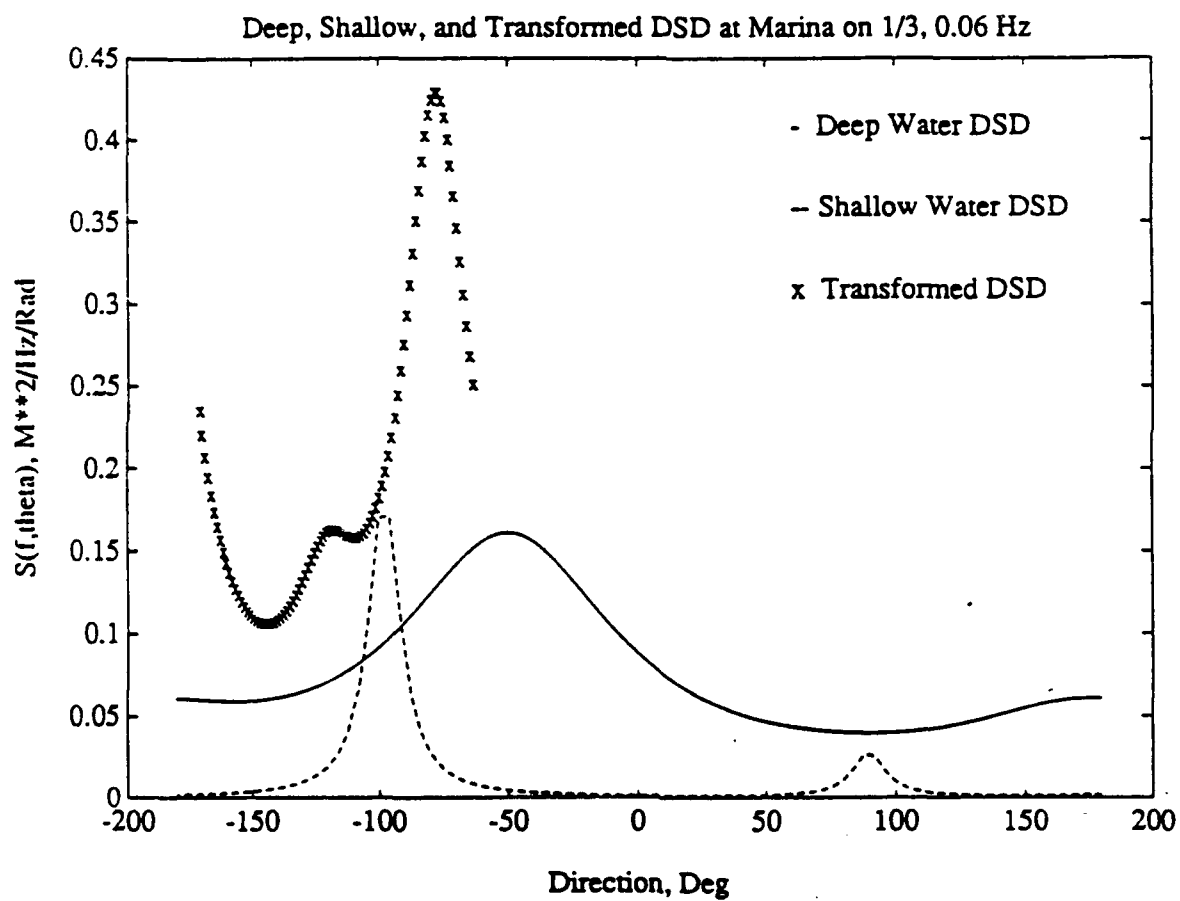


Figure 37. The deep, shallow, and transformed DSD: On 3 Jan 1988 at Marina, 0.06 Hz.

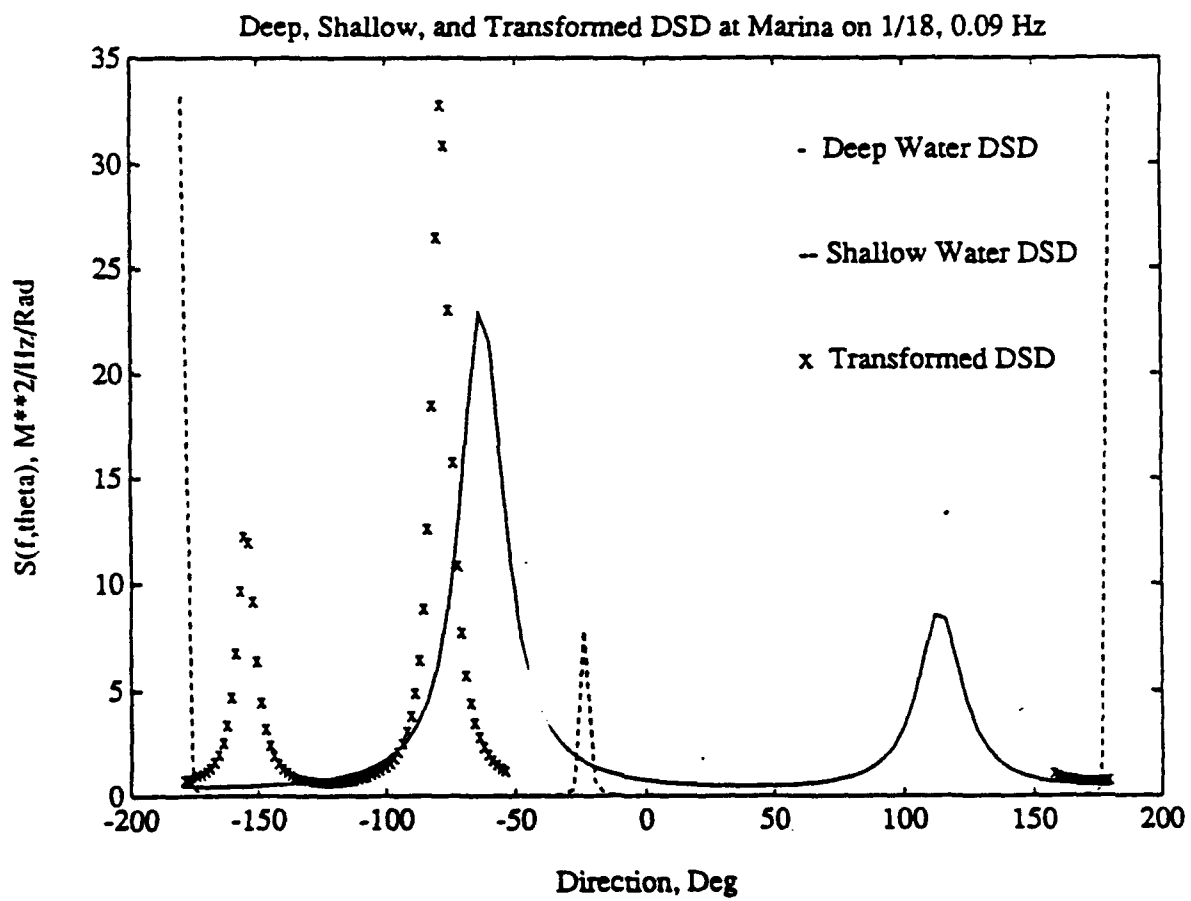


Figure 38. The deep, shallow, and transformed DSD: On 18 Jan 1988 at Marina, 0.09 Hz.

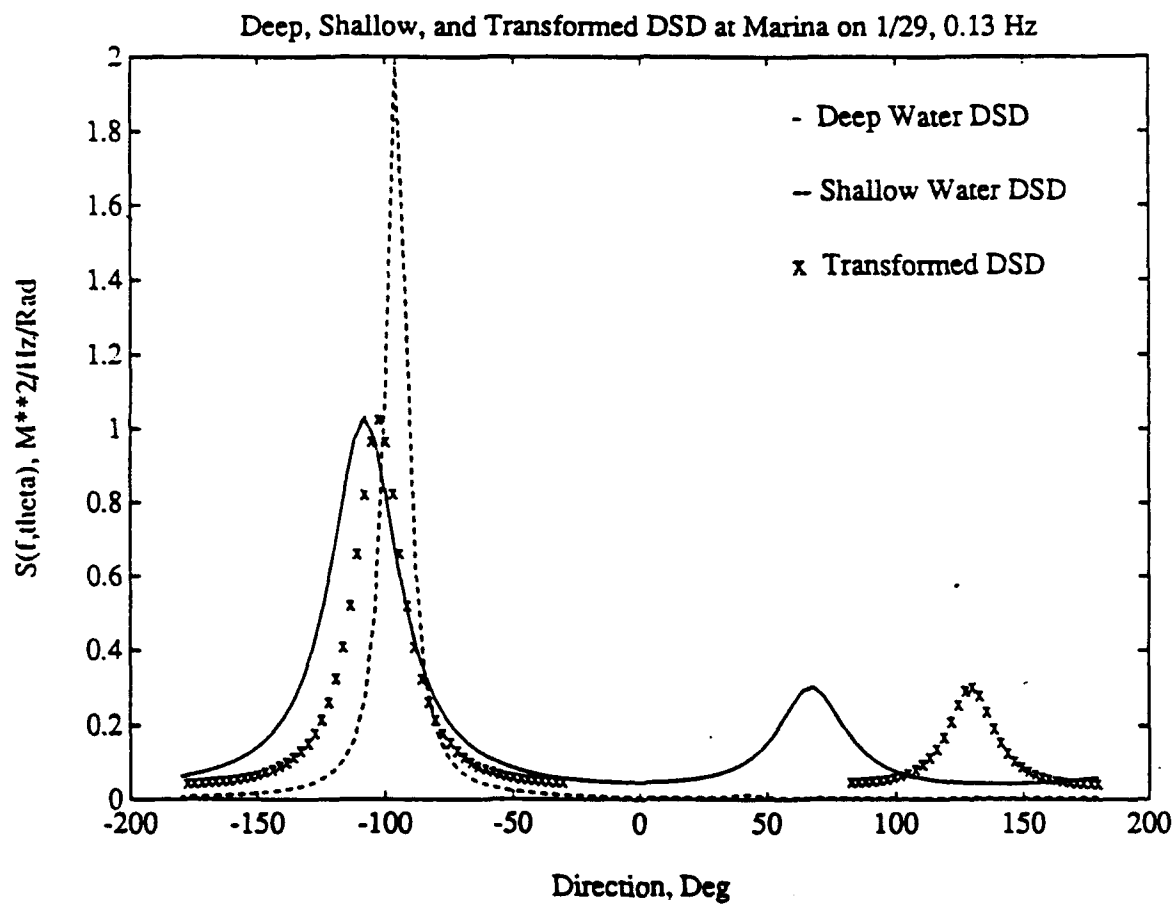


Figure 39. The deep, shallow, and transformed DSD: On 29 Jan 1988 at Marina, 0.13 Hz.

a 30 angle degree difference on 18 January 1988, on the same day, the measured energy is four times larger than predicted, but on 3 and 29 January 1988 errors are the same for between measured and predicted. At Santa Cruz, the directional difference is almost the same on 18 and 29 January 1988, but has a 30 angle degree difference on 3 January 1988. From an energy point of view, 3 and 18 January 1988 show the same energy, but on 29 January 1988, the predicted energy is almost two times the measured energy.

Summarizing, the energies at the peak frequency were similar except at Marina on the 18th (x4) and Santa Cruz on the 29th (x2). The angles at the peak frequencies were within 5 degrees except at Santa Cruz on the 3rd (30°) and Marina on the 18th (30°). There is no obvious correlation with error on deep water wave directions (~275° on the 3rd, 300° on the 18th and 245° on the 29th)

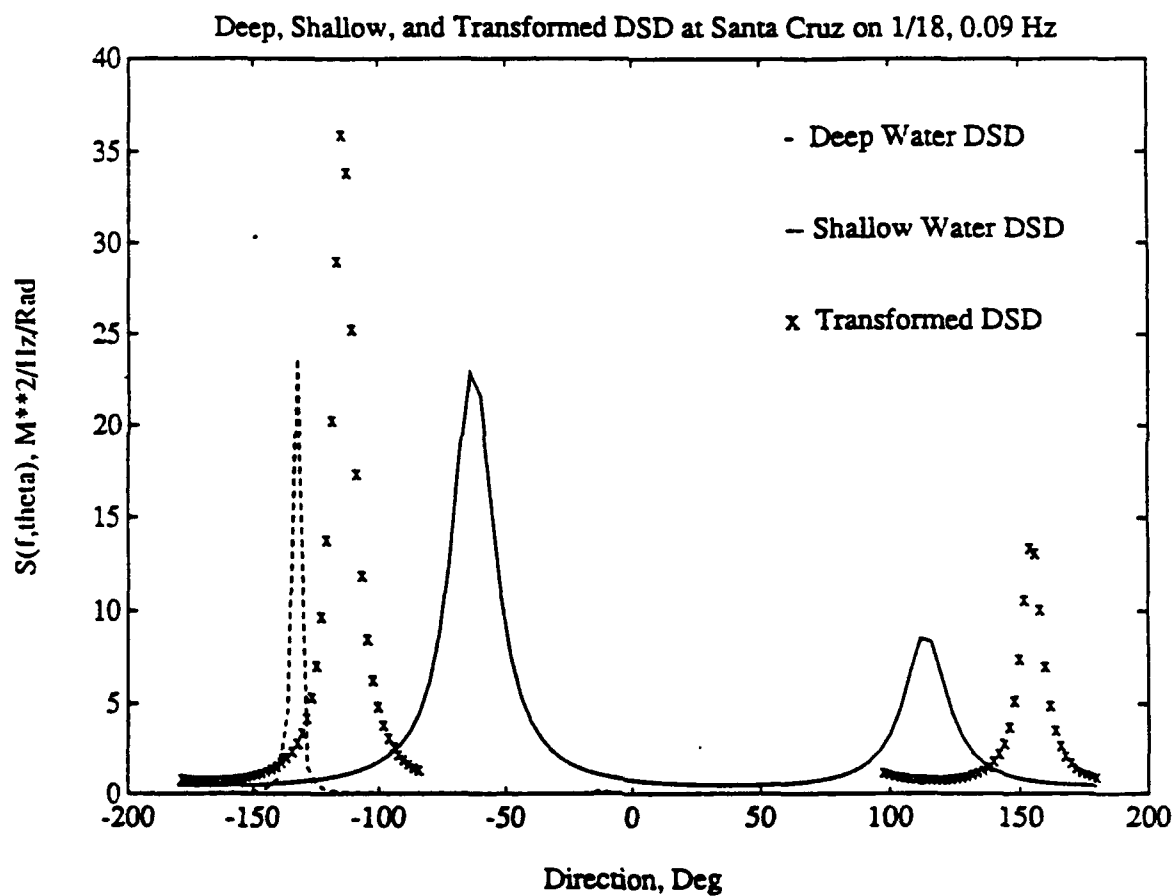


Figure 40. The deep, shallow, and transformed DSD: On 18 Jan 1988 at Santa Cruz, 0.09 Hz.

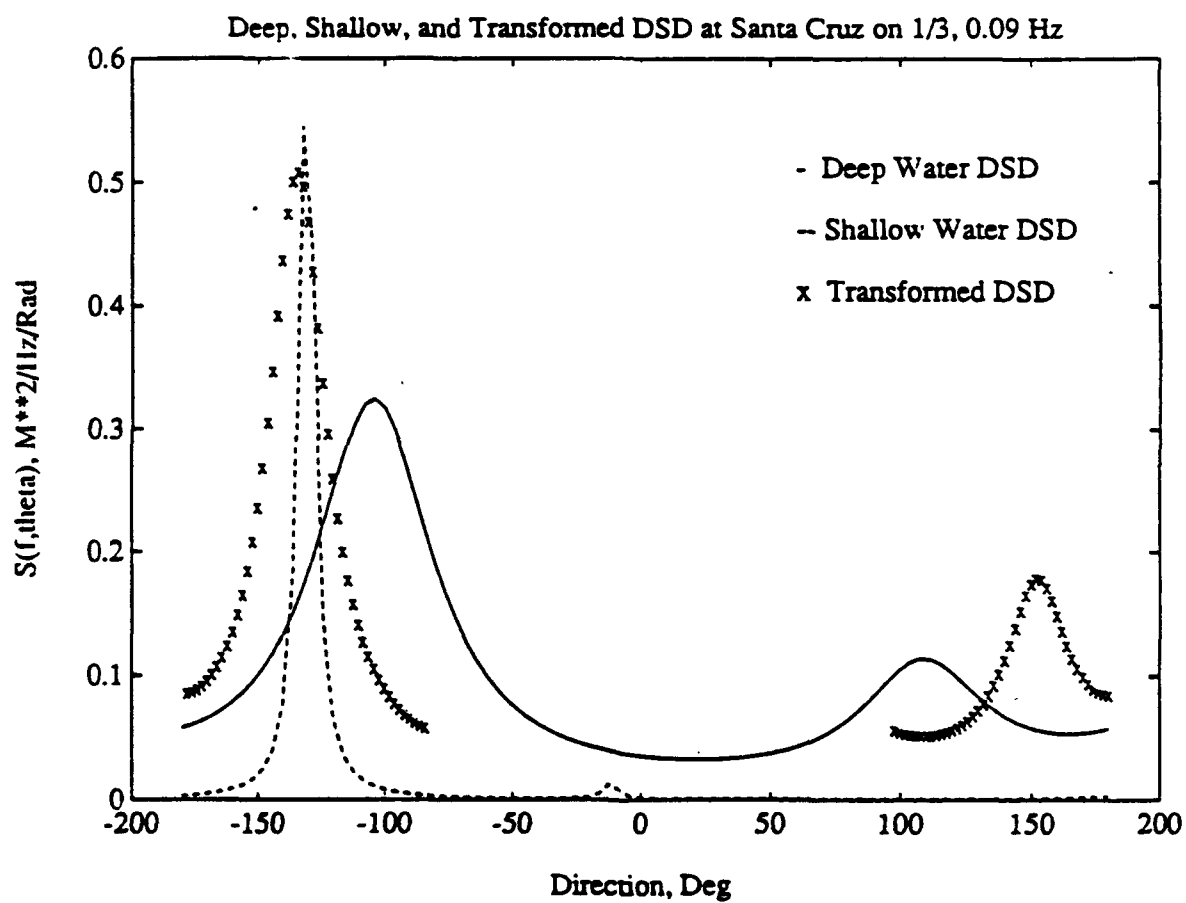


Figure 41. The deep, shallow, and transformed DSD: On 3 Jan 1988 at Santa Cruz, 0.09 Hz.

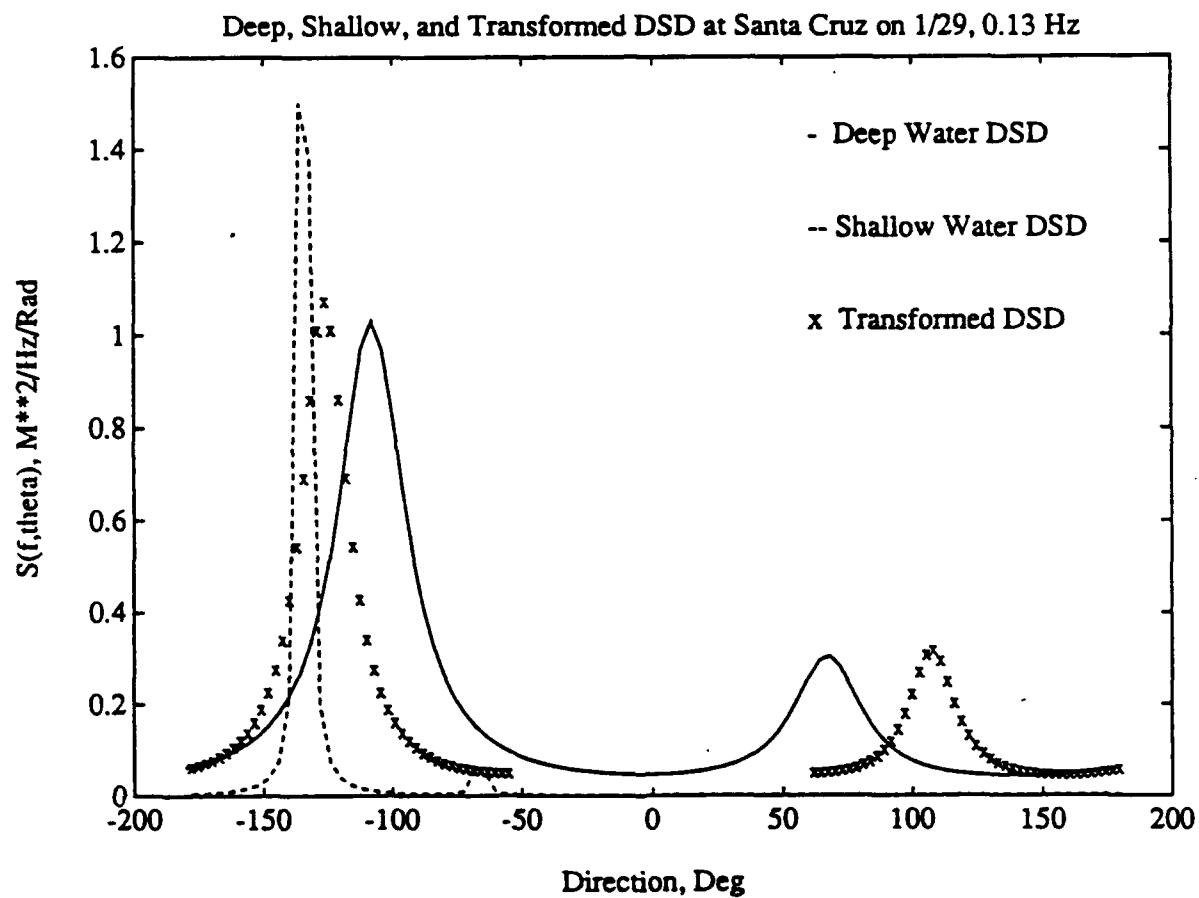


Figure 42. The deep, shallow, and transformed DSD: On 29 Jan 1988 at Santa Cruz, 0.13 Hz.

V. CONCLUSION

Deep water directional wave spectra were calculated from data acquired from the NDBC buoy and transformed over the highly complex bathymetry of Monterey Bay to shallow water using a linear wave refraction model. The transformed spectra were compared with measured shallow wave spectra at Marina and Santa Cruz.

Two methods of calculating the directional spectrum were employed, the LCS and EFC techniques. The results show that the two techniques give the same peak densities and energies, but that the EFC method has much superior resolution.

The comparison of measured and transformed spectra show that higher frequency wave conditions exhibit more accurate results, which are less refracted, and with relatively larger errors occurring at lower frequencies. In general, linear refraction can give reasonable energy and direction estimates starting with deep water spectra, but notable exceptions can occur. The largest prediction errors occurred at Marina on 18 January 1988 for the case of a severe storm. This is presumably due to diffractive and non-linear effects of the high waves causing loss of accuracy. The linear refraction model is not suitable for handling such problems. Further modeling efforts for Monterey Bay including diffractive and non-linear effects are needed.

APPENDIX A. THE SHALLOW WATER ANGLE VERSUS DEEP WATER ANGLE

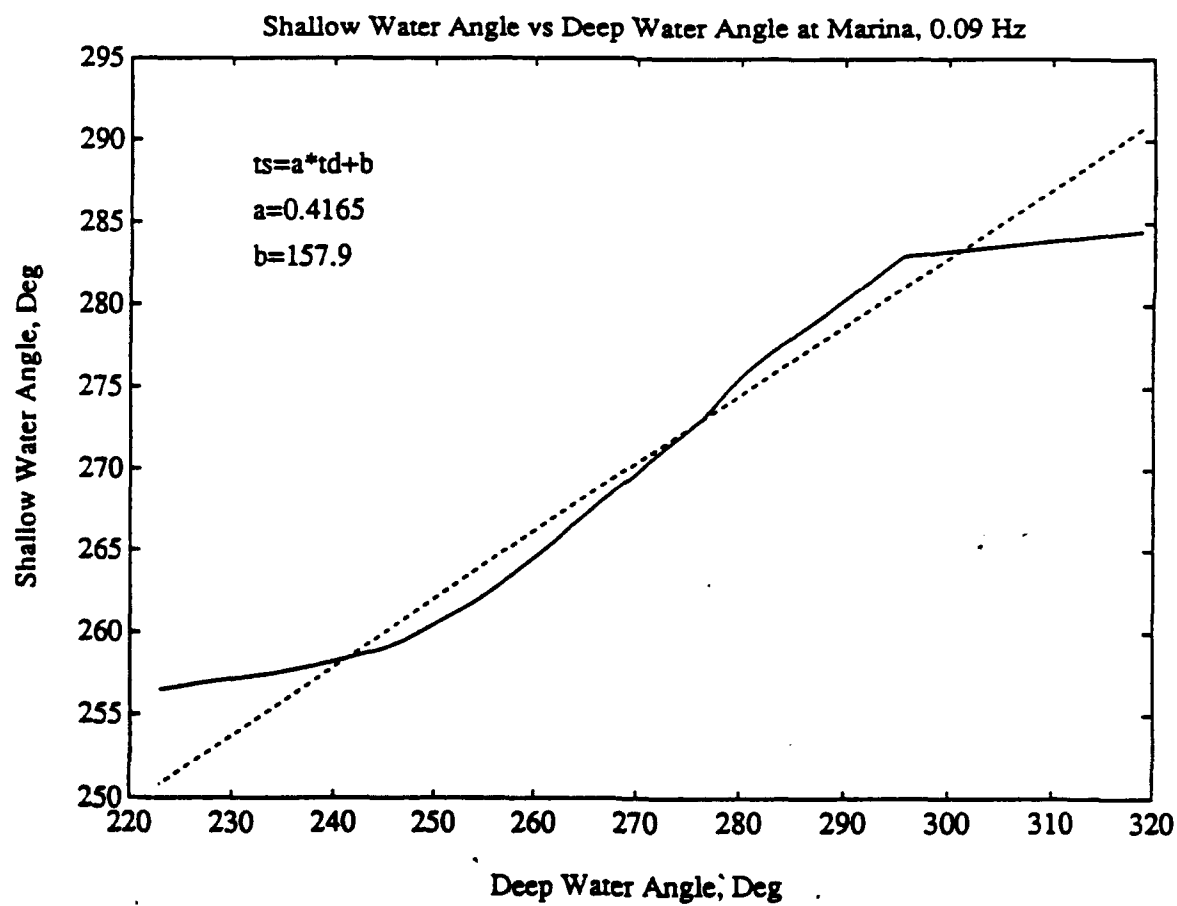


Figure 43. The shallow water angle versus deep water angle at Marina 0.09 Hz.

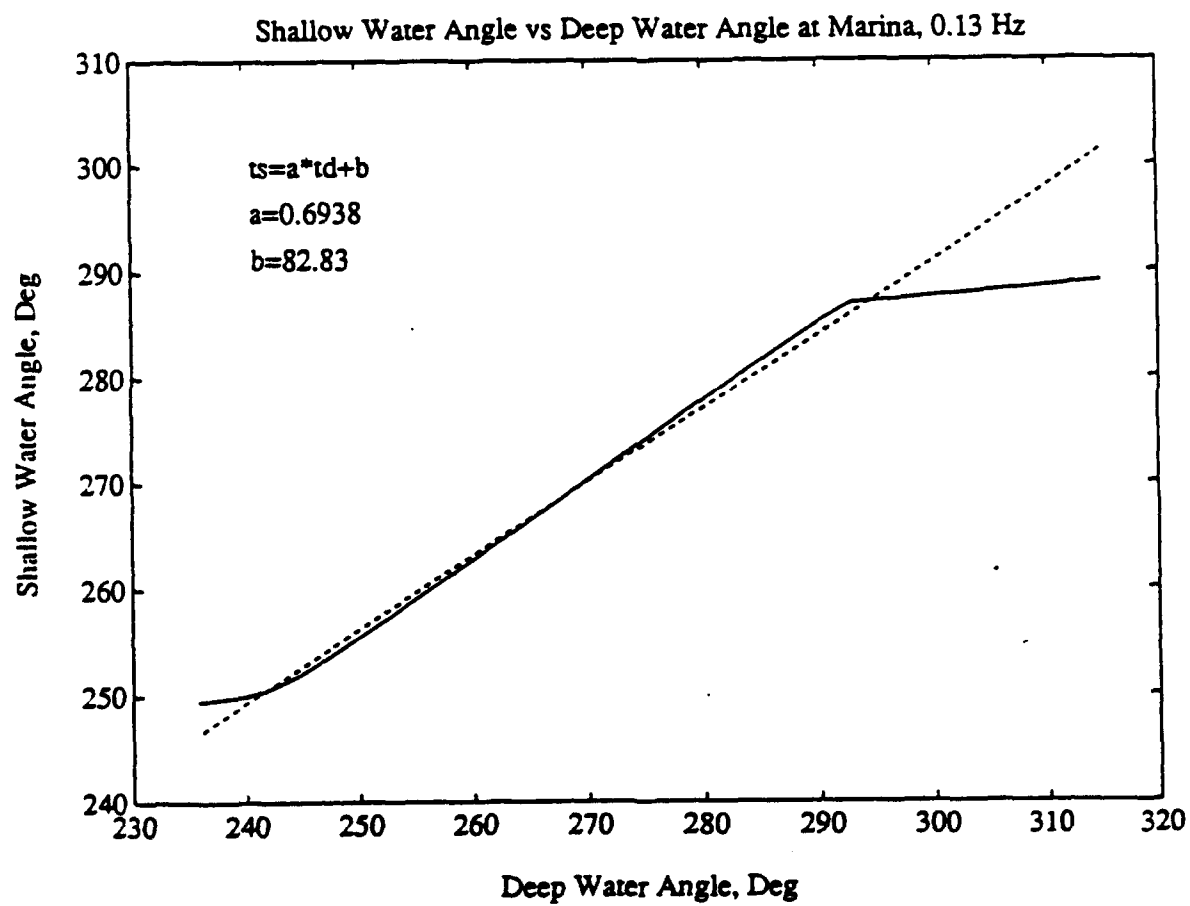


Figure 44. The shallow water angle versus deep water angle at Marina 0.13 Hz.

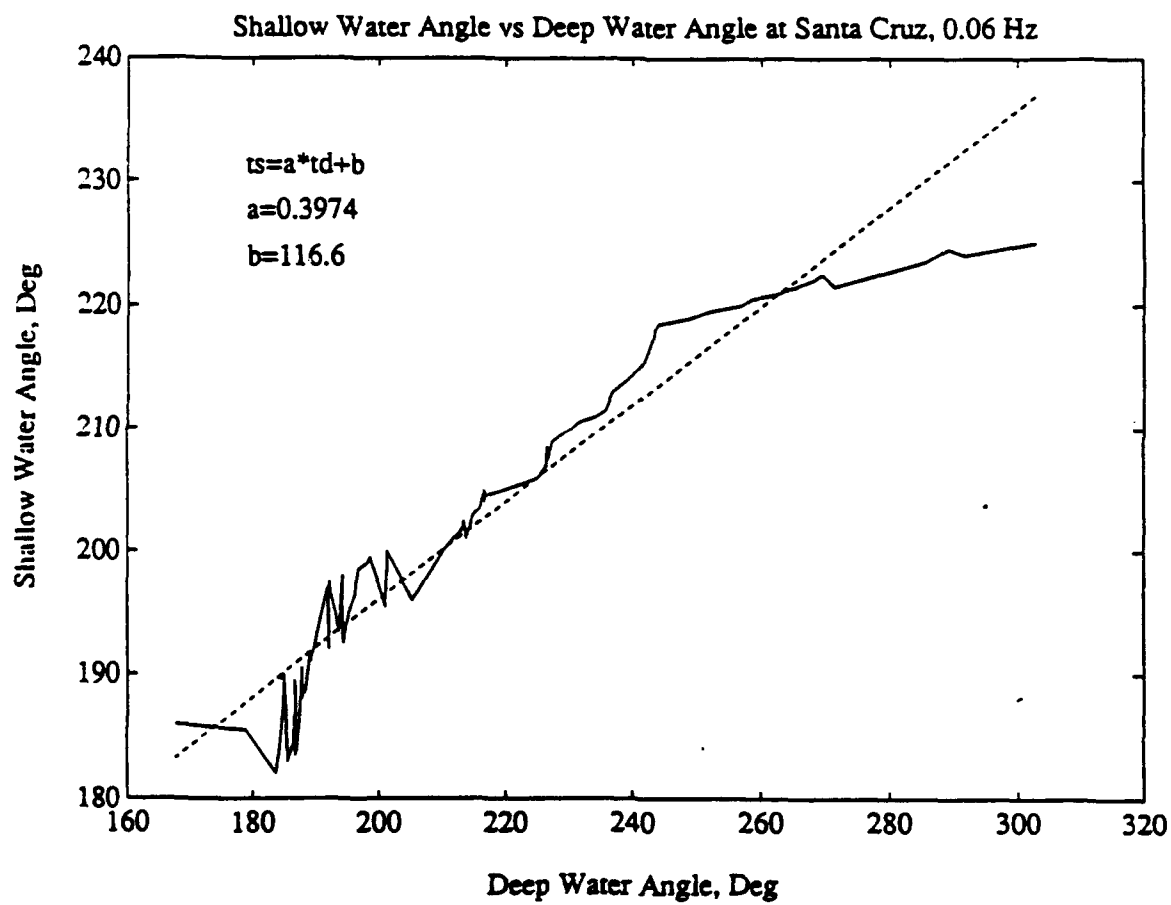


Figure 45. The shallow water angle versus deep water angle at Santa Cruz 0.06 Hz.

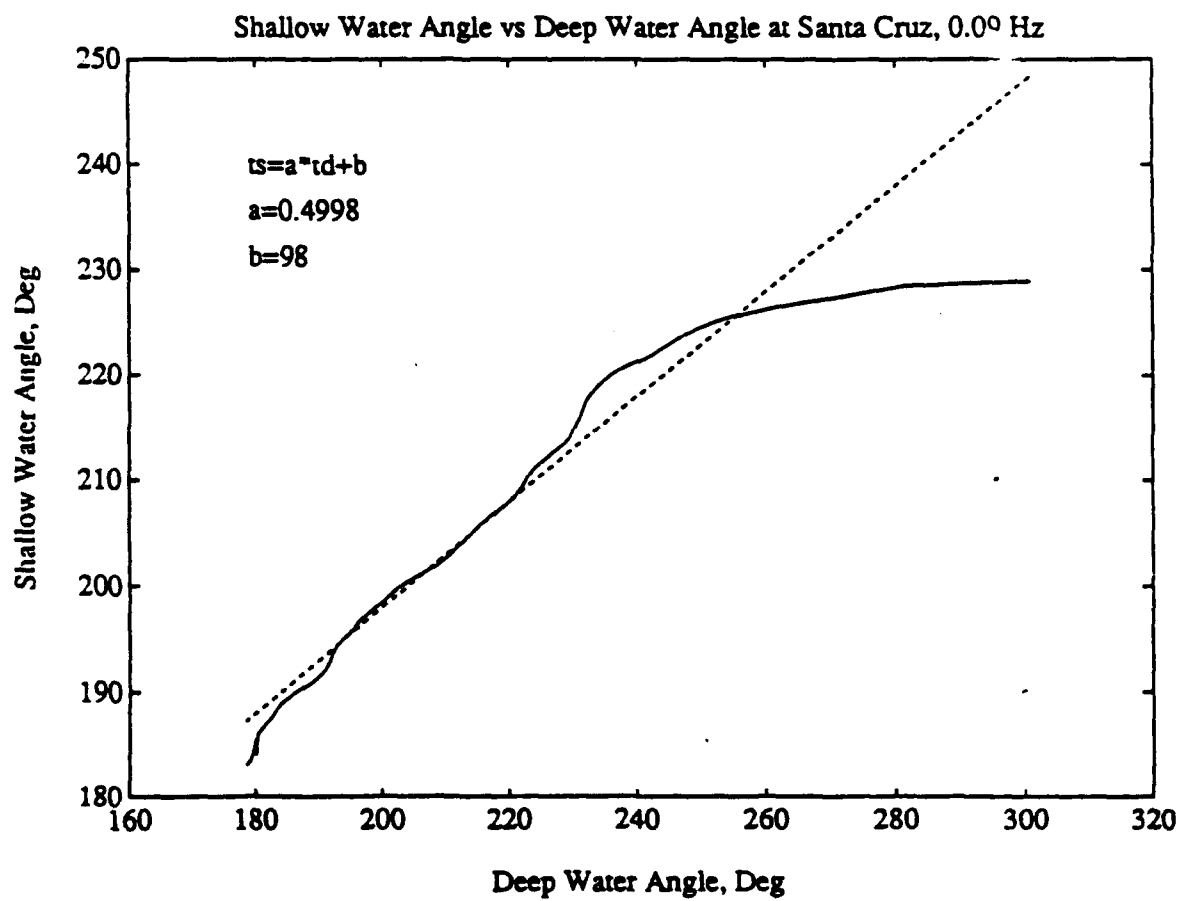


Figure 46. The shallow water angle versus deep water angle at Santa Cruz 0.09 Hz.

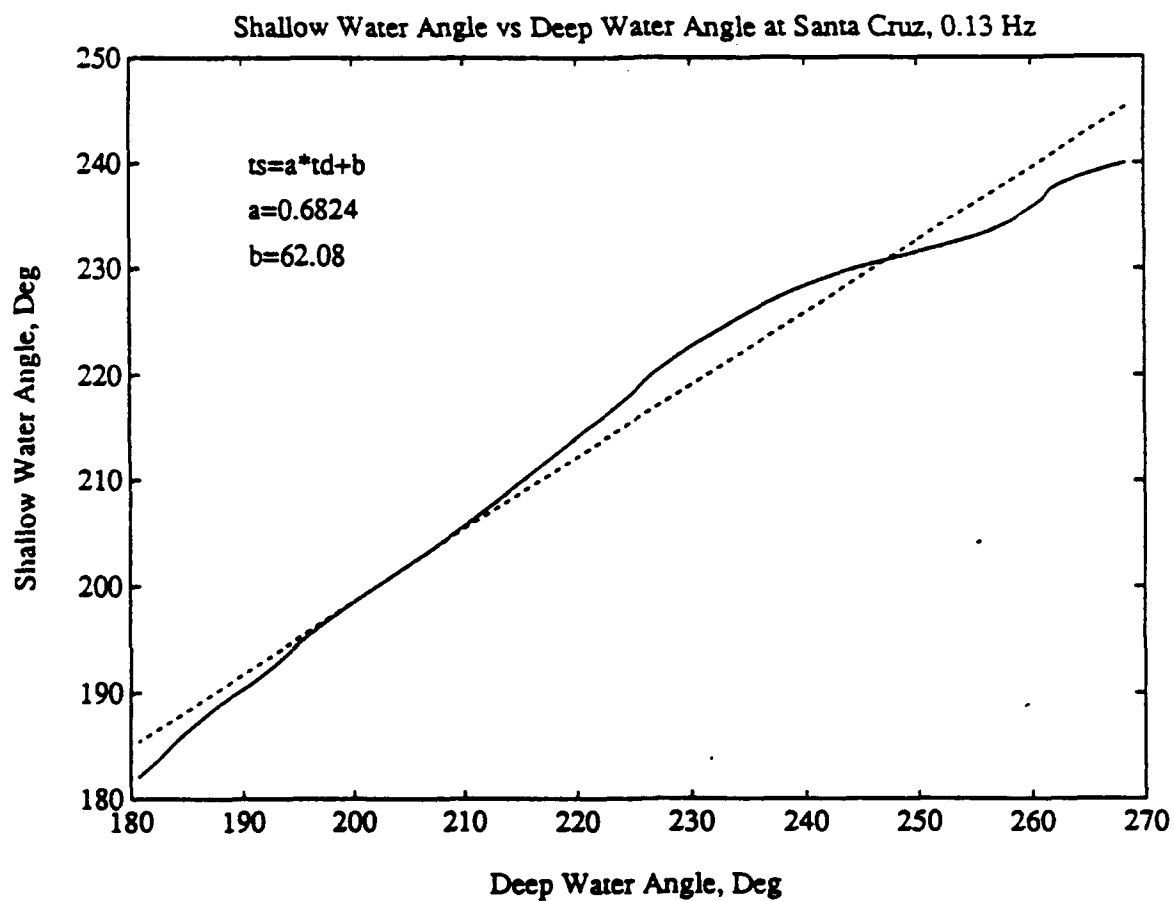


Figure 47. The shallow water angle versus deep water angle at Santa Cruz 0.13 Hz.

APPENDIX B. THE DEEP, SHALLOW, AND TRANSFORMED DSD

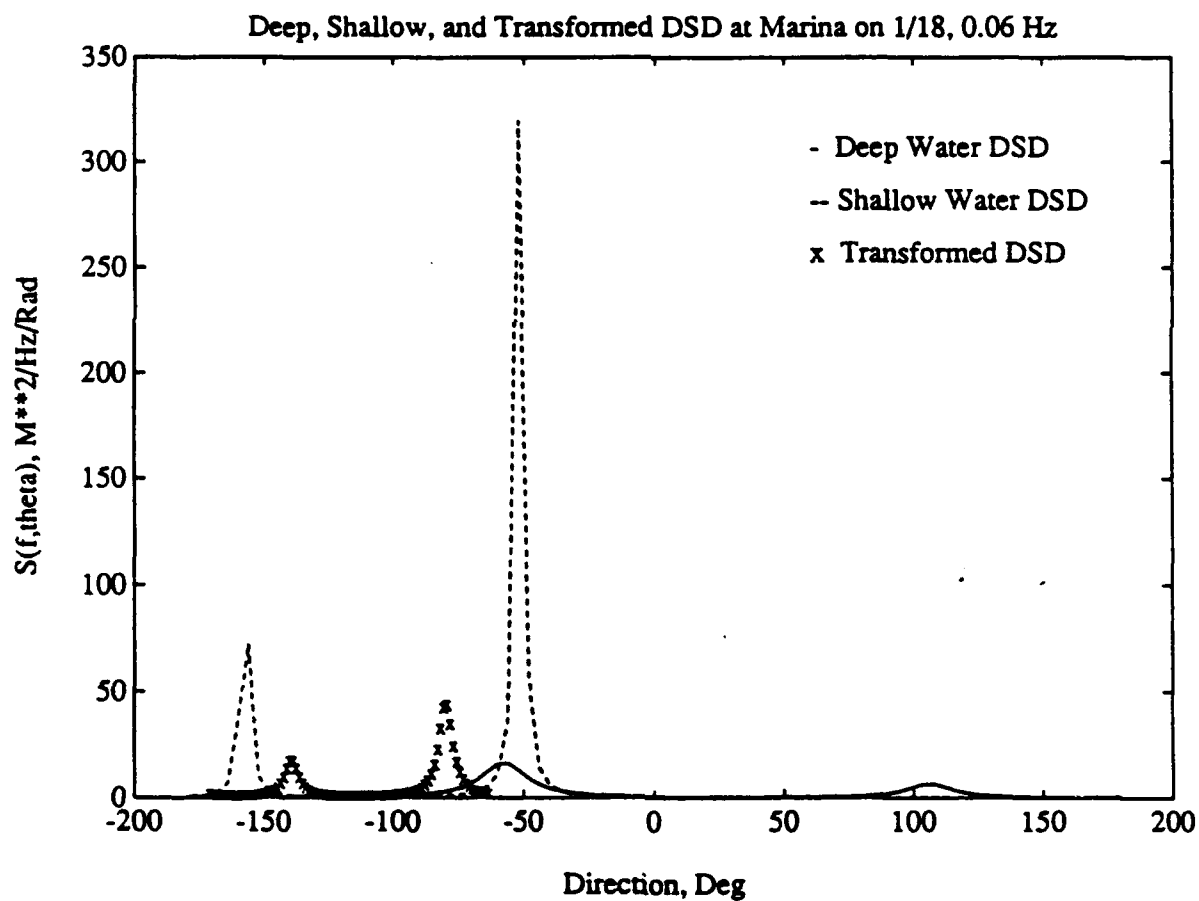


Figure 48. The deep, shallow, and transformed DSD: On 18 Jan 1988 at Marina, 0.06 Hz.

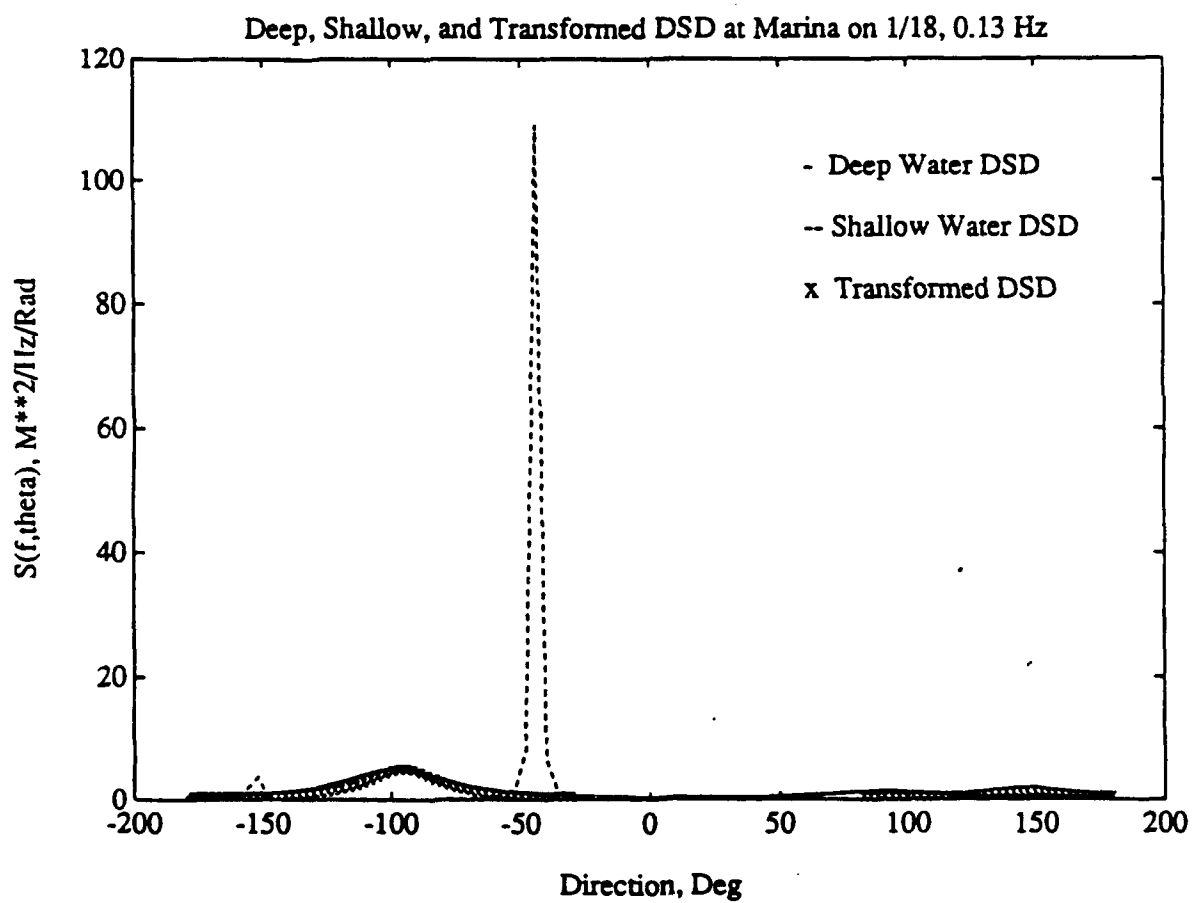


Figure 49. The deep, shallow, and transformed DSD: On 18 Jan 1988 at Marina, 0.13 Hz.

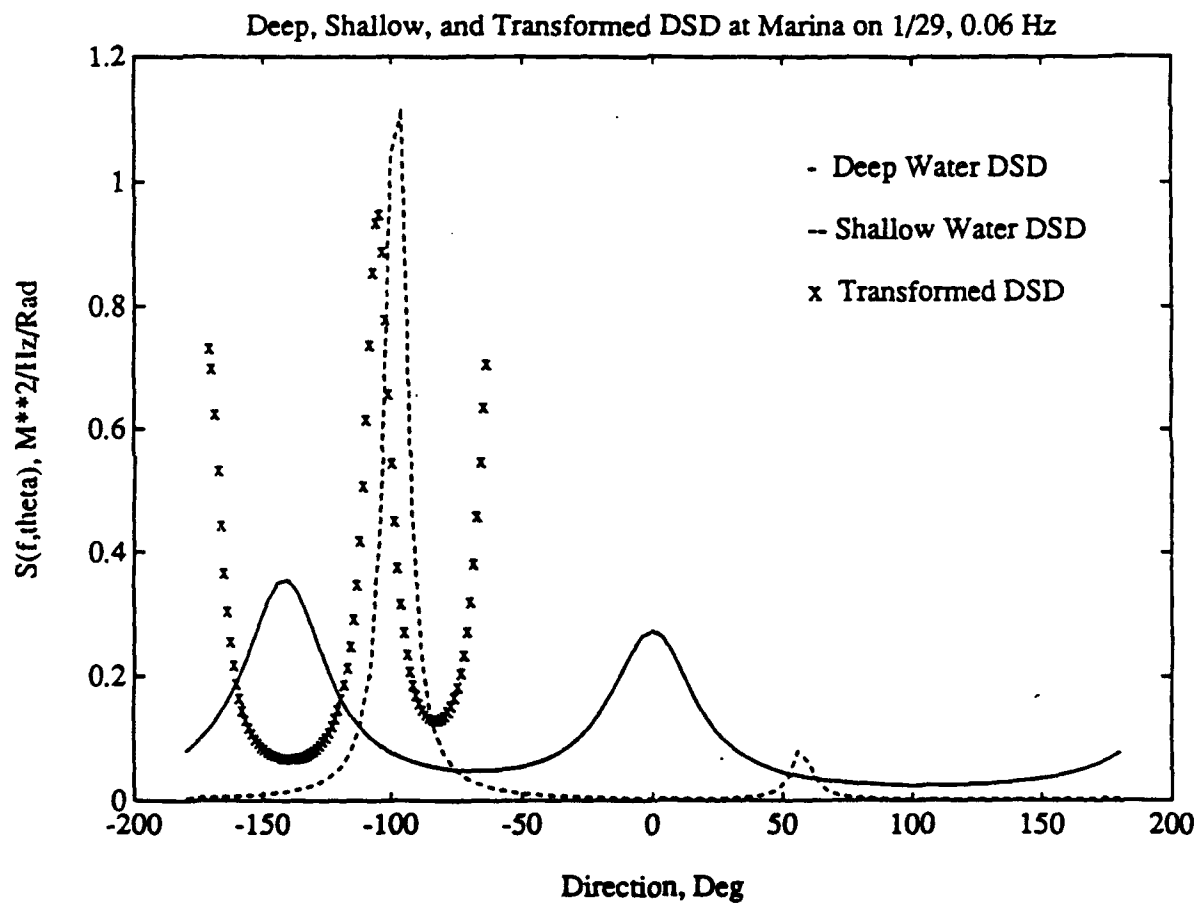


Figure 50. The deep, shallow, and transformed DSD: On 29 Jan 1988 at Marina, 0.06 Hz.

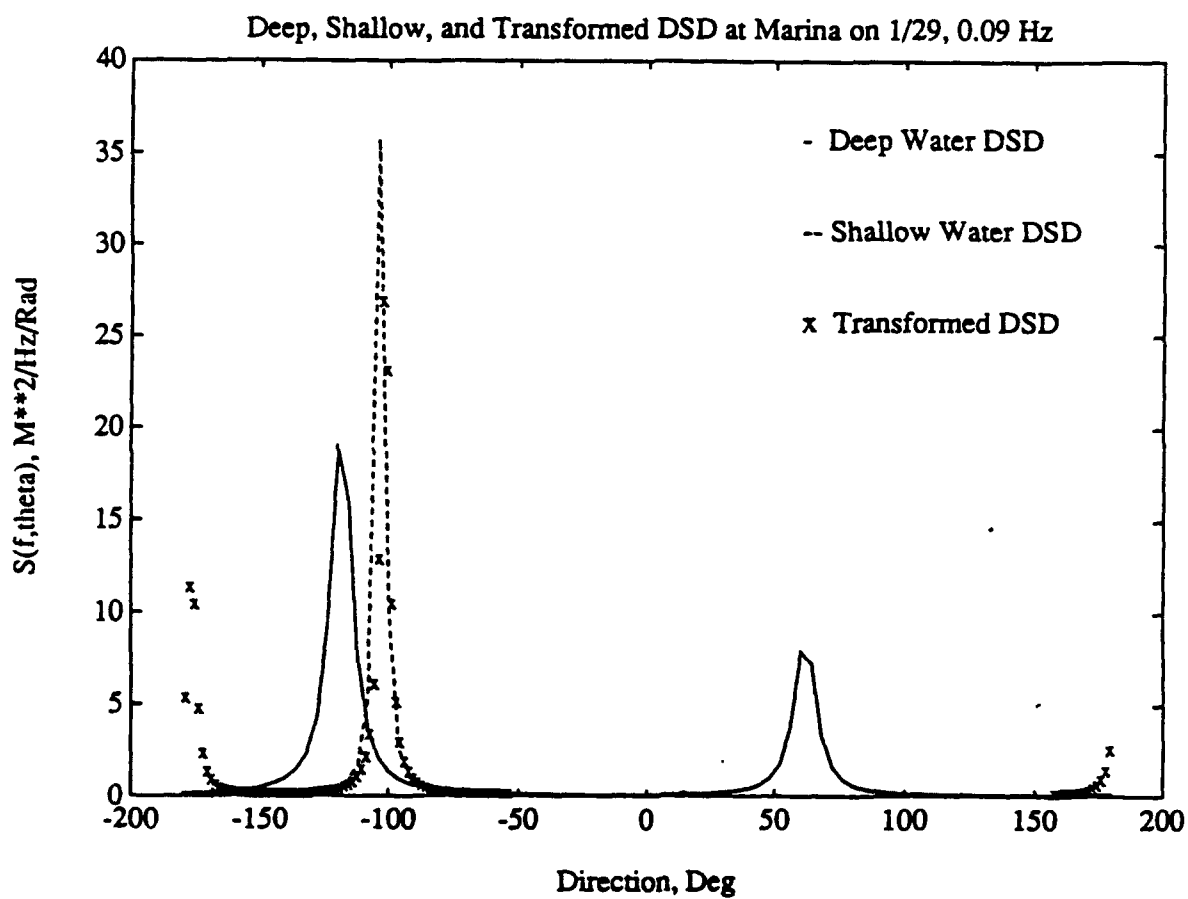


Figure 51. The deep, shallow, and transformed DSD: On 29 Jan 1988 at Marina, 0.09 Hz.

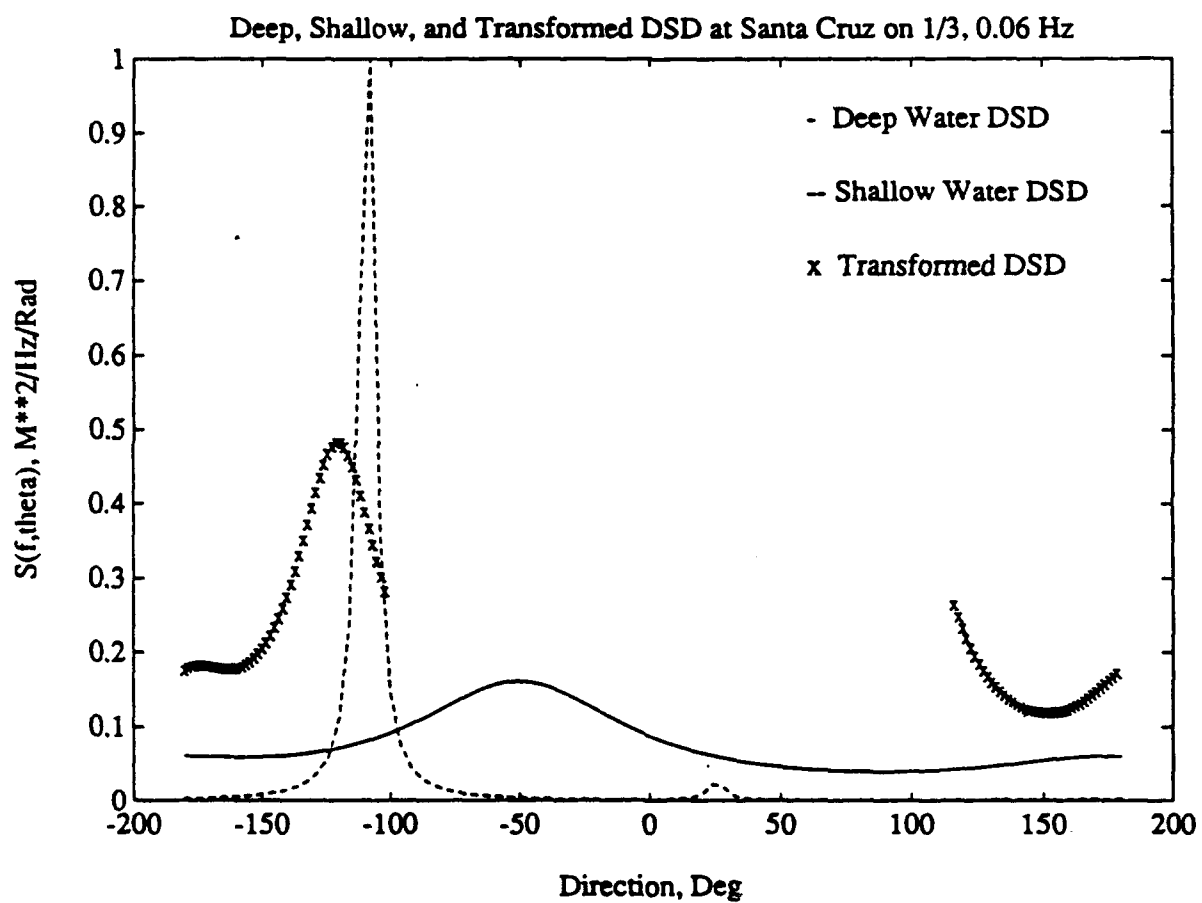


Figure 52. The deep, shallow, and transformed DSD: On 3 Jan 1988 at Santa Cruz, 0.06 Hz.

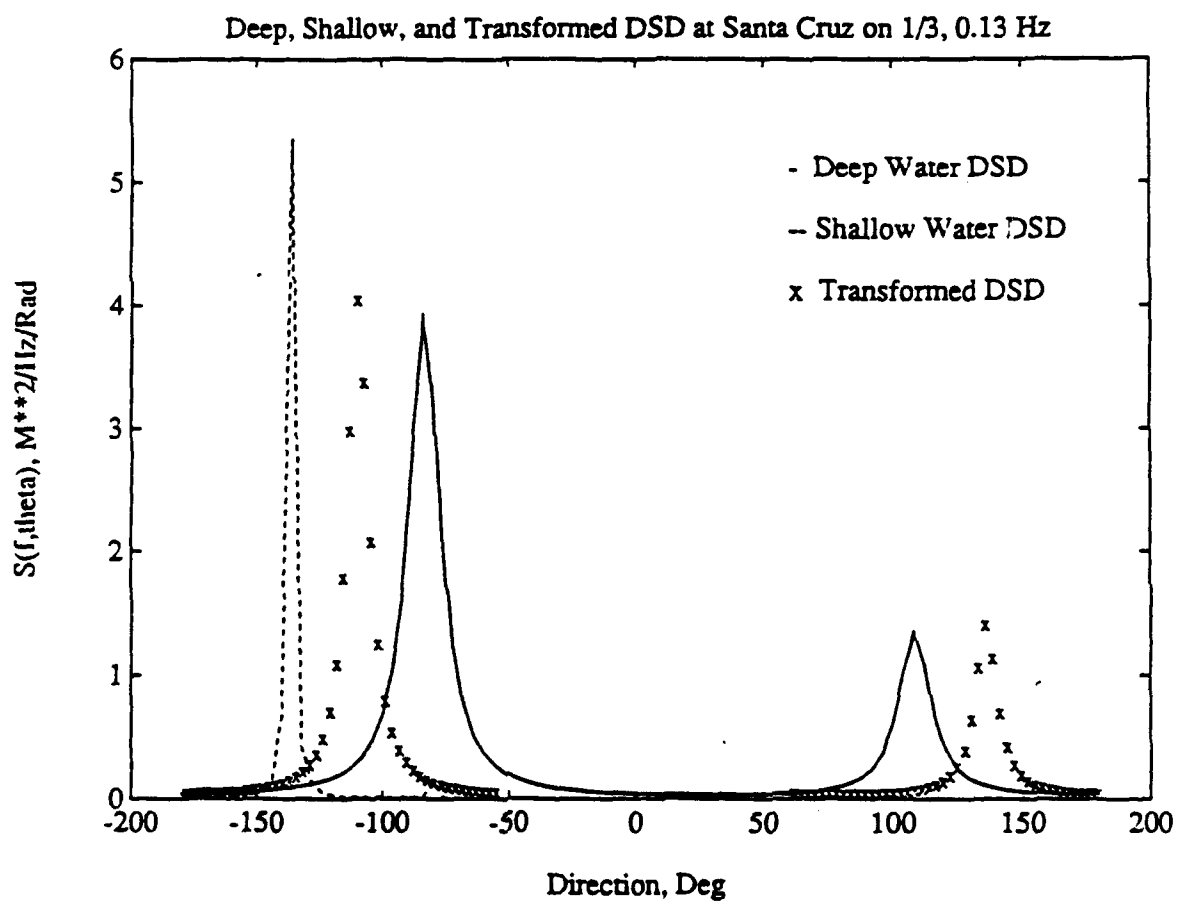


Figure 53. The deep, shallow, and transformed DSD: On 3 Jan 1988 at Santa Cruz, 0.13 Hz.

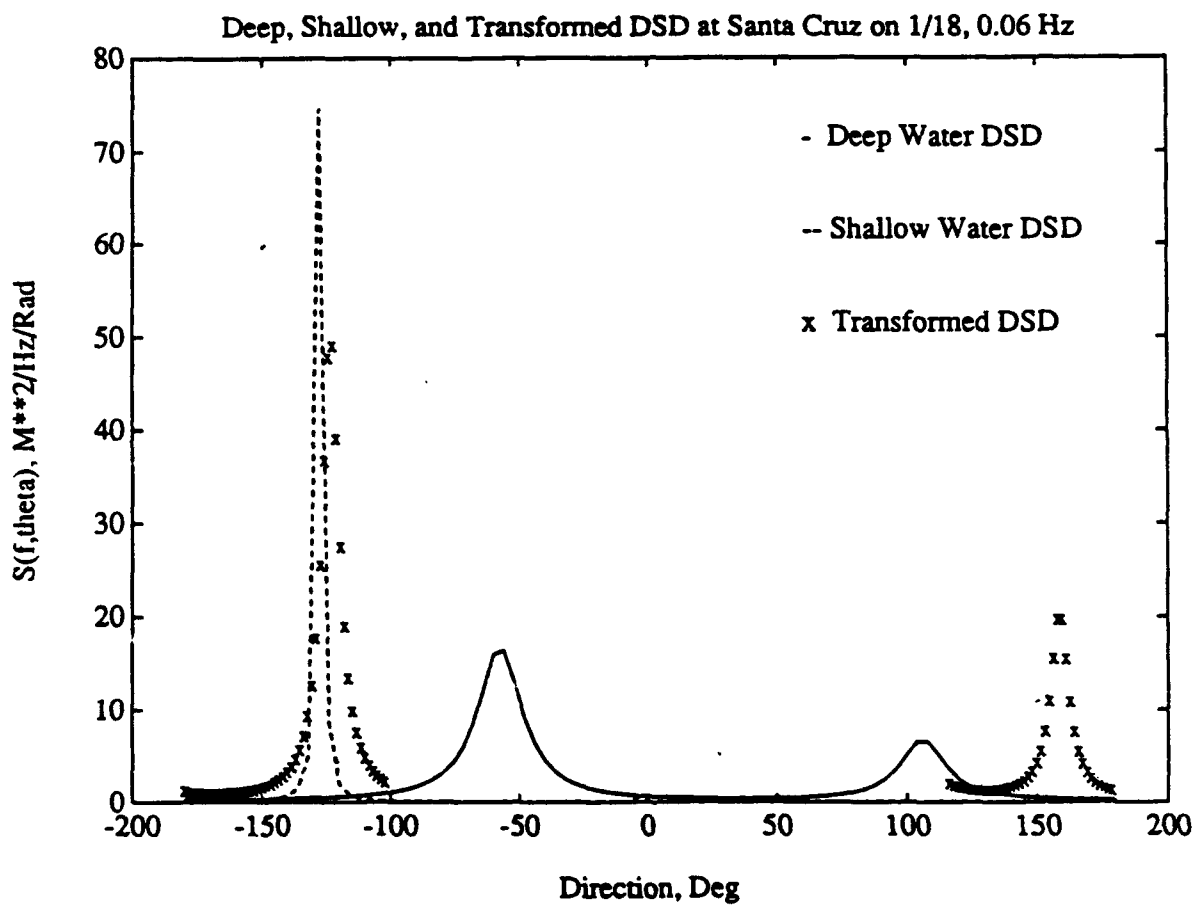


Figure 54. The deep, shallow, and transformed DSD: On 18 Jan 1988 at Santa Cruz, 0.06 Hz.

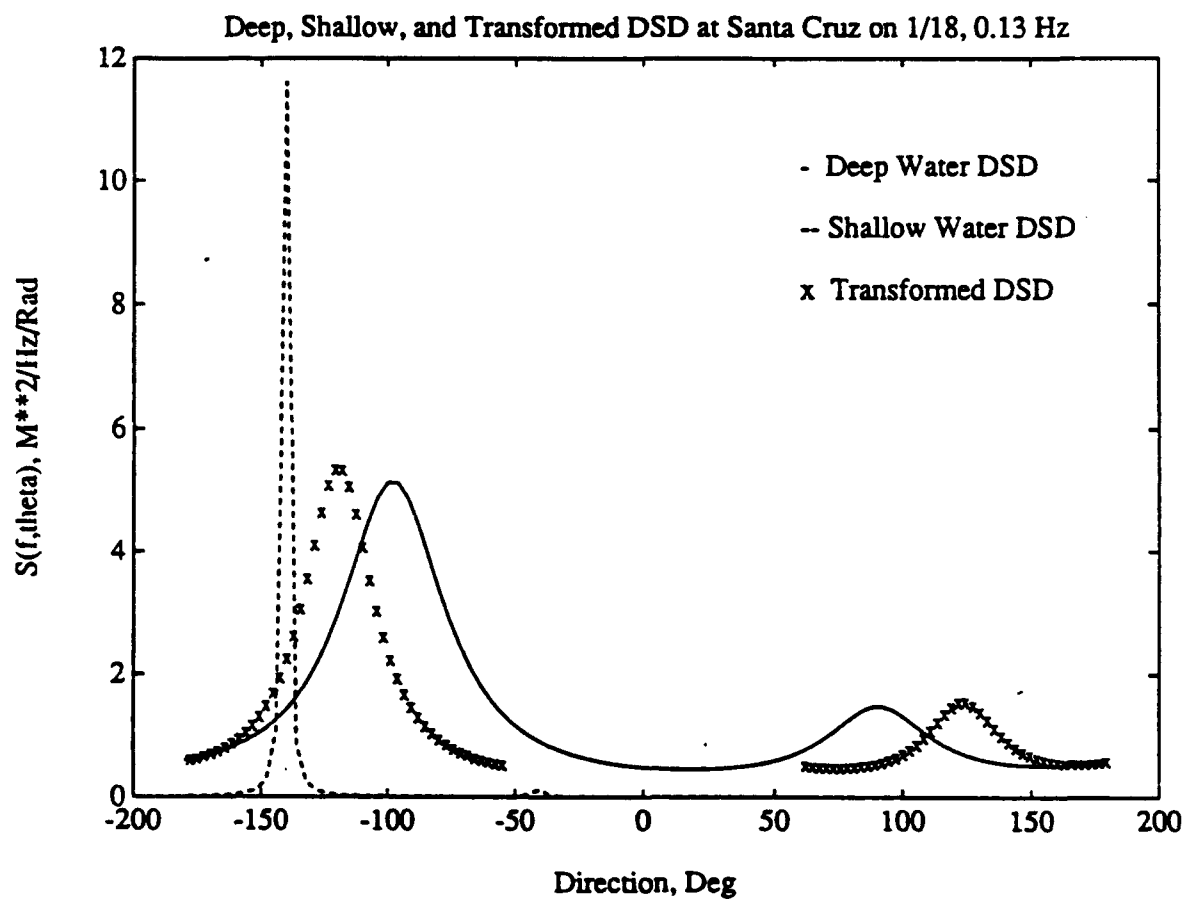


Figure 55. The deep, shallow, and transformed DSD: On 18 Jan 1988 at Santa Cruz, 0.13 Hz.

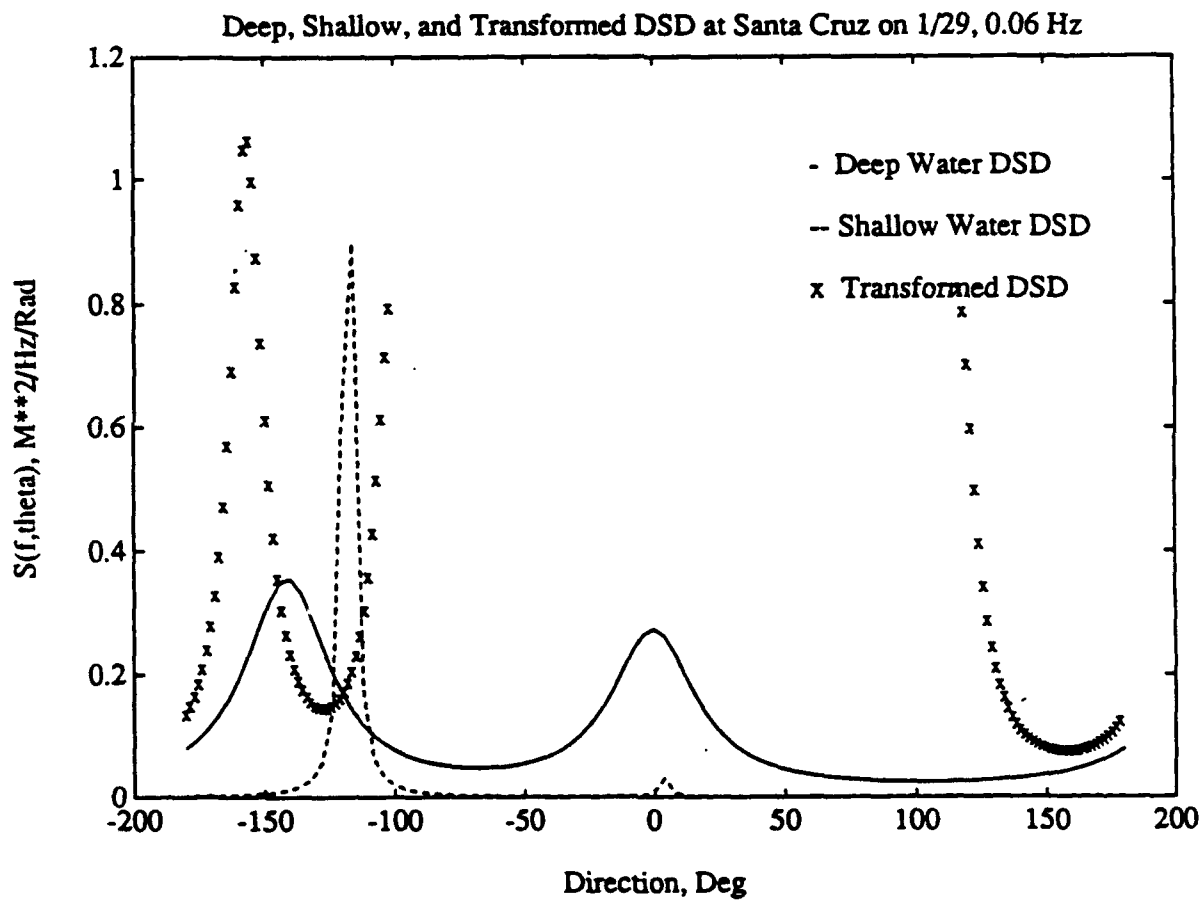


Figure 56. The deep, shallow, and transformed DSD: On 29 Jan 1988 at Santa Cruz, 0.06 Hz.

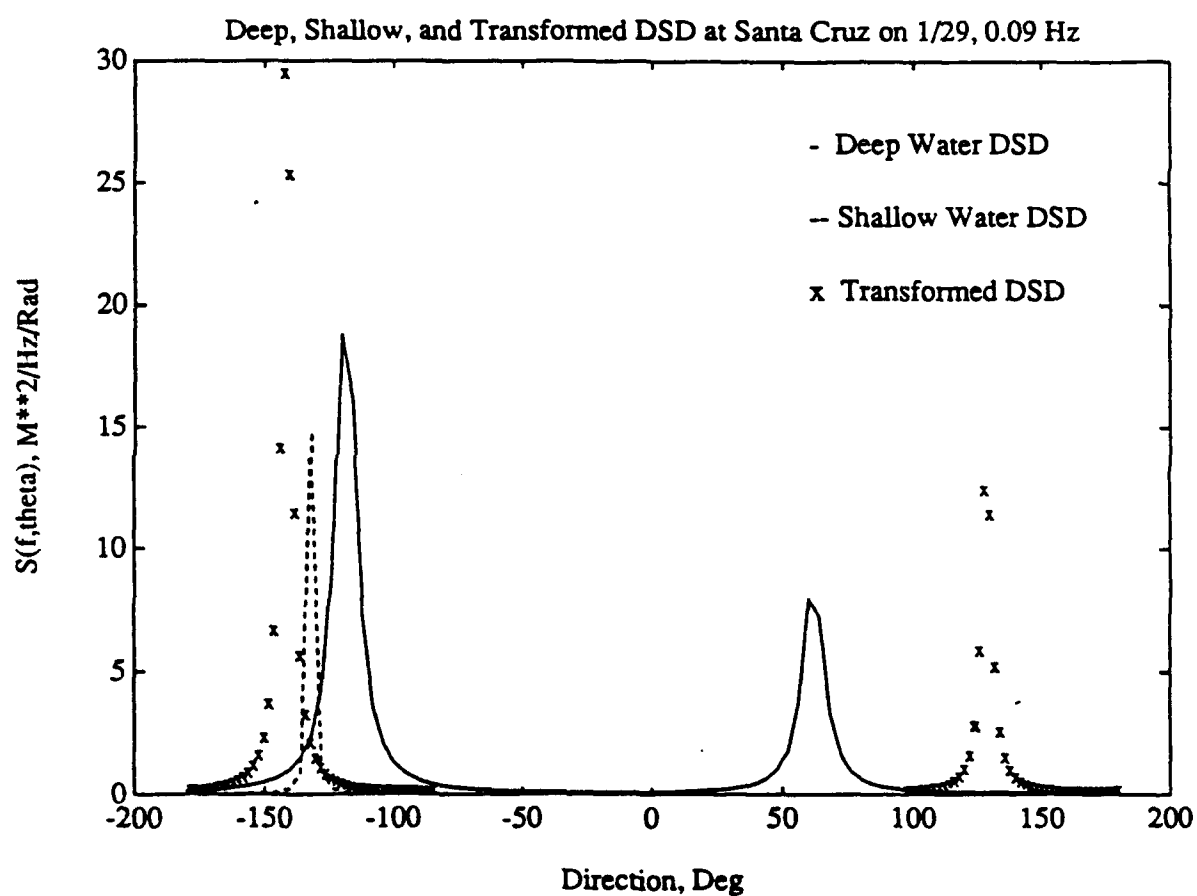


Figure 57. The deep, shallow, and transformed DSD: On 29 Jan 1988 at Santa Cruz, 0.09 Hz.

RERERENCES

- Abreu, M.P., 1989: Kinematics under wind waves., M.S. thesis, Department of Oceanography, Naval Postgraduate School, 4-19 pp.
- Arnal, R.E., Dittmer, E., and Shumaker, E. 1973: Sand transport studies in Monterey Bay, California. *Moss Landing Marine Laboratory Tech. Pub.*, , 73-75.
- Barber, N.F., 1946: Measurements of sea conditions by the motion of a floating buoy. *Admiralty Res. Lab. Report*, 103/ n2/W.
- Cayan, D.R. et al. 1988: January 16-18, An unusual severe southern California coastal storm, CSBPA Newsbreaker.
- Davis, R.E. and L.A. Regier, 1977: Methods for estimating direction : wave spectrum from multi-element array. *J. Mar. Res.* 35(3), 453-477.
- Dorman, C.E. 1968: Southern Monterey bay littoral cell. A preliminary sediment report, M.S. thesis, Naval Postgraduate School, Monterey, California.
- Khalid, M.A., 1989: Comparison of measured and transformed directional wave spectra using linear refraction model., M.S. thesis, Department of Oceanography, Naval Postgraduate School. 18-55 pp.
- Kinsman, B. 1965: Wind waves, Prentice Hall, 676 pp.
- Longuet-Higgins, M.S., 1957: On the transformation of a continuous spectrum by refraction. *Proceedings of the Cambridge Philosophical Society*, Vol. 53, No. 1, pp.226-229.
- Longuet-Higgins, M.S., Cartwright, D.E., and Smith, N.D. 1963: Observation of the directional spectrum of sea waves using the motions of a floating Buoy. *Ocean Waves Spectra*.
- McGee, T. 1986: Coastal Erosion Along Monterey Bay., M.S. thesis, Department of Oceanography, Naval Postgraduate School.
- Méhauté B.L., and Wang, J.D., 1982: Wave spectrum changes on sloped beach. *J. of the Waterway, Port, Coastal and Ocean Division*, ASCE, 108, 33-44.
- Oradiwe, E.N., 1986: Sediment Budget for Monterey Bay., M.S. thesis, Department of Oceanography, Naval Postgraduate School.
- Phillips, O.M., 1977: Dynamics of the upper ocean., Cambridge University Press, 261 pp.
- Thornton, K.B., 1978: Maximum wave forces on proposed Monterey bay regional sewage outfall due to 50 years storm waves. Prepared for Engineering Science, Inc..

Thornton, K.B., 1980: Wave design criteria and related environmental impacts., Unpublished Report for Monterey Bay Aquarium.

Wiegel, R.L., 1964: Oceanographical engineering., Prentice Hall.

INITIAL DISTRIBUTION LIST

		No. Copies
1.	Defense Technical Information Center Cameron Station Alexandria, VA 22304-6145	2
2.	Library, Code 52 Naval Postgraduate School Monterey, CA 93943-5002	2
3.	Chairman (Code OC/Co) Department of Oceanography Naval Postgraduate School Monterey, CA 93943-5000	1
4.	Chairman (Code MR/Hy) Department of Meteorology Naval Postgraduate School Monterey, CA 93943-5000	1
5.	Professor Edward B. Thornton (Code 68TM) Department of Oceanography Naval Postgraduate School Monterey, CA 93943-5000	2
6.	LCDR Cheng liu Department of Oceanography 6, Alley 3, Lane 115, Shi-Tzung Rd. Taipei, Taiwan, R. O. C.	2
7.	Commanding Officer Navy Headquarters Taipei, Taiwan, R.O.C.	1
8.	Commanding Officer Naval Weather Center bar-li, Taipei, Taiwan, R.O.C.	1

- | | | |
|-----|--|---|
| 9. | Commander
Naval Oceanography Command
Stennis Space Center, MS 39529-5000 | 1 |
| 10. | Commanding Officer
Naval Oceanography Command
Stennis Space Center, MS 39522-5001 | 1 |
| 11. | Mr. George Armstrong
Department of Boating and Waterways
1629 S Street
Sacramento, CA 95814 | 1 |